MARTIN MARIETTA ENERGY SYSTEMS LIBRARIES
3 4456 0364409 1

CENTRAL RESEARCH LIBRARY
DOCUMENT COLLECTION

ORNL-3164
UC-40 – Radiation Effects on Materials
TID-4500 (17th ed.)

EFFECTS OF FAST-NEUTRON IRRADIATION AND HIGH TEMPERATURE ON BERYLLIUM OXIDE

R. P. Shields
J. E. Lee, Jr.
W. E. Browning, Jr.

CENTRAL RESEARCH LIBRARY
DOCUMENT COLLECTION
LIBRARY LOAN COPY
DO NOT TRANSFER TO ANOTHER PERSON
If you wish someone else to see this document, send in name with document and the library will arrange a loan.

OAK RIDGE NATIONAL LABORATORY
operated by
UNION CARBIDE CORPORATION
for the
U.S. ATOMIC ENERGY COMMISSION

Printed in USA. Price $2.00 cents. Available from the

Office of Technical Services
U. S. Department of Commerce
Washington 25, D. C.

LEGAL NOTICE

This report was prepared as an account of Government sponsored work. Neither the United States, nor the Commission, nor any person acting on behalf of the Commission:

A. Makes any warranty or representation, express or implied, with respect to the accuracy, completeness, or usefulness of the information contained in this report, or that the use of any information, apparatus, method, or process disclosed in this report may not infringe privately owned rights; or

B. Assumes any liabilities with respect to the use of, or for damages resulting from the use of any information, apparatus, method, or process disclosed in this report.

As used in the above, "person acting on behalf of the Commission" includes any employee or contractor of the Commission to the extent that such employee or contractor prepares, handles or distributes, or provides access to, any information pursuant to his employment or contract with the Commission.

ORNL-3164

Contract No. W-7405-eng-26

REACTOR CHEMISTRY DIVISION

EFFECTS OF FAST-NEUTRON IRRADIATION AND HIGH TEMPERATURE ON BERYLLIUM OXIDE

R. P. Shields
J. E. Lee, Jr.
W. E. Browning, Jr.

DATE ISSUED

MAR 19 1962

OAK RIDGE NATIONAL LABORATORY
Oak Ridge, Tennessee
operated by
UNION CARBIDE CORPORATION
for the
U.S. ATOMIC ENERGY COMMISSION

MARTIN MARIETTA ENERGY SYSTEMS LIBRARIES

3 4456 0364409 1

CONTENTS

ABSTRACT..... 1

INTRODUCTION..... 2

BERYLLIUM OXIDE IRRADIATION-CAPSULE DESIGN AND MEASUREMENT AND CONTROL OF IRRADIATION CONDITIONS..... 5
- Thermal Stress in BeO Specimens..... 6
- Design of Capsules..... 8
- Design of In-Pile Assembly..... 9
- Measurement of Temperature..... 13
- Control of Temperature..... 14
- Flux Monitoring..... 16
- Summary of Conditions of Irradiation..... 16

DESCRIPTION OF BeO MATERIAL USED IN TESTS..... 18
- High-Density BeO Bodies..... 18
- Low-Density BeO Bodies..... 19

EXAMINATION OF IRRADIATED BeO..... 20
- Physical Appearance of Irradiated BeO..... 20
- Changes in Physical Dimensions of Irradiated BeO Specimens..... 35
- Gas Analysis of Irradiated BeO..... 40
- Changes in Thermal Conductivity of BeO During Irradiation..... 43
- Changes in Crystal Structure of Irradiated BeO..... 44
- Electron Microscopy Studies of Irradiated BeO..... 48
- Metallographic Examination of Irradiated BeO..... 61

DISCUSSION OF RESULTS..... 70
- Effects of Thermal Stress..... 70
- Chemical Decomposition of Compounds..... 74
- Effects of Atomic Displacements..... 74
- Effects of Gas Generation..... 78

CONCLUSIONS..... 83
- Behavior of BeO Under Irradiation..... 83
- Implications for Reactor Design..... 85

ACKNOWLEDGMENTS..... 85

EFFECTS OF FAST-NEUTRON IRRADIATION AND HIGH TEMPERATURE ON BERYLLIUM OXIDE

R. P. Shields J. E. Lee, Jr. W. E. Browning, Jr.

ABSTRACT

Beryllium oxide bodies irradiated in the Engineering Test Reactor experienced changes ranging from negligible to major, including complete deterioration to a fine powder. The ranges of conditions were: 1.4×10^{20} to 2.8×10^{21} fast neutrons/cm^2 (>1 Mev), irradiation times of 2.03×10^5 to 5.60×10^6 sec, 110 to 1025°C, 0.428- to 1.18-in. specimen diameter, and gamma heat generation rates of 18 to 25 w/g.

The greatest damage appeared in bodies irradiated for high neutron doses at low temperatures. Greater doses could be tolerated at higher temperatures. Specimens irradiated at 110°C powdered at an accumulated dose of 1.5×10^{21} neutrons/cm^2. Specimens irradiated at 444°C at a dose of 1.1×10^{21} neutrons/cm^2 and at 737°C at a dose of 1.6×10^{21} neutrons/cm^2 remained intact. Specimens irradiated at 827 to 950°C at a dose of 2.1 to 2.6×10^{21} neutrons/cm^2 fractured.

Changes in linear dimensions up to 4% were observed. X-ray diffraction measurements revealed changes in the c lattice parameter up to 7×10^{-3} $\Delta c/c_0$ for material irradiated at 110°C but only 1 to 2×10^{-3} $\Delta c/c_0$ at 444 to 1025°C. The $\Delta c/c_0$ value appeared to saturate at a dose of 3×10^{20} neutrons/cm^2 in the latter temperature range. All temperatures above 444°C were equally effective in suppressing the $\Delta c/c_0$ values. Changes in the a parameter were smaller by a factor of 7.

Helium was retained even at irradiation temperatures of 1025°C. Gases could be removed only by dissolving the BeO in fused salt. The helium content of the BeO varied linearly with fast-neutron dose up to 1.6×10^{21} neutrons/cm^2, with a slope of 205 standard μl per g of BeO per 10^{21} neutrons/cm^2. The tritium content of BeO irradiated at 110°C followed a (neutrons/cm^2)^2 curve up to 6.4 ppm at 2.1×10^{21} neutrons/cm^2. Specimens irradiated above 444°C contained much less tritium.

Voids 0.1 to 0.3 μ in diameter which were not in the original material were found by electron microscopy in the interior of grains and at grain boundaries. No evidence of chemical decomposition was observed.

Radial temperature differences during irradiation increased by 50 to 100%, indicating a decrease in thermal conductivity.

It was concluded that the observed changes could be caused either by gas generation or atomic displacements. The hypothesis that thermal stress alone produced failure was rejected.

The results of this series of experiments indicate that great caution must be exercised in designing BeO moderators for nuclear reactors. Under some conditions physical deterioration occurs to such a degree as to render the material unsuitable for use. For greatest life the moderator should be kept above 400°C, and probably 800 to 1000°C is more desirable.

The design of the irradiation assembly is described. Temperatures were controlled by varying the composition of a helium-argon mixture in an annulus. Sixty-three specimens were irradiated in six assemblies.

INTRODUCTION

Beryllium oxide is of interest as a moderator in reactors of advanced design because of its favorable physical and nuclear properties. These include its strength at elevated temperature, high thermal conductivity, low density with consequent low heating by gamma radiation, and its small cross section for thermal neutrons. The unresolved question of its stability under irradiation has caused its consideration in reactor design to be postponed until recent years. Proposed designs for aircraft nuclear propulsion reactors and for gas-cooled reactors have specified BeO as a moderator, and this recommendation has been based on somewhat limited studies of irradiation effects made by investigators from several countries.

During the past ten to fifteen years, irradiation studies have been made on a limited scale with small pieces of beryllium oxide and for radiation doses of 10^{19} neutrons/cm^2 or less. Among the first studies of this kind were those done in 1946 at Oak Ridge and Argonne National Laboratories as a part of a feasibility study led by Farrington Daniels. This

group reported minor changes in such parameters as structural strength, thermal conductivity, and modulus of elasticity.[1,2]

More recently, beryllium oxide irradiation studies have been done by the British at Harwell, who also have reported radiation-induced changes in thermal conductivity, production of free gases under irradiation, and changes in creep properties of BeO under reactor conditions.[3-7]

Laboratories at Saclay, France, have investigated the irradiation effects in conjunction with purification of BeO and fabrication of BeO bodies.[8-10] These laboratories also have reported changes in the parameters mentioned above and, in one case, reported the powdering of a BeO specimen which was irradiated in the MTR to 2×10^{20} fast neutrons/cm^2.

Similar, more extensive studies are being made in this country on beryllium oxide—uranium oxide compacts. These experiments have produced information on the ability of beryllium oxide to withstand reactor conditions. The BeO-UO_2 bodies of various and intricate shapes have been reported to have satisfactory stress characteristics and resistance to water-vapor corrosion for 1000 hr at about 2600°F. Another laboratory

---

[1] J. R. Gilbreath and O. C. Simpson, "The Effect of Reactor Irradiation on the Physical Properties of BeO," A/Conf.15/P/621, USA (1958).

[2] W. M. Manning, Argonne National Laboratory Chemistry Division Progress Report, December 1948, ANL-4204.

[3] R. C. McGill and J. A. G. Smith, The Thermal Conductivity of Irradiated and Unirradiated BeO, AERE-R-3019 (1959).

[4] T. K. Ghosh and F. J. P. Clarke, An Experiment Concerning the Presence of Free Gases in Irradiated Beryllia, AERE-R-2889.

[5] F. J. P. Clarke and J. Williams, The Stability of BeO Under Reactor Conditions, AERE-M/M-229 (1959).

[6] F. J. P. Clarke and G. Tappin, Physical Property Changes in BeO Due to Reactor Irradiation, AERE-R-3164 (1960).

[7] F. J. P. Clarke, "Recent Results on Irradiation of Ceramic Materials," AIC-P-19.

[8] J. Elston, C. GeWiss, and C. Labbe, Compt. rend. 249, 1635–37 (1959).

[9] J. Elston and R. Caillat, A/Conf.15/P/1159 (1958).

[10] H. Frisbie, A. Bisson, and R. Caillat, J. Nuclear Materials 1, 106–8 (1959).

reports satisfactory retention of fuel by the BeO-UO_2.[1,11-13] Although radiation doses in BeO adjacent to UO_2 grains were very high, the BeO surrounding the UO_2 beyond the range of fission fragments generally received doses less than 10^{20} fast neutrons/cm^2.

A review of the effects of radiation on BeO appeared in a recent Russian article.[14]

Although the studies outlined above indicated that changes occur in the physical properties of the BeO when it is subjected to reactor conditions, its reactor life was considered favorable for use as a moderator in some aircraft reactor designs and in certain advanced-design gas-cooled reactors.

These proposed uses made it necessary to assess the thermal stress resistance in reactors of larger pieces than had been previously tested and at larger radiation doses. Since it is not practical to produce thermal stresses of the desired magnitude by internal heating except in a nuclear reactor, a series of in-pile experiments was designed to obtain information about the resistance of BeO to thermal stress. The experiments were irradiated in the Engineering Test Reactor (ETR) because its high power provided gamma heating of about 25 w/g, which would produce the large temperature gradients necessary to effect the desired thermal stresses. With the availability of a fast flux of 3 to 5×10^{14} neutrons cm^{-2} sec^{-1}, a high neutron dose could be acquired in a relatively short time. Experimental equipment was developed for irradiation in these gamma and neutron fluxes of the ETR, and six assemblies containing 63 specimens were irradiated under several temperature and radiation dose conditions.

---

[11] E. R. Dytko, Fueled BeO for Nuclear Reactors, CNLM-3160 (Nov. 25, 1960).

[12] A. J. Rothmer, BeO and BeO-UO_2 Work at Livermore Laboratory, UCRL-6231-T (Dec. 1, 1960).

[13] D. E. Johnson and Martin Tobin, Irradiation of BeO-UO_2 Fuel Pellets, GA-1845.

[14] P. P. Budnikov and R. A. Belyayef, Zhur. Priklad. Khim. 33, 1921 (1960).

Material for these tests originated from two sources: high-density specimens were cut from large hexagonal blocks of BeO which were produced for the Aircraft Reactor Experiment (ARE) by hot pressing, and low-density specimens were produced by isostatic pressing and firing to about 1500°C. Cylinders of BeO 1 in. long with nominal diameters of 0.4, 0.6, and 0.8 in., and 3 in. long with a diameter of 1.18 in., were irradiated for doses up to 2.5×10^{21} nvt (>1 Mev) at temperatures over a range of 120 to 1025°C. The highest dose was received by the low-density material, and extensive damage, ranging from cracking to powdering, was observed in this material. A crack was observed in only one capsule of the high-density material which was irradiated to 4.5×10^{20} nvt.

In addition to information on the resistance of BeO to thermal stresses acquired during this series of tests, extensive data on highly irradiated BeO were obtained by x-ray analysis, electron microscopy, analysis for neutron-generated gases, and metallurgical and petrographic analyses. Observations were made on dimensional changes and apparent changes in thermal conductivity. Such information will assist in identifying the mechanisms by which irradiation causes the observed changes. These tests, however, are limited in scope, and a more extensive series of irradiations, wherein exact physical-property measurements are made on specimens both before and after irradiation, is needed to determine adequately the way in which nuclear radiation damages BeO, so that predictions regarding its behavior and life in a reactor can be made.

This preliminary report is issued to make the results of the first five BeO irradiation experiments available as promptly as possible. A later report will be issued containing information from the sixth experiment, the results from additional measurements on the first five experiments, and additional analysis and interpretation of these results.

BERYLLIUM OXIDE IRRADIATION-CAPSULE DESIGN AND MEASUREMENT AND CONTROL OF IRRADIATION CONDITIONS

The BeO specimens in this series were irradiated in the H-10 position in the core of the ETR in equipment designed to provide the desired environment around the specimens and at the same time measure and control

their temperature. In-pile absorption of gamma radiation provides internal heat generation with the resultant desired thermal stresses and also provides heat by which the specimens are brought up to the desired temperature. Temperatures were controlled by adjustment of the composition and consequently the thermal conductivity of the insulating gas in an annulus surrounding the capsules. A cylindrical configuration was selected as being compatible with the simplest possible experiment design while at the same time affording minimum complexity in stress-calculation models. Specimen diameters in these tests were 0.428, 0.636, 0.798, and 1.180 in., or nominally 400, 600, 800, and 1100 mils. Each specimen was 1 in. long, regardless of diameter, with the exception of the 1100-mil specimens, which were 3 in. long. A group of three 1-in.-long cylinders was usually encapsulated as a single unit to reduce end effects and to provide a more nearly uniform thermal environment for at least some of the material. A 12-specimen capsule was used for one test, however, and the 3-in.-long specimens were installed as single units.

Thermal Stress in BeO Specimens

Stress calculations for proposed specimens at temperatures of interest were performed as a part of the engineering design of the BeO irradiation assembly. It was desired to produce stresses over such a range that some specimens would fail and others would survive, thus defining the maximum calculated thermal stress which could be tolerated in reactor designs. In an infinitely long, solid cylinder with internal heat generation, the maximum tensile stress appears at the surface and has the value

$$\sigma = \frac{\alpha E}{1 - \gamma} \frac{qb^2}{8K} .$$

The circumferential and longitudinal stresses are equal. The symbols have the following meanings, and values for BeO are listed:[15]

α = linear thermal expansion coefficient, $5.86 \times 10^{-6}/°F$ (25 to 900°C),

E = modulus of elasticity, 38×10^6 psi (900°C),

[15] Nuclear Engineering Handbook, pp 9–13, Table I, and pp 10–53, Table 44, McGraw-Hill, New York, 1958.

γ = Poisson's ratio, 0.34,

q = internal heat generation (based on a gamma heat intensity of 25 w/g and a BeO density of 2.9 g/cm^3), 4060 Btu hr^{-1} in.$^{-3}$,

b = specimen diameter, 0.428 to 1.18 in.,

K = thermal conductivity, 1.31 Btu hr^{-1} in.$^{-1}$ (°F)$^{-1}$ (900°C).

At the ends of a cylinder of finite length the maximum tensile stress is a combination of circumferential, longitudinal, and shear stresses and is about 1.25 times the stress calculated with the expression above.[16] Table 1 gives the calculated maximum stresses for 25 w/g gamma heat in cylinders of BeO at 900°C, for the diameters used in this series of experiments. These stresses should be compared with the tensile strength of BeO at 900°C, which is given in Fig. 1 as 12,000 psi. The tensile strength of BeO depends upon fabrication history, of course, and probably varies over a considerable range.[15] Calculations for other temperatures yield very similar results.

Table 1. Calculated Maximum Thermal Stresses in BeO Cylinders for 25 w/g Gamma Heat at 900°C

Diameter (in.)	Maximum Tensile Stress (psi)	Capsules Using Specimens of Listed Diameter
0.428	7,600	3-1
0.636	16,780	1, 2-1, 2-3, 3-3
0.800	26,560	3-5, 3-7, 4, 5-1 to 5-7
1.180	57,700	6

These calculations indicate that specimens 0.636 in. or greater in diameter would experience thermal stresses greater than the tensile strength of BeO and would be expected to fail.

The values of the physical properties used are not believed to be sufficiently accurate to permit a reliable prediction as to the survival

[16] R. J. Roark, Formulas for Stress and Strain, Part B-15, p 337, McGraw-Hill, New York, 1954.

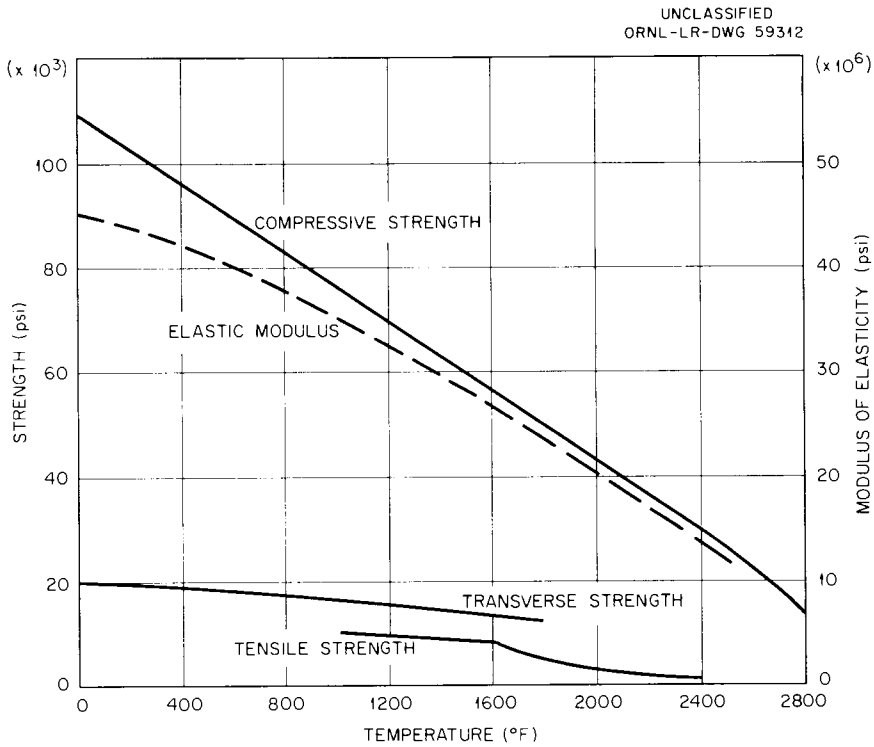

Fig. 1. Mechanical Strength Properties of BeO.

of the BeO. Also, these stress calculations do not take into consideration the effects of stress relaxation which may be important at higher temperatures. Accordingly, a wide range of specimen diameters and gamma heat intensities was selected.

Design of Capsules

An encapsulation material which does not restrict the expansion of BeO was chosen so that the stresses in the test material would be equivalent to the thermal stresses in an unclad cylinder. Stainless steel type 430, with a mean coefficient of thermal expansion of 5.6×10^{-6} in. in.$^{-1}$ (°F)$^{-1}$ at 68 to 1500°F, serves this purpose as can be seen by comparison with the value for BeO given in Fig. 2.

Beryllium oxide specimens were lightly press-fit into their capsules to ensure minimum eccentricity. Type 347 stainless steel was used for the water-cooled capsules because of its superior resistance to corrosion, its higher coefficient of thermal expansion being of no importance at low temperature. A wall thickness of 0.035 in. was specified

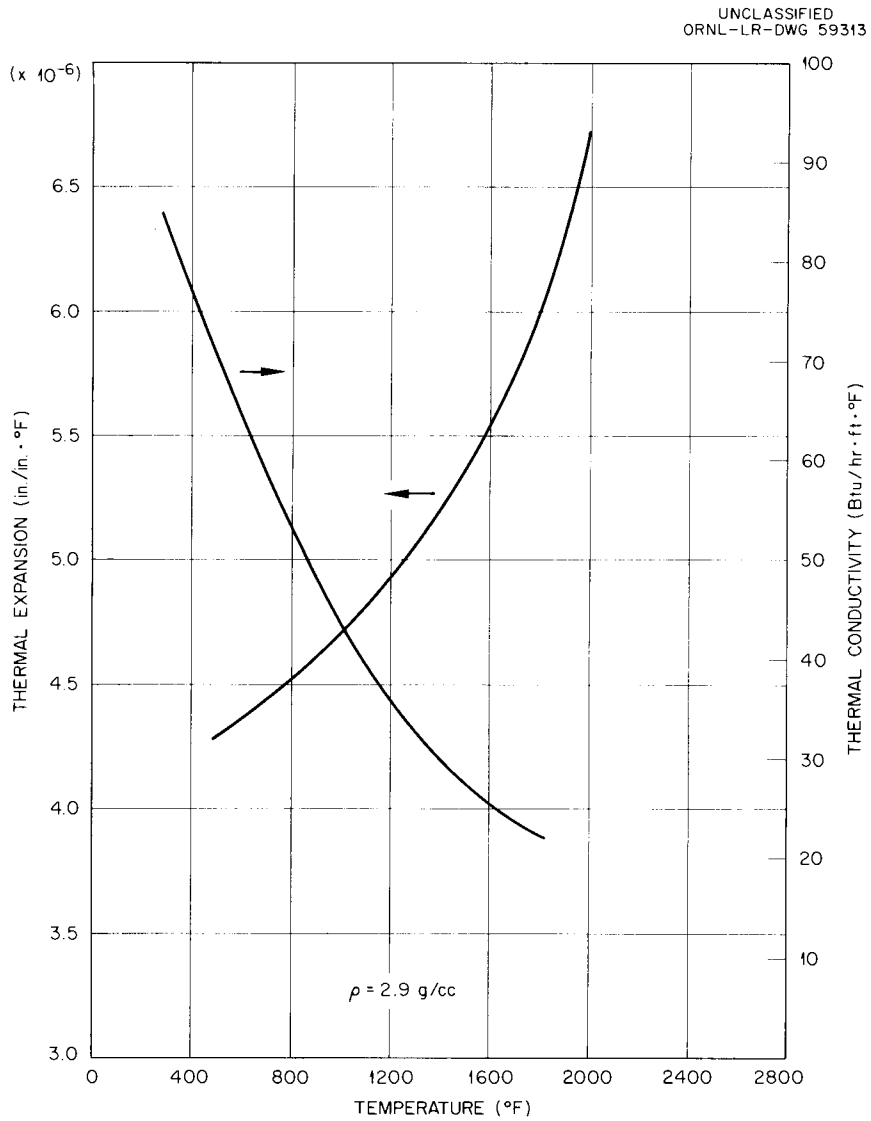

Fig. 2. Mechanical Strength Properties of BeO.

as adequate for strength at anticipated temperature without excessive contribution to extraneous gamma heat generation. The burst strength of an 800-mil-diam cylinder of 35-mil wall thickness is about 7000 psi at 100°C.

Design of In-Pile Assembly

The problem of installing a capsule is concerned primarily with three objectives. They are: (1) achieve and maintain concentricity of

the cylindrical capsules in a coolant or thermal barrier annulus of proper thickness, (2) accommodate thermal expansion of the capsule without impairing the concentricity of its position, and (3) provide thermocouples to monitor temperature and thermal gradient in the BeO. These objectives were satisfactorily attained by the unique design of in-pile hardware described in the following paragraphs. This design operated satisfactorily for the first experiment and was used for the entire test series.

An extension of the cladding cylinder is provided at both ends of each capsule. An inverted end cap is fusion-welded to the cylinder extension, which effects a seal of the capsule end and provides an inside bearing sleeve. A concentric centering ring is installed inside the bearing sleeve and serves as the positioning mount for each end of the capsule. This internal ring is flanged radially to the walls of the primary containment cylinder for its support and is perforated to allow longitudinal passage of the thermal-barrier gas to adjacent hardware. A schematic diagram of this capsule mount is shown in Fig. 3. Longitudinal thermal expansion is accommodated entirely at the upper mount by a reduction of the interference tolerance of the bearing at that end. In

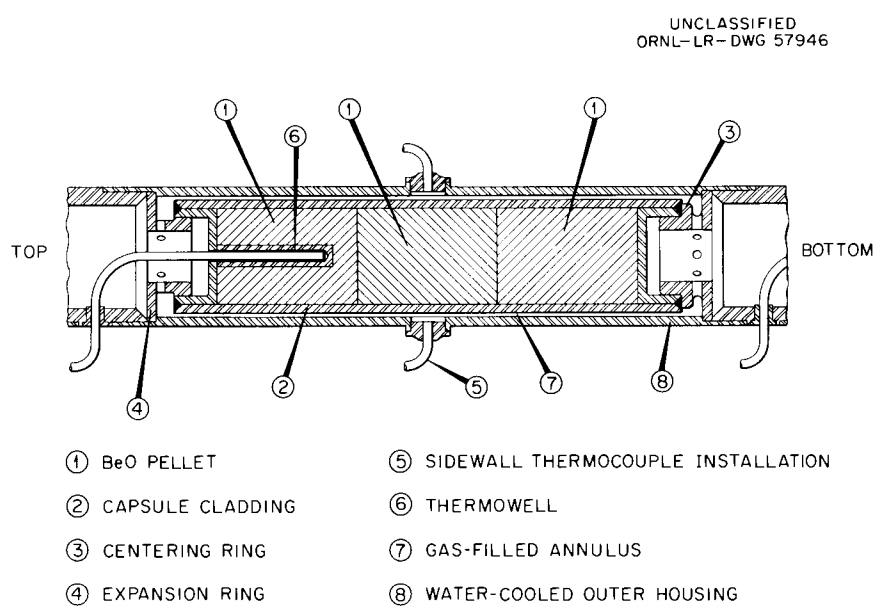

Fig. 3. BeO Irradiation Capsule.

contrast, the lower end is assembled by a cold shrink fit of the internal member to ensure permanent attachment at this point. Referring to Fig. 3, it may be seen that, as the capsule, insulated in its gas annulus, heats and expands, the upper bearing flange will leave its mount and become free to extend itself as needed. The internal ring receives radiant heat from the capsule flange which it can dissipate only on a limited basis; consequently it approaches the higher temperature of the flange, thereby maintaining the dimensional symmetry thermostatically.

Beryllia temperatures of 600 to 1000°C were to be of primary interest for the irradiation. In order to achieve these temperatures it was necessary to install the capsules in a gas-annulus thermal-barrier type of mount for the required insulation from reactor coolant water and to provide for temperature control through variation in annulus-gas composition. An annular space surrounding a capsule is provided by a cylindrical sleeve which extends the length of the capsule and terminates in a transition ring. This transition piece is also the support for the capsule-centering mounts and serves to align both the annulus and capsule. It also becomes the coupling unit for joining several capsules in an end-to-end assembly and provides a site for the exit of certain thermocouples. Details of this annulus as used for a thermal barrier and the route of the gas mixture with which it is filled are also shown in Fig. 3. A combination of six capsules, typical of most experiments, may be seen in Fig. 4. The transition sections connect the several capsules, and a conical end unit completes the group.

Reactor cooling water is used to dissipate the heat transferred through the annulus gas to the primary jacket wall. The primary jacket wall is cooled by water flowing at high velocity through an annulus formed by an aluminum sleeve surrounding the annulus wall. This sleeve is held off by pins to maintain an annulus dimension which will provide the necessary water film coefficient. The aluminum sleeve is also channeled along its exterior to provide a passageway for thermocouple lines and the annulus gas exhaust tube. Internal spacer spools support the capsule assembly in proper vertical orientation to the reactor-core midplane. A final casing of stainless steel tubing encloses the components described above. An annular plug forms the lower closure and

UNCLASSIFIED
ORNL-LR-DWG 57947

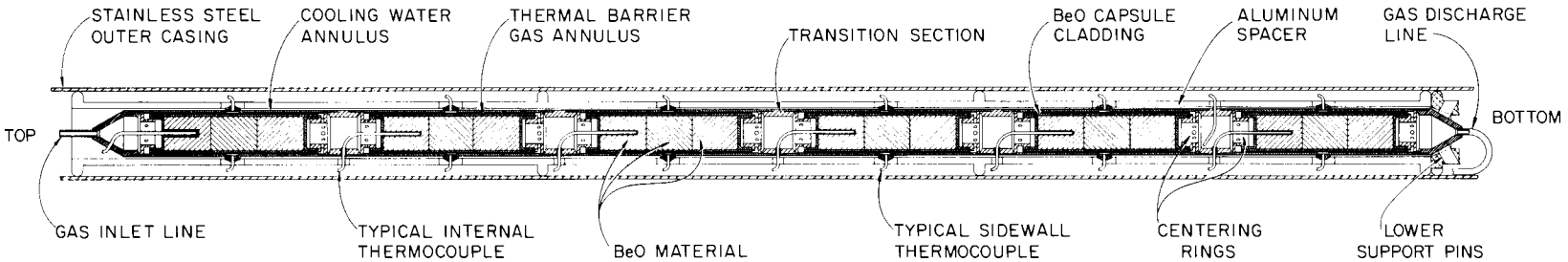

Fig. 4. Typical 6-Capsule BeO Moderator Irradiation Assembly.

water discharge, while the casing is supported from the top by a length of stainless steel pipe doubling as the thermocouple wire conduit and coolant-water inlet. The casing section stands in a fuel element filler piece which is counter-bored to accept the experiment and is externally dimensioned to be compatible with water-channel tolerances for adjacent fuel elements in the reactor.

Measurement of Temperature

A major problem in monitoring temperatures of these experiments was installation of thermocouples on the wall of a capsule mounted in a small gas annulus. Gas-annulus radii at operating temperatures were in many cases equivalent to the diameter of a single thermocouple wire, making it extremely difficult to provide temperature measurements at the capsule walls. A method of attachment was developed in which the wires were installed through radial ports, 1/4 in. in diameter, spaced 180° apart at a position halfway between the capsule ends. Bench-test experiments with electrical-resistance-heated capsule wall mockups showed that an opening of this size did not cause appreciable hot spots in the general area of the side ports and that 10-mil thermocouple wires could be spot-welded to the capsule wall with as limited an access as this. Stainless-steel-sheathed thermocouple wire was used, with the sheath removed to expose the element wires at a point just inside the access-port sealing plug. The wires were formed into a flat helix and welded individually to the capsule wall. Figures 3 and 4 show the details of the thermocouple installation. The access port and thermocouple sheath are both joined leak-tight when the plug is brazed into place. The turns in the exposed wire provide the necessary flexibility as the capsule wall moves past the port during thermal expansion.

The internal temperature of the encapsulated BeO was measured in a more conventional manner by the use of sheathed thermocouples with the element wires fusion-welded to the tip of the sheath. This type of couple was then inserted in an axial thermowell at one end of a capsule. The first pellet inside the capsule was core-drilled to a depth of 0.75 in., corresponding to a one-quarter penetration along the capsule axis.

The other two specimens were not exposed to possible effects of the axial hole and of the thermocouple. The temperature measured by the thermocouple inserted to the bottom of this well was assumed to sample the peak center temperature of the BeO. Heat transfer calculations showed that the temperature rise in the thermocouple assembly produced by gamma heating would be negligible.

The radial thermal gradient across the BeO specimen during irradiation was indicated by the difference in the readings of the axial and sidewall thermocouples. Drift or fluctuation in the thermal gradient was taken as evidence of the anticipated changes in thermal conductivity.

In order to utilize the superior mechanical stability of fused sheath-type thermocouples for measuring the thermal gradient in the BeO specimens, one experiment (No. 6) was fitted with two thermowells in each specimen. An axial well was used for the central couple, and a second thermowell nearly parallel to the first was drilled to a point just below the surface of the pellet, halfway between the ends of the cylinder. The larger diameter, 1.180 in., and longer length, 3 in., of the BeO specimens made this type of thermal-gradient monitoring possible. The distance between thermocouples rather than the radius of the specimen must be used in evaluating thermal gradients. An x-ray photograph is used to determine the location of the thermocouple junctions with respect to the dimension of the BeO body. This type of thermocouple installation is much simpler to assemble and provides a temperature monitoring system with greater longevity.

Control of Temperature

The use of a gas-annulus thermal barrier for insulation of capsules to be irradiated at high temperatures in a water-cooled reactor permits temperature control by varying the thermal conductivity of the annulus gas. This method of regulation was employed in all the BeO experiments to control capsule temperatures by automatically regulated dilution of argon with helium. In practice all of the gas annuli are connected in series and supplied with a continuous flow of argon. When the reactor is at sufficient power to generate temperatures in excess of the set

point, a monitoring thermocouple actuates a Brown recorder–Moore controller combination to meter helium into the argon supply. The higher thermal conductivity of the helium effectively increases the heat transfer across the annulus, causing the temperature to be restored to the control point. It was necessary to specify the annulus dimension carefully, considering the heat generation of the capsules, so that the required thermal conductivity would be that of a reasonable gas mixture. Heat transfer calculations performed for these experiments, although based on extrapolated values for high-temperature thermal conductivity of BeO and gas mixture and on imprecise gamma-heating rates, proved to be well within the range of control flexibility. The effectiveness of the control system can be seen in Fig. 5, which shows the center temperatures of the various capsules in experiment 5. Note the range over which temperature could be controlled at 50 Mw reactor power by varying gas composition. The hottest capsule, No. 4, could be adjusted from 300°C with pure helium to 790°C with pure argon.

There are some practical considerations which should be listed here. Response time of the control system is entirely compatible with the rate of change in gamma heating for a normal reactor power excursion when the control gas diluent is fed to the experiment at the closest

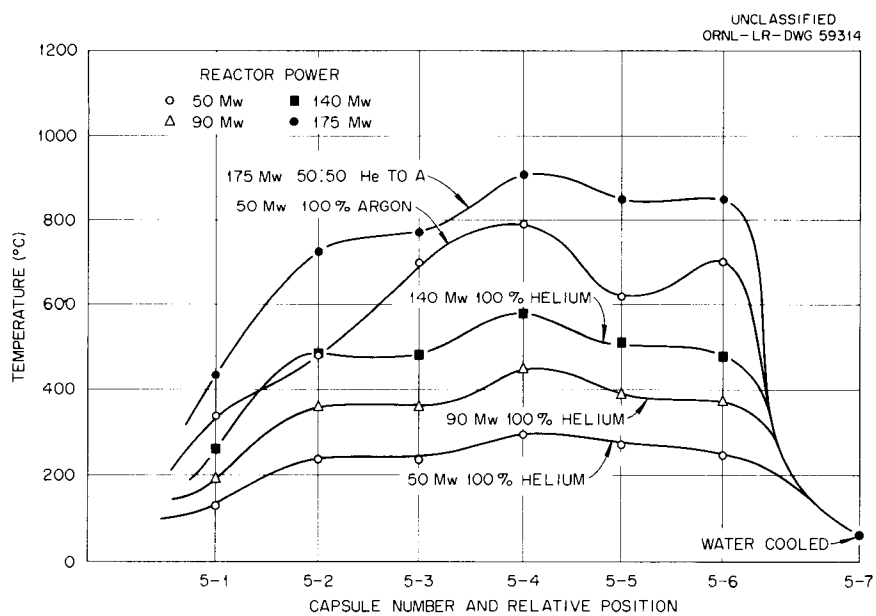

Fig. 5. Effectiveness of Temperature Control by Gas Composition.

possible point. This was determined in a thermal mockup of the control system and worked well in practice when the mixing point was about 48 in. from the first capsule, at flow rates of about 10 to 50 std cc/sec, through a 0.125-in.-ID supply line. It proved expedient to provide a supply of helium in addition to the controlled supply at a small, constant, but manually adjustable flow rate to prevent response delay or overshoot caused by back-diffusion of argon into the helium supply line. This provision has the additional advantage of improved safety in that it limits the extent of accidental high-temperature excursion caused by malfunction of the automatic metering of control helium. Completely manual operation of the low-conductivity gas supply, argon, prevents a similar sort of incident due to runaway condition of the argon metering system if it too were supplied on a temperature-dependent basis.

Flux Monitoring

Since the purpose of this series of experiments is to determine the behavior of BeO exposed to nuclear radiation, measurement of the intensities of the various kinds of nuclear radiations is necessary. The important kinds of radiation in the ETR are thermal neutrons, fast neutrons, and gamma radiation. Their intensities were measured by radioassay of components of the in-pile assembly.

Thermal neutron flux was determined by measuring the Co^{60} induced in cobalt in the Inconel thermocouple sheath. Fast neutron flux was determined by measurement of Mn^{54} induced in the stainless steel capsule wall. The results were validated by comparison with those obtained from U^{238}, Np^{237}, and Ni specimens included in some of the experiments.

The gamma heat intensity was determined by comparison of observed initial temperature profiles with those calculated. A value of 25 w/g was obtained for the position of maximum intensity.

Summary of Conditions of Irradiation

Predictable and controlled operation of the in-pile experiments has been possible with the system described above. The later experiments were operated without connections to the reactor safety circuits. There

were no high-temperature excursion events recorded for the series, although some of the early tests were terminated prematurely because a sufficiently large number of thermocouple failures had caused undesirable omissions in the temperature history records.

Table 2 is a summary of the conditions of irradiation for the various capsules.

Table 2. Summary of Irradiation Conditions

Capsule Number	Irradiation Time (sec)	Fast Flux (> 1 Mev)	Integrated Fast Flux (neutrons/cm^2)	Center Temperature (°C)	Observed ΔT (°C)
		$\times 10^{14}$			
1-1	2.029×10^5	6.90	1.4×10^{20}	722	47
2-1	8.803×10^5	1.25	1.1×10^{20}	219	
2-2	8.803×10^6	2.09	2.3×10^{20}	388	
2-3	8.803×10^6	3.18	3.5×10^{20}	500	
3-1	1.101×10^6	1.00	1.1×10^{20}	458	
3-3	1.101×10^6	2.82	3.1×10^{20}	858	
3-5	1.101×10^6	4.09	4.5×10^{20}	1025	167
3-7	1.101×10^6	4.00	4.4×10^{20}	120	20
4-11	5.600×10^6	3.21	1.8×10^{21}	110	
4-14	5.600×10^6	4.11	2.3×10^{21}	120	
4-17	5.600×10^6	4.82	2.7×10^{21}	120	
4-110	5.600×10^6	5.00	2.8×10^{21}	110	
4-19	5.600×10^6	5.00	2.8×10^{21}	120	
5-1	4.953×10^6	2.22	1.1×10^{21}	444	
5-2	4.953×10^6	3.23	1.6×10^{21}	737	
5-3	4.953×10^6	4.24	2.1×10^{21}	827	35
5-4	4.953×10^6	5.25	2.6×10^{21}	900	130
5-5	4.953×10^6	4.64	2.3×10^{21}	944	60
5-6	4.953×10^6	4.24	2.1×10^{21}	950	107
5-7	4.953×10^6	3.03	1.5×10^{21}	110	20

DESCRIPTION OF BeO MATERIAL USED IN TESTS

Two kinds of BeO material have been tested in this series of experiments. One material was selected on the basis of its immediate availability for the first three experiments. The other material was selected to test a fabrication method which was being developed.

High-Density BeO Bodies

The high-density BeO used in the first three experiments was cut from blocks of hot-pressed material with a density of approximately 2.9 g/cm^3 which had been fabricated for the Aircraft Reactor Experiment at ORNL. As seen in Fig. 6, this material has a gray color and discolorations which appear to be carbon from the mold. These specimens were very hard and could not be notched with a file. The following results were obtained by spectrographic analysis: Si, 0.6%; Ca, < 0.08%; Fe, 0.1%; Ni, < 0.08%; and Pb, Cu, Cr, and Al, < 0.05%. These values are approximate, within a factor of 2.

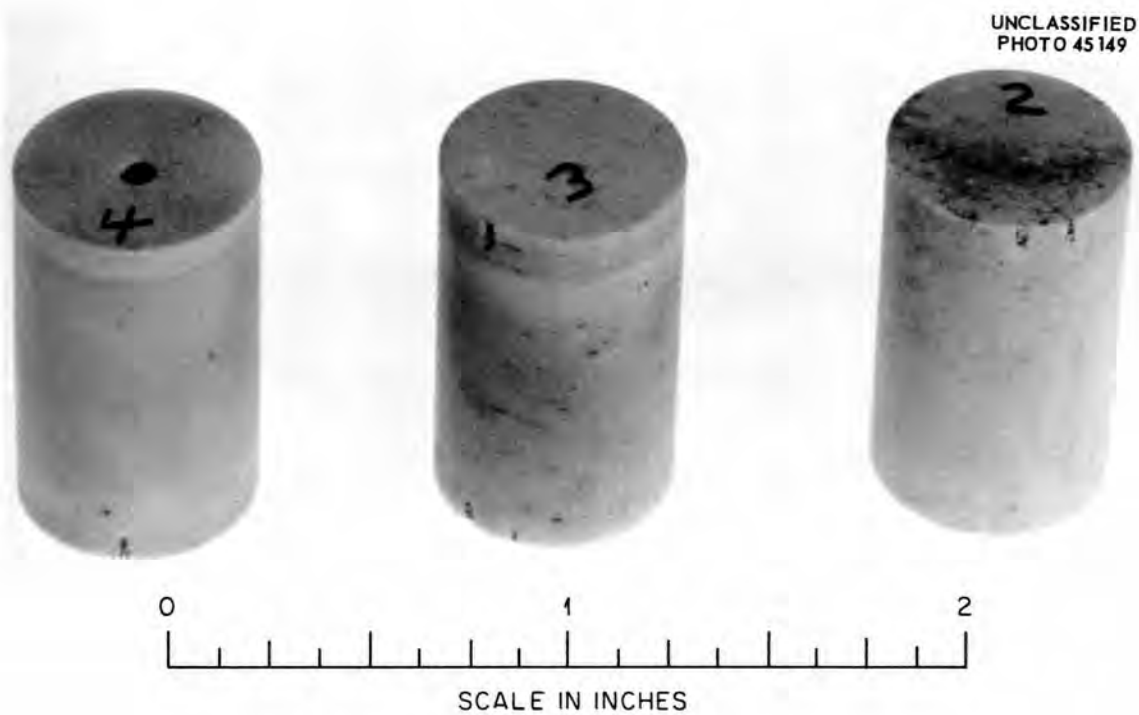

Fig. 6. Specimens of High-Density BeO.

Photomicrographs of this material indicate that the grain size is about 20 μ and that the grains have well-defined boundaries. The photographs show areas where whole grains had pulled out during polishing and also reveal that three or four voids are present in each grain, on the average. These voids represent less than 1% of the area of the grain.

Low-Density BeO Bodies

Beryllia for experiments 4, 5, and 6 had a density of 2.65 to 2.70 g/cm^3 and was prepared in the Ceramics Laboratory of the Metallurgy Division from UOX grade BeO powder from the Brush Beryllium Company. The fabrication procedure for producing these specimens is as follows. Powders were prepressed isostatically in a rubber bag, and the resultant hard mass was broken down in a chromium-plated mix muller, then granulated by passing through a coarse screen (~35 mesh). The granules of BeO powder were loaded into rubber molds and pressed isostatically in the form of a rough cylindrical slug. The slugs were sintered at about 1500°C in a carbon tube induction furnace using a nitrogen atmosphere. They were ground with a diamond wheel to dimensions specified and were cleaned and normalized (annealed) by firing in an oxidizing atmosphere. Figure 7 shows the finished specimens of this type.

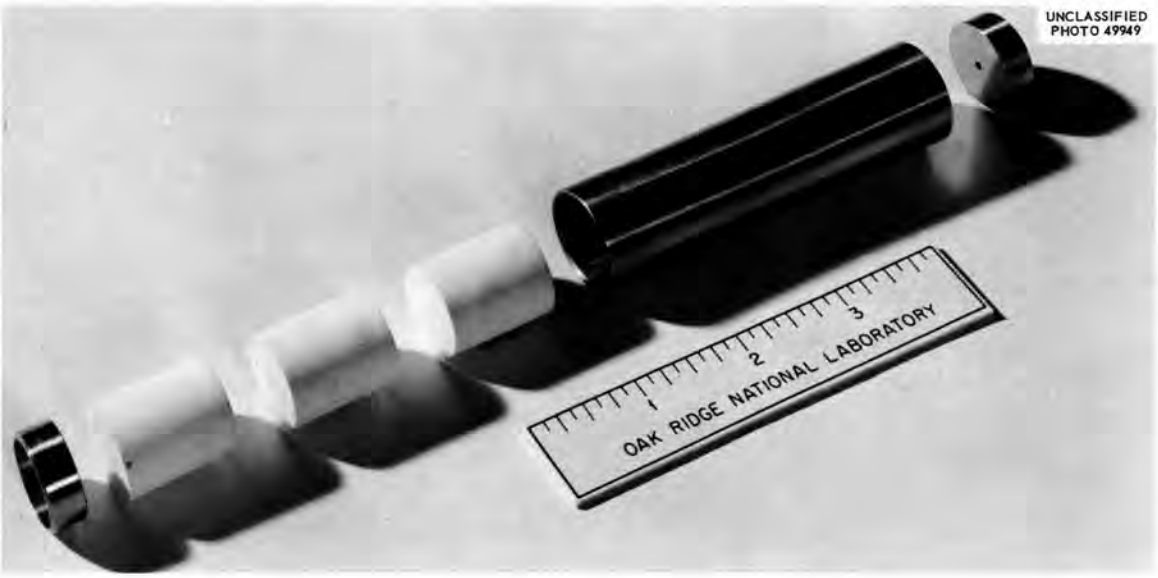

Fig. 7. Low-Density BeO Unirradiated.

Spectrographic analysis of the low-density material showed the following impurities, in parts per million: Al, 100; Ca, 50; Cr, 20; Fe, 20; K, 100; Mg, < 70; Mn, < 20; Mo, < 50; Ni, < 20; and Si, 110.

Photomicrographs of the isostatically pressed material revealed a poor grain pattern. There was much pullout of grains during the polishing operation. The best approximation of grain size is 2 μ. Table 3 shows which of the two types of material was used in each experiment.

Table 3. Type of BeO Used in the Various Experiments

Experiment Number	Type of Material	Number of Specimens	Nominal Dimensions (in.)	
			Diameter	Length
ORNL-41-1	Hot pressed	3	0.636	1.000
2	Hot pressed	9	0.636	1.000
3	Hot pressed	3	0.428	1.000
		3	0.636	1.000
		6	0.800	1.000
4	Isostatically pressed	12	0.800	1.000
5	Isostatically pressed	21	0.800	1.000
6	Isostatically pressed	6	1.180	3.000

EXAMINATION OF IRRADIATED BeO

Physical Appearance of Irradiated BeO

The following descriptions of the capsules of the first five experiments represent information obtained by observation in the BMI hot cells by ORNL personnel and from reports of observations made by the BMI hot-cell personnel. Additional information regarding the condition of the irradiated BeO was obtained while sampling the specimens for the various analyses. Photographs have been selected to give a representative picture from each capsule.

A code has been used to identify the various specimens. The number of the experiment is used for the first number, and in the two-digit number which follows, the first digit represents the number of the capsule and the second digit identifies the specimen within the sample. Capsules and specimens are both numbered from top to bottom, relative to the position of the experiment when it was in the reactor lattice. As an example, 5-53 designates the third specimen of the fifth capsule in experiment five. Figure 8 is a graphic display of the first five experiments and some of the pertinent information about them.

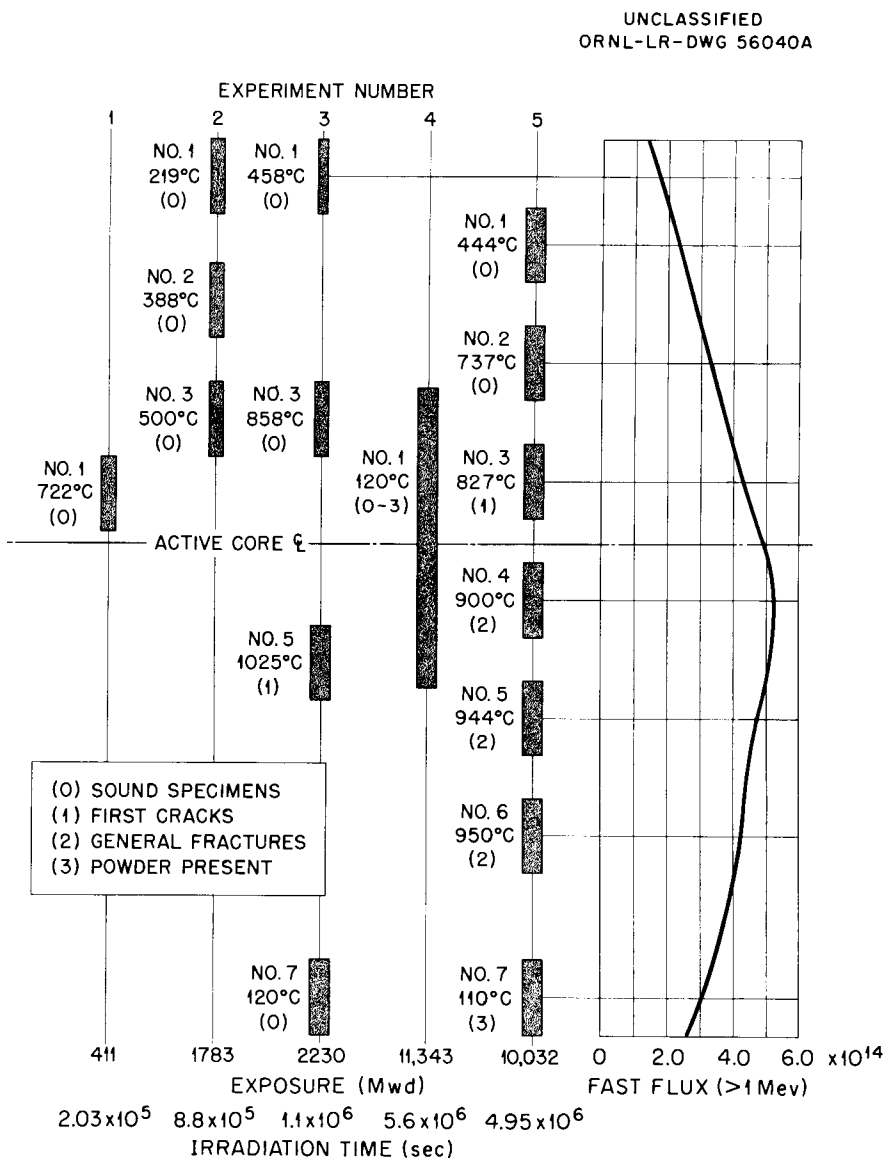

Fig. 8. BeO Irradiation Conditions.

Descriptions of individual specimens are given below. The integrated fast (> 1 Mev) neutron dose in neutrons/cm^2 and the irradiation temperature are given in parentheses following each capsule number. Positions 3-2, 3-4, 3-6, and 3-8 were occupied by a material other than BeO. Experiment 6 was irradiated but had not been examined at the time of this report.

1-1 (1.4×10^{20}, 722°C). – As shown in Fig. 9, none of the specimens showed any change.

2-1 (1.1×10^{20}, 219°C). – No change in physical condition is noticeable. Figure 10 shows the pellets of capsule 1 viewed from one end.

2-2. – This capsule was lost in the hot cells.

2-3 (3.5×10^{20}, 500°C). – The specimens had about the same general appearance as before irradiation (Fig. 11). No chipping or cracks are visible.

3-1 (1.1×10^{20}, 458°C). – Figure 12 is a display of the specimens of this capsule. The rough area on the bottom specimen is epoxy resin. On the side of two of the cylinders a flake of BeO has been broken by the cutting operation. Figure 13 is a closeup of specimen 3-13 showing this breaking and indicating the brittleness.

3-3 (3.1×10^{20}, 858°C). – The top surface of specimen 3-31 showed some discolored areas near the edges, and the BeO in these areas was flaky and could be peeled off by slight abrasion. These specimens are shown in Fig. 14. A piece was broken from specimen 3-33 rather easily with vise-grip pliers. A small piece was crushed in a mortar and broke easily into grains, all of which passed through a 100-mesh screen.

3-5 (4.5×10^{20}, 1025°C). – All three specimens in this capsule showed cracks but did not break into pieces. Figure 15 shows the general appearance of the BeO in this capsule. The center specimen, 3-52, has what appears to be a crack running diametrically across the top. Figure 16 shows the sides of this specimen. The longitudinal crack along one side is a continuation of the crack across the end face. The cylinder did not break apart when removed from the capsule. Specimen 3-53 seems to be cracked across the top, but the longitudinal cracks do not extend very far down the sides (see Fig. 17).

3-7 (4.4×10^{20}, 120°C). – This capsule was irradiated at 120°C, and as seen in Fig. 18 the specimens are all intact except for chipping from the removal operation; they show no cracks. This material seems to be abnormal, as discussed below. Approximately half a

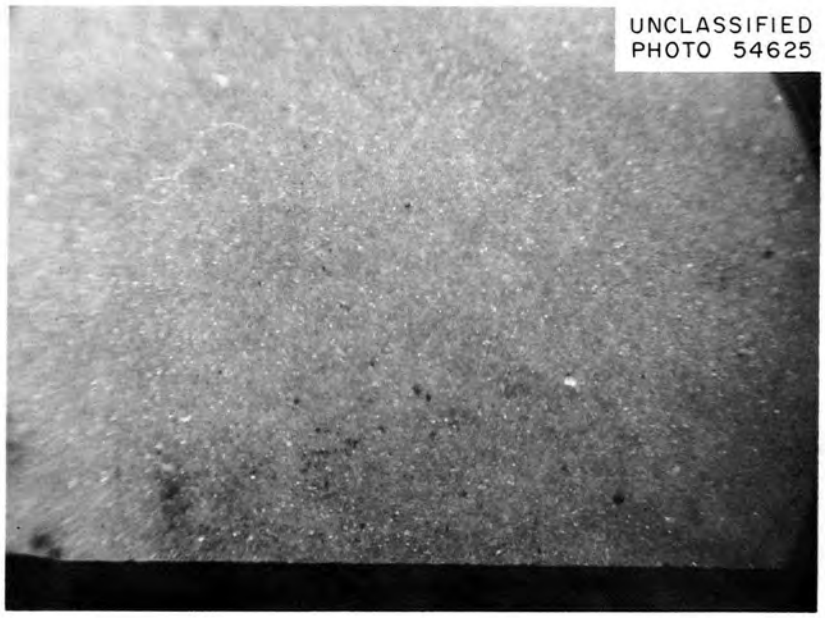

Fig. 9. BeO from Capsule 1-1; nvt = 1.4×10^{20}. Irradiated at 722°C. 10X.

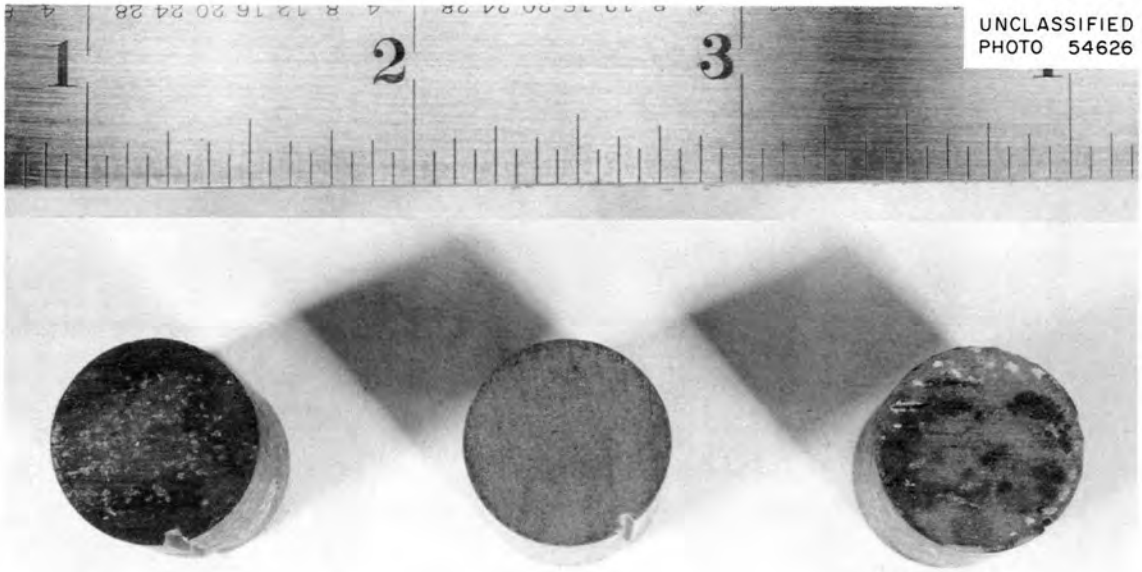

Fig. 10. BeO from Capsule 1, Experiment 2; nvt = 1.1×10^{20}. Irradiated at 219°C.

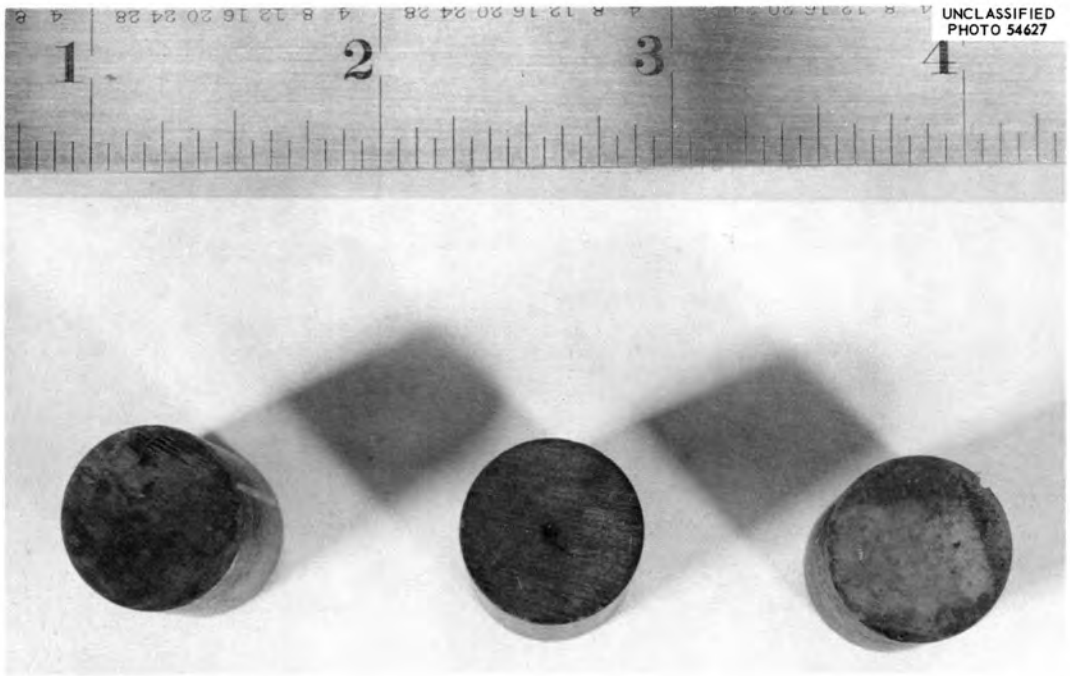

Fig. 11. BeO Pellets from Capsule 3, Experiment 2; nvt = 3.5×10^{20}. Irradiated at 500°C.

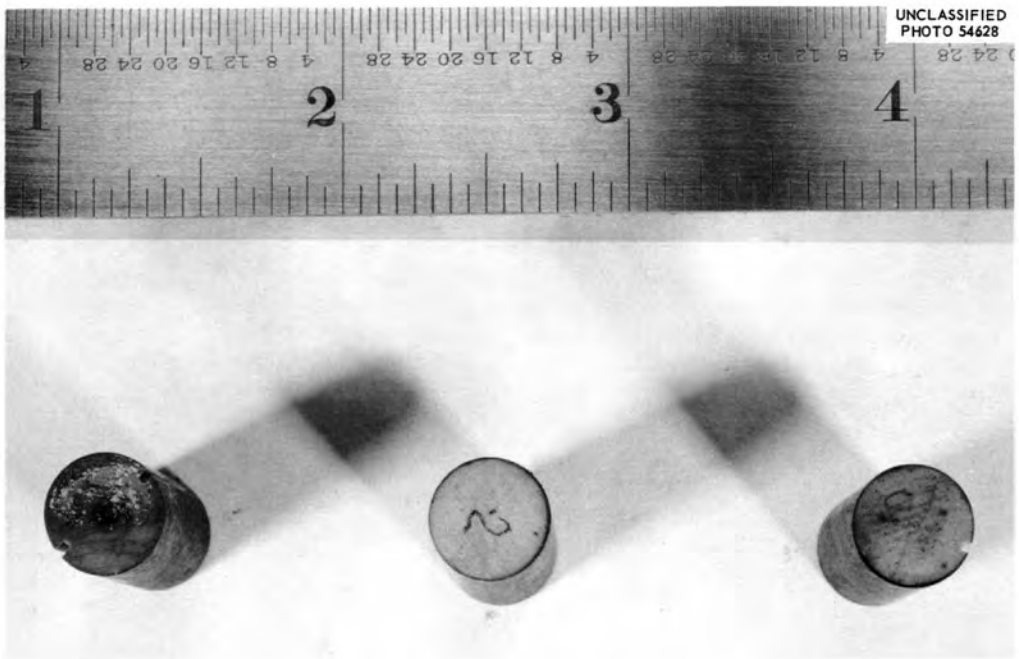

Fig. 12. BeO Pellets from Capsule 1, Experiment 3; nvt = 1.1×10^{20}. Irradiated at 458°C.

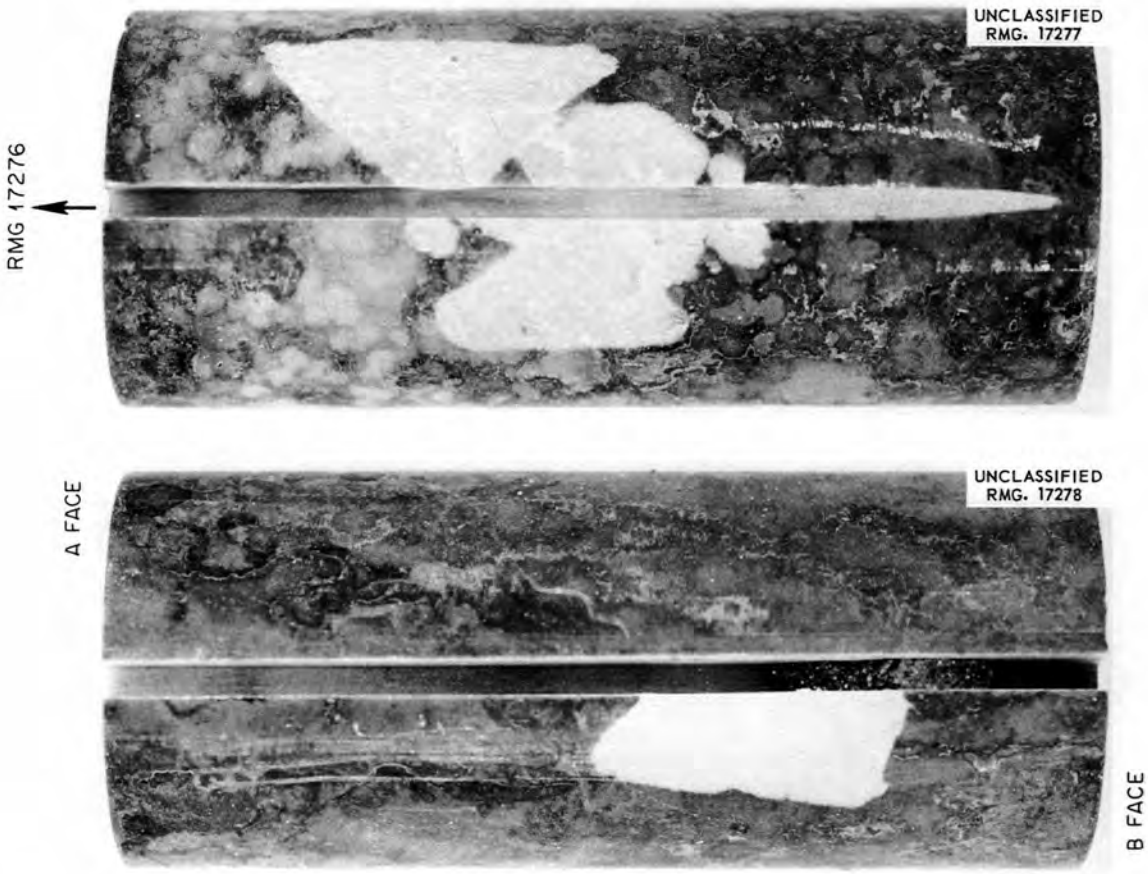

Fig. 13. Chipping (White Area) of BeO of Capsule 3-1 Caused by Sawing During Recovery Operations.

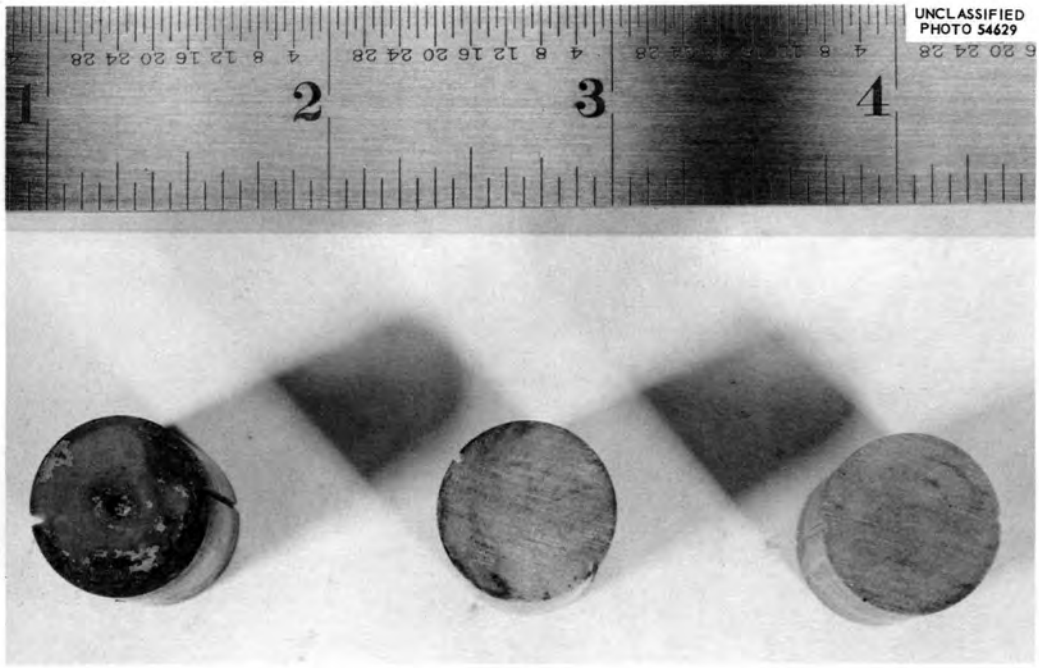

Fig. 14. BeO from Capsule 3, Experiment 3; nvt = 3.1×10^{20}. Irradiated at 858°C.

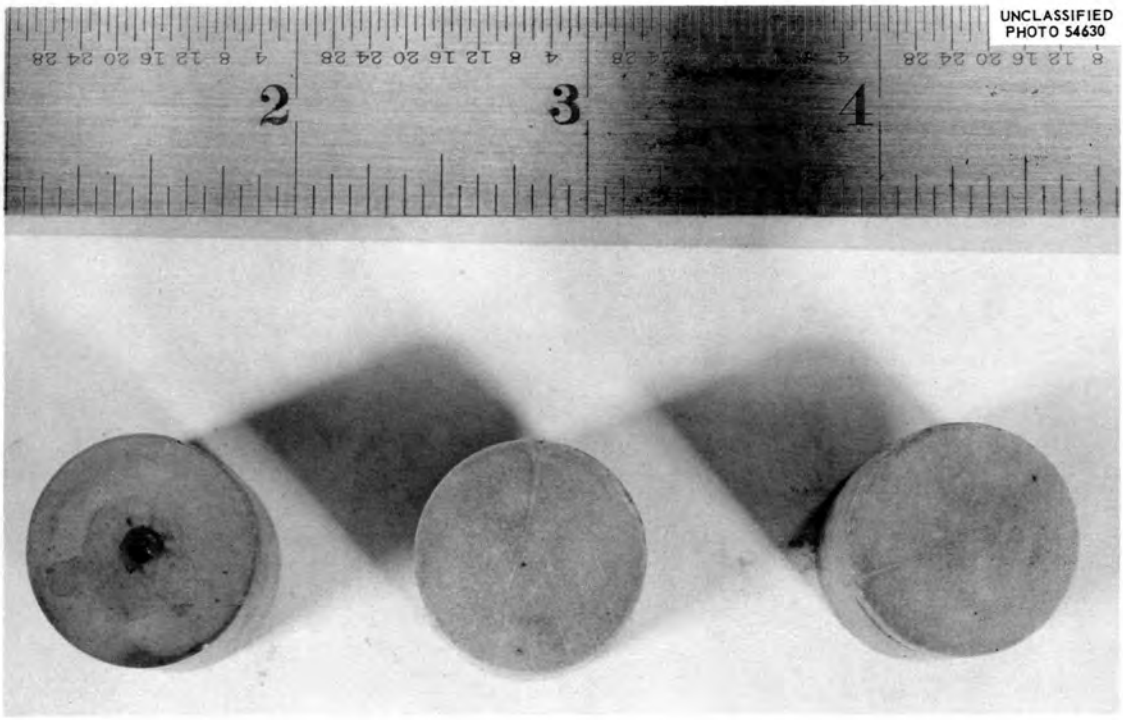

Fig. 15. BeO from Capsule 5, Experiment 3; nvt = 4.5×10^{20}. Irradiated at 1025°C.

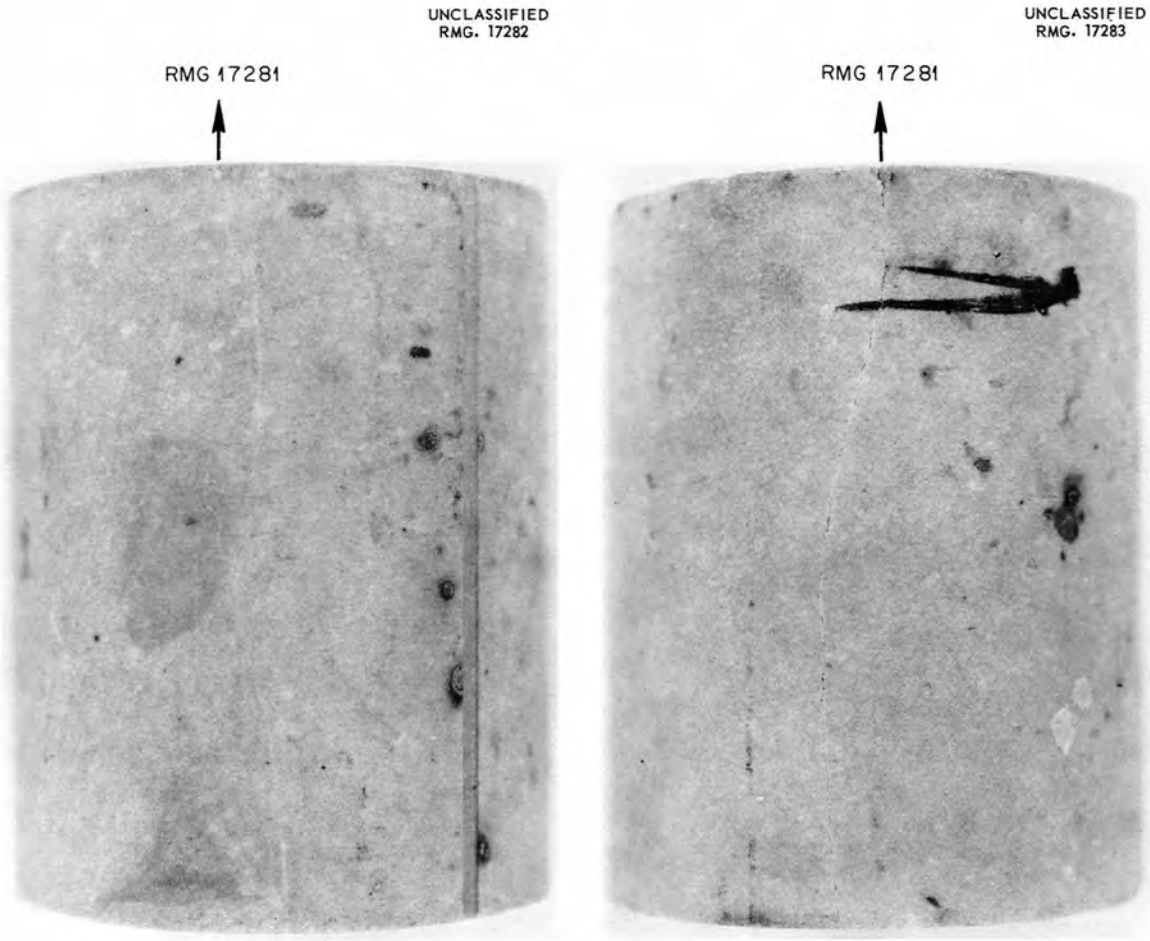

Fig. 16. Opposite Sides of 3-52, Showing Cracking. Note center specimen, Fig. 15, for top view.

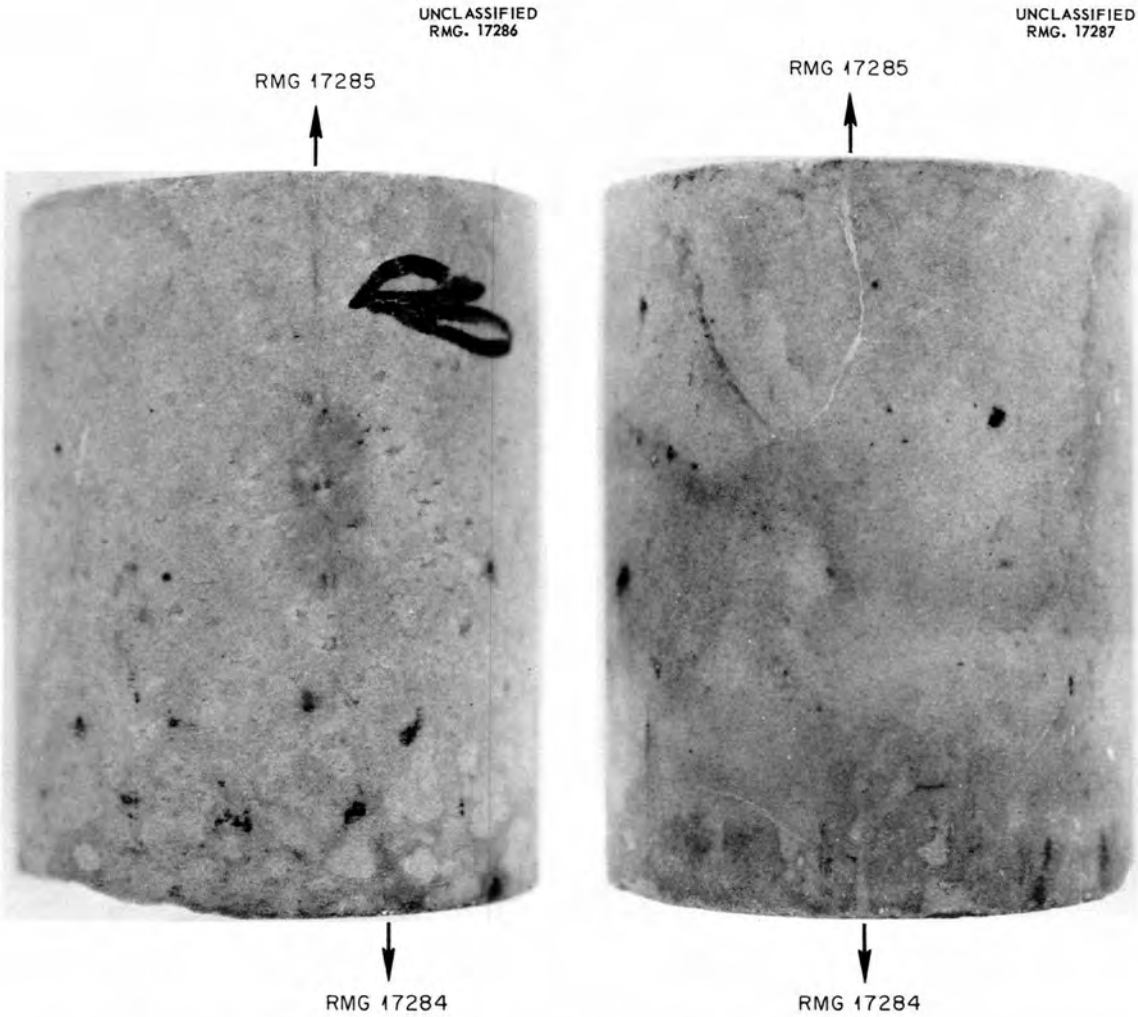

Fig. 17. Opposite Sides of Specimen 5-53. See specimen on right in Fig. 15 for top view.

Fig. 18. BeO from Capsule 3-7; nvt = 4.4×10^{20}. Irradiated at 120°C.

gram of powder shattered from one of the specimens when it was broken with vise-grip pliers. All of this powder passed through a 100-mesh sieve. All specimens are much more brittle than before irradiation. Figure 19 shows an end view of 3-71 and the chipping. This is representative of the general condition of the specimens in this capsule.

4-1 ($1.8–2.8 \times 10^{21}$, 120°C). – This experiment is a single capsule constructed differently from the other test assemblies. The capsule contains 12 specimens, each of which was a 1-in.-long cylinder, 0.8 in. in diameter. One pellet near the top in the region of lower flux did not crack. The damage becomes progressively greater lower in the experiment, where there was greater flux. Breaking chips from the pieces with vise-grip pliers was quite difficult for the top specimen but was easier for lower samples. The bottom pellet could be broken by hand. Figure 20 is a composite picture of the BeO for the entire experiment. Since some of the material was so badly broken, it was photographed after removing only a part of one side of the capsule. The top pellet is shown at the upper left, and the rest are in order with pellet No. 12 at the lower right.

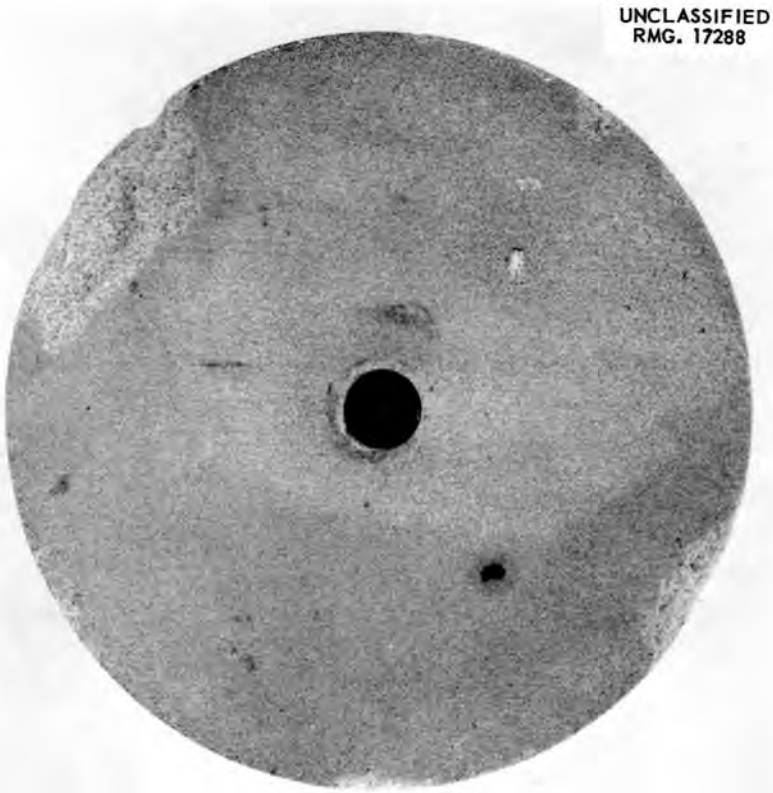

Fig. 19. Top View of Specimen 3-71, Showing Chipping of Edges. This is representative of the general condition of the specimen in this capsule. 5X.

5-1 (1.1×10^{21}, 444°C). – The BeO in this capsule maintained its integrity. Figure 21 is a view of the end of specimen 5-11 and is representative of the conditions of the specimens in this capsule.

5-2 (1.6×10^{21}, 737°C). – The specimens in this capsule experienced some diametrical cracking. Fig 22

5-21. – This capsule shows a circumferential cracking around the specimen about 1/16 in. in from the outer circumference. These conditions are pictured in Fig. 22.

5-3 (2.1×10^{21}, 827°C). – All the specimens in this capsule are broken along the diameter. There are also many cracks between the major breaks. Figure 23 shows a typical break from this capsule. When removed from the capsule, the material separated into many pieces. The pieces had sharp edges, however, and were very hard to break in the mortar.

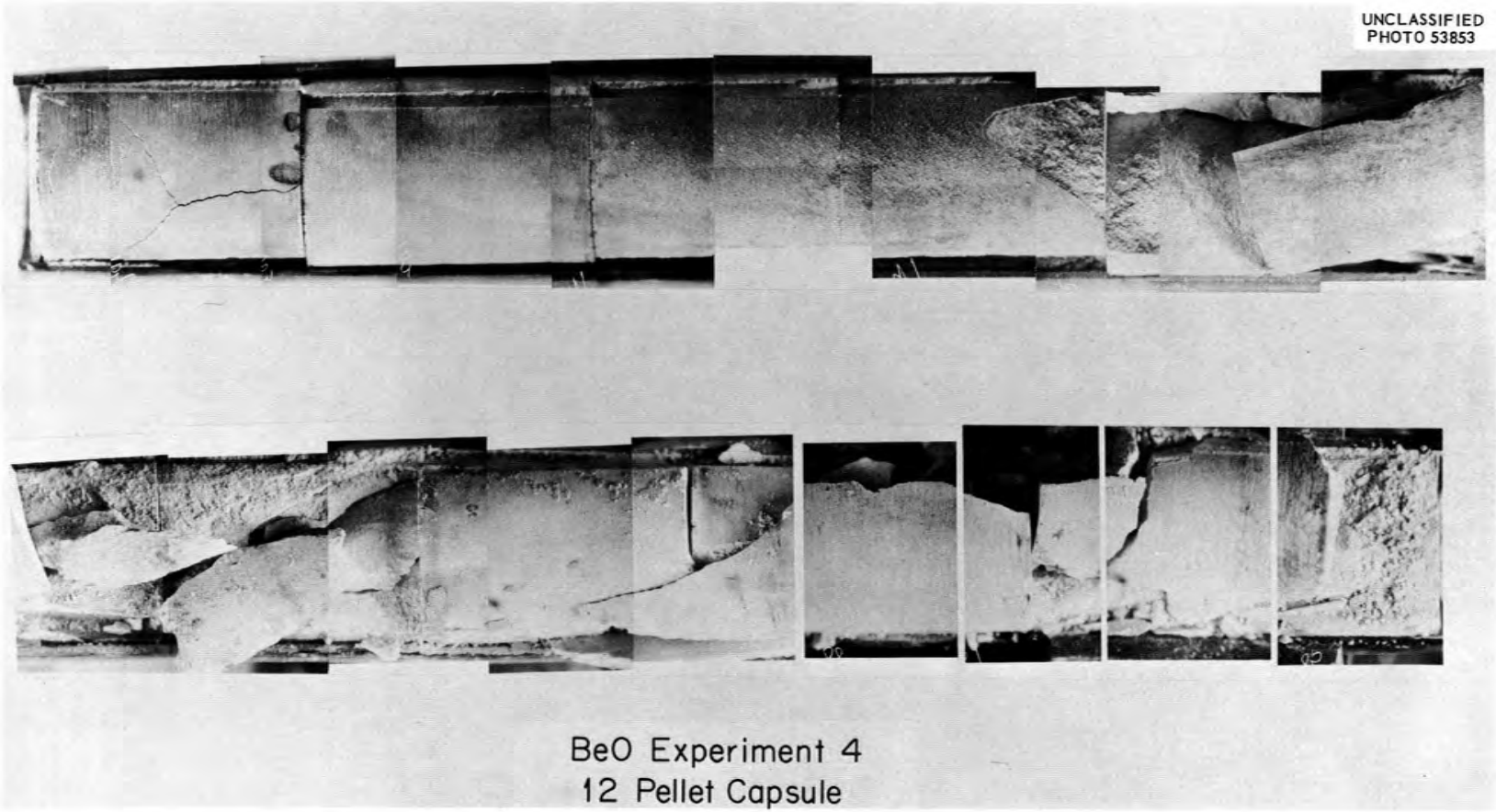

Fig. 20. Composite Photograph of BeO for Capsule 4-1; nvt = 1.8–2.8 x 10^{21} (>1 Mev). Irradiated at 120°C.

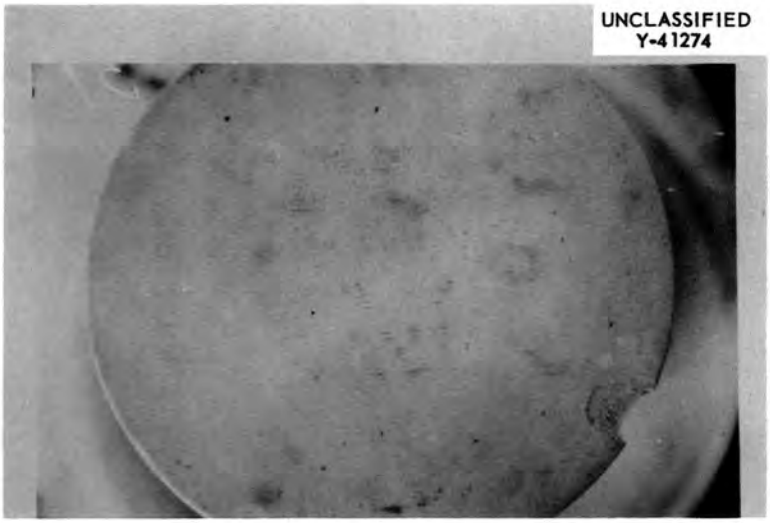

Fig. 21. End View of BeO Pellet 5-11B, a Representative Pellet in This Capsule; nvt (>1 Mev) = 1.1×10^{21}. Irradiated at 444°C.

Fig. 22. End View of BeO Specimen 5-21A; nvt = 1.6×10^{21}. Irradiated at 737°C.

5-4 (2.6×10^{21}, 900°C). – The top specimen of this capsule was completely broken into pieces approximately 3/8 in. in diameter. The second specimen was broken into ten pieces and exhibited a tendency to break into quarters. The third pellet had more small chips, with quartering tendencies still evident but not as pronounced. Figure 24 shows specimens of this capsule.

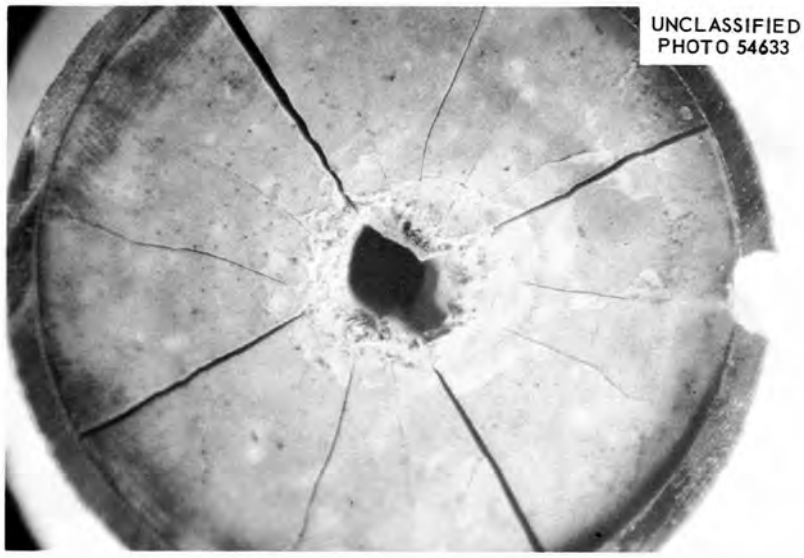

Fig. 23. End View of BeO Pellet 5-31A in Capsule 5-3; nvt = 2.1×10^{21}. Irradiated at 827°C.

Fig. 24. Section of Specimen from Capsule 5-4; nvt = 2.6×10^{21}. Irradiated at 900°C.

5-5 (2.3×10^{21}, 944°C). – Specimens 5-51 and -52 had many radial breaks and a tendency to quarter. The specimens also had many fine cracks. Specimen 5-53 was broken into half cylinders, and the outside had a beige color. Figure 25 is a composite picture of this capsule.

UNCLASSIFIED
PHOTO 53855

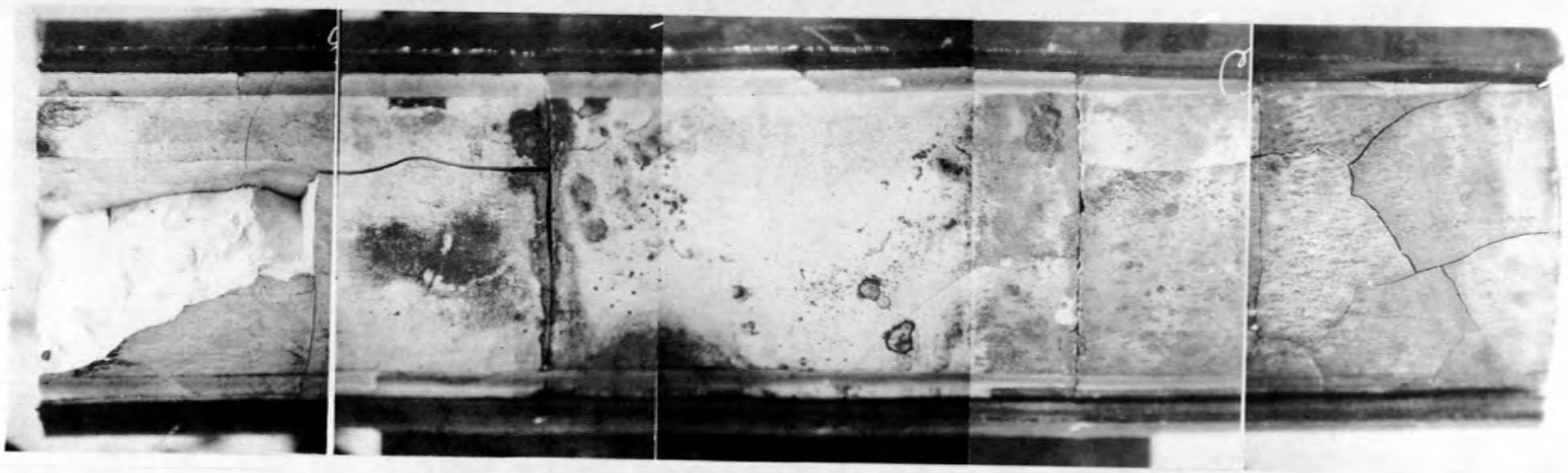

BeO Experiment 5

Capsule 5

Fig. 25. Composite Photograph of Capsule 5-5; nvt = 2.3×10^{21}. Irradiated at 944°C.

5-6 (2.1×10^{21}, 950°C). – Specimen 5-61 of this capsule had breaks of a more random nature, and there was evidence of some powdering. Specimen 5-62 was not at all like 5-61. It appeared to be hard with very sharp edges. Specimen 5-63 was very much like -62; however, there were more chips evident from the breakages. Figure 26 is a composite picture of the specimens from this capsule.

5-7 (1.5×10^{21}, 120°C). – This capsule was irradiated at low temperature in direct contact with water. During irradiation the capsule was split both circumferentially and diametrically. Figure 27 is a photograph of this breakage. All specimens in this capsule were completely powdered or in chunks which were easily crushed with the fingers. Figure 28 is an example of the condition of the BeO in this capsule.

Changes in Physical Dimensions of Irradiated BeO Specimens

Specimens of BeO irradiated in this series were measured with a micrometer both before and after exposure to reactor conditions. Post-irradiation measurements were made by remotely operated micrometers, and the dimensions, per cent changes, and irradiation conditions are listed in Table 4.

There are some omissions in the data. Capsule 2-2 was accidentally discarded, as mentioned above. In several cases extensive fracture occurred, and no fragment existed on which diameter or length measurements could be made. Specimens for which the length is given but not the diameter are those which fractured into full-length fragments and retained a portion of each original end face. The negative values of pellets 1-11 and 1-13 are attributed to experimental error. The abnormally high value for pellet 3-52 is believed to be caused by the crack, which is more completely cleaved in this specimen; it is described in an earlier paragraph.

During the disassembly of experiments 4 and 5 it was observed that in addition to rupture of the 5-7 capsule, the cladding of the other capsules had increased in diameter from the preirradiated dimension. The diameter of each capsule was measured remotely at its approximate midpoint and compared with the original dimension. This comparison is shown in Table 5. The long capsule of experiment 4 was measured at the several points indicated. Here again the reported values are the result of duplicate or a greater number of measurements.

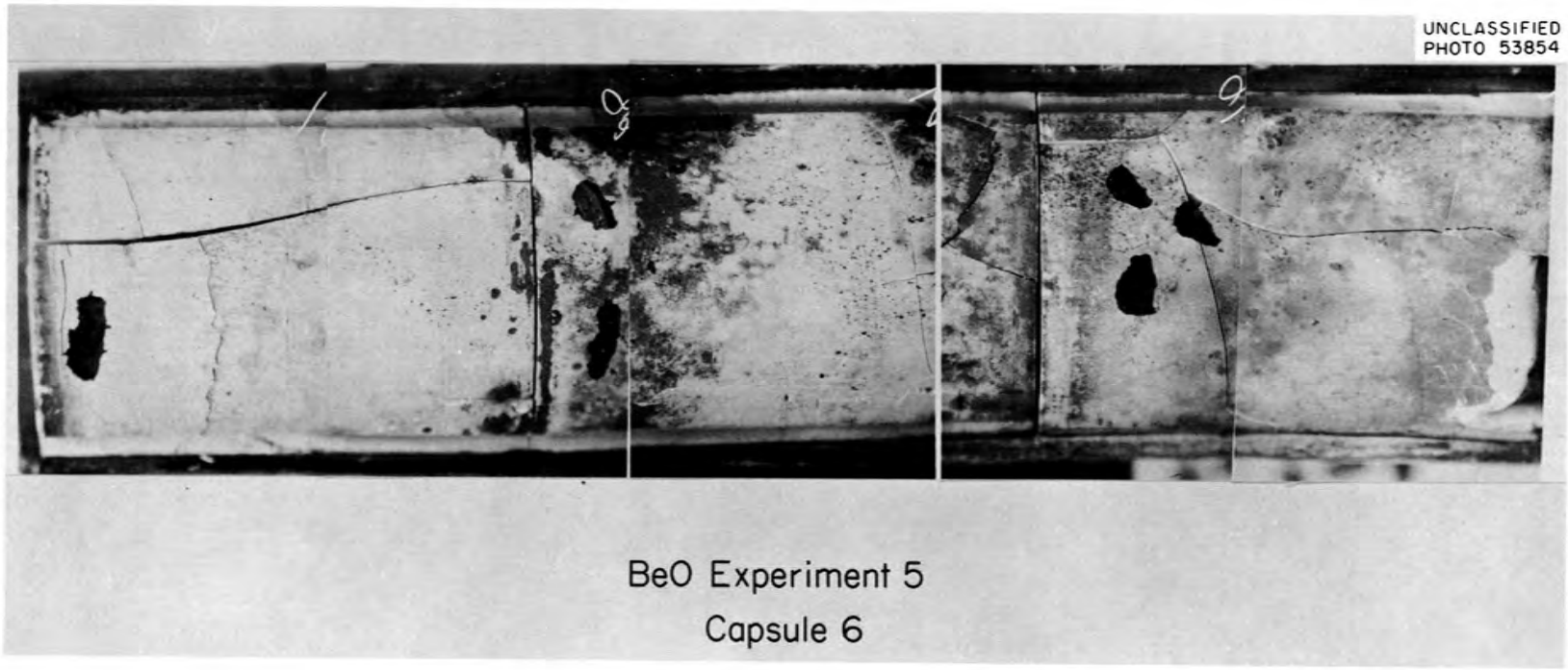

Fig. 26. Composite Photograph of Capsule 5-6; nvt = 2.1×10^{21}. Irradiated at 950°C.

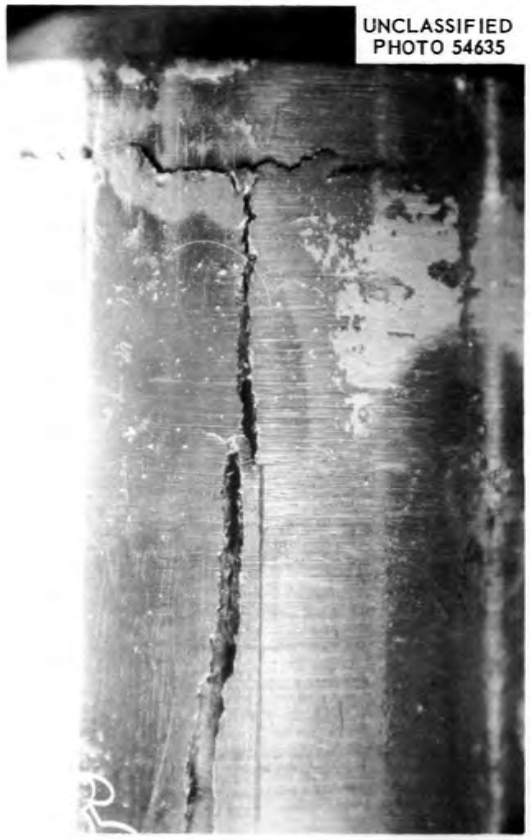

Fig. 27. View of Rupture in Cladding of Capsule 5-7.

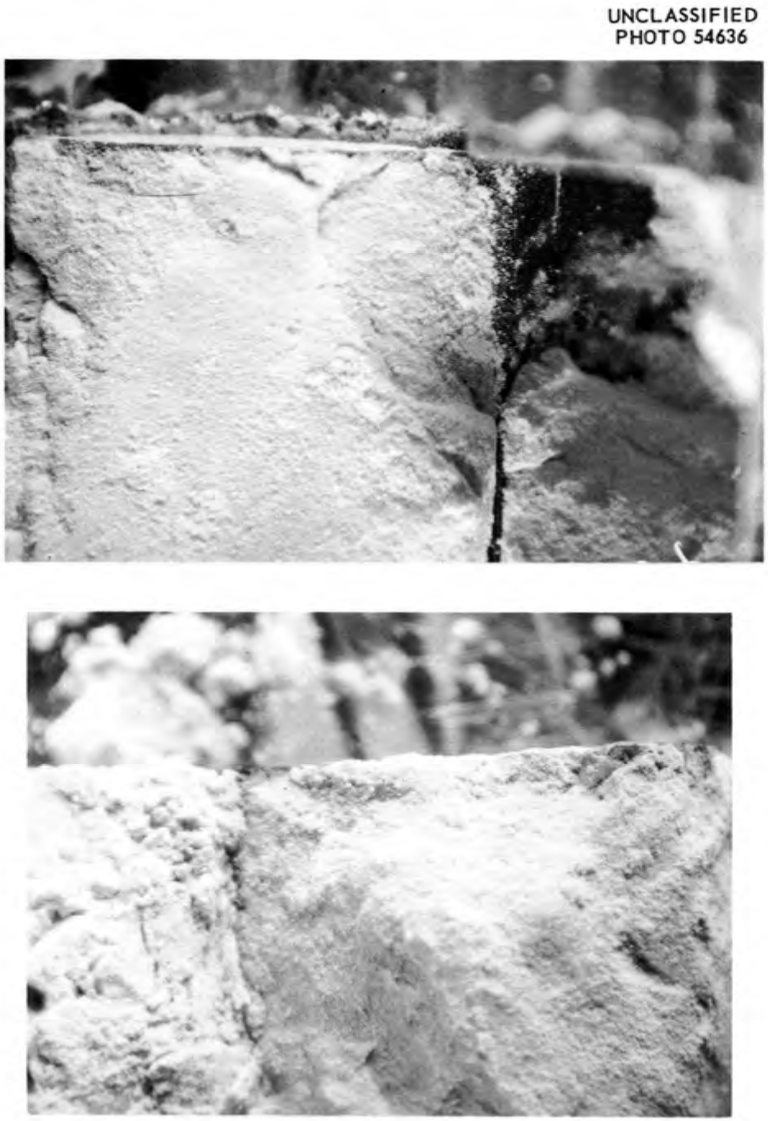

Fig. 28. BeO Specimens 41-5-72 and -73; nvt = 1.5×10^{21}. Irradiated at 120°C.

Table 4. Dimensional Changes in Irradiated BeO

Specimen	nvt (> 1 Mev)	Temperature (°C)	Length (in.) Preirrad	Mils Growth	Per Cent Change	Diameter (in.) Preirrad	Mils Growth	Per Cent Change
1-11	1.4×10^{20}	722	1.001	-7.4	-0.74	0.637	-1.6	-0.251
12			1.002			0.637		
13			1.003	0.7	0.7	0.637	-1.2	-0.188
2-11	1.1×10^{20}	219	0.9980	0.9	0.09	0.6353	0.8	0.126
12			1.0022	1.1	0.11	0.6354	0.5	0.0787
13			1.0025	-4.3	-0.43	0.6355	0.9	0.142
31	3.5×10^{20}	500	1.0025	3.2	0.32	0.6355	1.7	0.268
32			1.0020	3.2	0.32	0.6355	2.0	0.315
33			1.0020	3.7	0.37	0.6359	1.8	0.283
3-11	1.1×10^{20}	458	1.0010	0.6	0.06	0.4280	0.3	0.0701
12			1.0020	0.2	0.02	0.4277	0.4	0.0935
13			1.0020	0.2	0.02	0.4280	0.3	0.0701
31	3.1×10^{20}	858	1.0030	2.1	0.21	0.6360	1.1	0.173
32			1.0000	1.5	0.15	0.6360	0.8	0.126
33			1.0010	1.7	0.17	0.6360	1.1	0.173
51	4.5×10^{20}	1025	1.0010	3.0	0.30	0.7982	1.2	0.150
52			1.0025	3.0	0.30	0.7982	13.4	1.68
53			1.0015	3.7	0.37	0.7981	1.8	0.226
71	4.4×10^{20}	120	1.0010	8.0	0.80	0.7980	4.4	0.551
72			1.0010	6.5	0.65	0.7980	4.0	0.501
73			1.0010	5.4	0.54	0.7980	3.4	0.426
4-12	1.8×10^{21}	120	1.000	21.6	2.16	0.7950	26.5	3.33
13	2.3×10^{21}	120	1.000	21.3	2.13	0.7950	28.5	3.58
14	2.4×10^{21}	120	1.000	18.7	1.87	1.7940	32.6	4.11
5-11	1.1×10^{21}	494	1.000	7.4	0.74	0.7987	5.2	0.652
12			1.000	6.6	0.66	0.7985	5.7	0.714
13			1.000	7.7	0.77	0.7983	5.6	0.701
21	1.6×10^{21}	737	1.000	6.3	0.63	0.7985	4.7	0.59
22			1.0005	5.5	0.55	0.7984	4.2	0.53
23			1.0010	4.7	0.47	0.7983		
31	2.1×10^{21}	827	1.0010	3.7	0.37	0.7983		
53	2.3×10^{21}	944	1.000	25.7	2.6	0.7980	21.1	2.64
63	2.1×10^{21}	950	1.0005	13.9	1.4	0.7984		

Table 5. Dimension Changes of Stainless Steel Cladding

Capsule Number	Postirradiation Outside Diameter* (in.)	Average Outside Diameter (in.)	Mils Increase	Per Cent	nvt	Temperature (°C)
					$\times 10^{21}$	
4-1 top	0.8893		21	2.4	2.5	120
4-1 top 1/4	0.8890		21	2.4	2.6	
4-1 middle	0.8907		23	2.6	3.3	
4-1 lower 1/4	0.8900		22	2.5	3.3	
4-1 bottom	0.8928		25	2.9	3.1	
5-1	0.8721 0.8723 0.8725	0.8723	4.3	0.50	1.1	494
5-2	0.8709 0.8708 0.8714	0.8710	3.0	0.35	1.6	737
5-3	0.8718 0.8719 0.8720	0.8719	3.9	0.45	2.1	827
5-4	0.8871 0.8890 0.8893	0.8885	20.4	2.35	2.6	900
5-5	0.8904 0.8905 0.8906	0.8905	22.5	2.59	2.3	944
5-6	0.8902 0.8901 0.8905	0.8903	22.3	2.57	2.1	950
5-7	Burst open				1.5	120

*Preirradiation dimension, 0.8680 in.

Gas Analysis of Irradiated BeO

Samples of the irradiated BeO were analyzed for He, H_2, O_2, N_2, CH_4, CO, Ar, CO_2, and tritium. Five- to ten-gram samples of the BeO were placed in a dissolver which was connected to a vacuum system, and the sample was subjected to pumping to collect for separate analysis the gases which could be removed without dissolving the BeO. Next, the sample was dissolved in a mixture of fluoride fused salts to release trapped gases.

The collected samples were then passed through a chromatographic column of Linde Molecular Sieve to separate the gases so they could be identified and measured. The total volumes of gases and the amounts of separated gases are listed in Table 6 in units of standard microliters per gram of BeO. The two fractions of gas are listed separately, CP being the fraction removed from the BeO by cold pumping, and HP being the fraction released by dissolving the BeO. Only a small fraction of the contained helium could be removed without dissolving the BeO. Since the oxygen/nitrogen ratio is approximately that of air, it is thought that most of the measured oxygen is of atmospheric origin. The maximum oxygen content observed was 64.5 μl/g, and the associated O_2/N_2 ratio was 0.186, compared with 0.2095 in the atmosphere.

The amounts of helium found in BeO samples are plotted vs integrated fast flux in Fig. 29. This plot shows a linear relationship up to 1.6×10^{21} neutrons/cm^2. Above this value the data are somewhat erratic and appear to level off at a maximum helium concentration of 400 μl per gram of BeO. The irradiation temperature and the degree of fracturing of the BeO during irradiation do not appear to be important factors in helium retention.

The amounts of tritium found in BeO samples are plotted vs integrated fast flux in Fig. 30. This plot shows that for BeO irradiated at low temperature the tritium concentration is proportional to the square of the integrated neutron flux. The curved line is drawn to show this relationship. The amount of tritium retained by the BeO is reduced at higher temperatures.

Table 6. Gas Contained in Irradiated BeO ($\mu l/g$ of BeO)

Capsule Number		He (ppm)	Total Gas	He	H_2	O_2	N_2	CH_4	CO	Ar	CO_2	Tritium (ppm of BeO)	Irradiation Conditions: Integrated Neutron (>1 Mev) Flux (neutrons/cm^2)	Irradiation Conditions: Temperature (°C)	O_2/N_2
3-33	CP*	0.86	98.0	5.0	13	17.8	32	0.4	12.0	0.7			3.1×10^{20}	858	0.556
	HP	13.3	322	75	250	1.9**	11.3								0.168
	Total	14.2	420	80	263	19.7	63	0.4	12.0	0.7		0.18			0.313
3-51	CP	1.9	845	10.6	32	9.8	87	0.6		0.8	576		4.5×10^{20}	1025	0.113
	HP	14.3	265	80.0	179	0.7**	7.2								0.097
	Total	16.2	1110	91	211	10.5	94	0.6		0.8		0.17			0.112
3-73	CP	0.45	429	2.5	20	8.3	329	0.1		4.4	0.4		4.4×10^{20}	120	0.205
	HP	11.8	802	66.5	659	56.2**	17	1.7	2.2						3.306
	Total	12.2	1231	69.0	679	64.5	346	1.8	2.2	4.4		0.29			0.186
4-1	CP	0.94	70	5.3	4.3	12.6	51	0.1		1.1	0.1		1.8×10^{21}	120	0.247
	HP	82.1	723	464	176	3.5**	17		68						0.206
	Total	83.0	793	469	180	16.1	68	0.1	68	1.1		4.60			0.237
4-3	CP	22	242	123	51	24**	42		12				2.0×10^{21}	120	0.571
	HP	33	317	187	79	11**	41								0.268
	Total	55	559	310	130	35**	83					5.6			0.422
4-5	CP	20.3	172	113	27	18.2**	84	0.3	7.7				2.3×10^{21}	120	0.216
	HP	56.5	342	316	53	1.7**	17								0.100
	Total	76.8	514	429	80	19.9**	101	0.3	7.7			6.4			0.197
5-13	CP	4.5	89	25.1	7.5	7.9	40	0.3	10.9	1.8	1.8		1.1×10^{21}	494	0.197
	HP	37.1	308	208	74	0.8**	35	0.2	3.1						0.023
	Total	41.6	396	223	81	8.7	75	0.5	14	1.8		1.2			0.116
5-22	CP	1.4	72	7.7	7.2	11**	43		6.2				1.6×10^{21}	737	0.255
	HP	58	822	322	337	6**	243	4	87						0.025
	Total	59	894	330	344	17**	286	4	93			0.34			0.059
5-33	CP	1.1	98	6.0	9.4	17.8	66	0.2	0.3	1.0	0.4		2.1×10^{21}	827	0.269
	HP	46.4	1280	260	710	2.2**	32	1.7	321						0.068
	Total	47.5	1378	266	719	20	98	1.9	321	1.0		0.23			0.204
5-41	CP	0.39	126	2.2	20	22.9	83	0.1		1.1			2.6×10^{21}	900	0.276
	HP	68.4	7790	396	7183	23.3**	112	7.8	78						0.208
	Total	68.8	7916	398	7203	46	195	7.9	78	1.1		0.52			0.235
5-63	CP	0.87	163	4.9	22	28	107			1.4			2.1×10^{21}	950	0.262
	HP	84.0	2642	470	1793	32**	285	11.6							0.112
	Total	84.9	2805	475	1815	60	392	12		1.4		0.21			0.153

*CP – Gas removed by pumping at room temperature.
HP – Additional gas removed by dissolving BeO in fused salt and pumping.
**Includes argon if present.

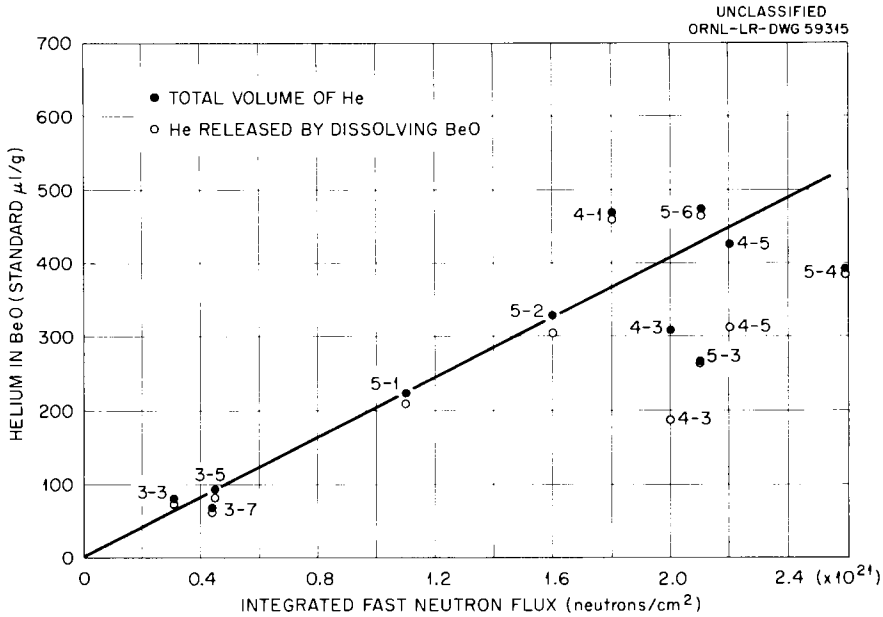

Fig. 29. Helium Contained in Irradiated BeO vs Integrated Fast Neutron Flux. (>1 Mev).

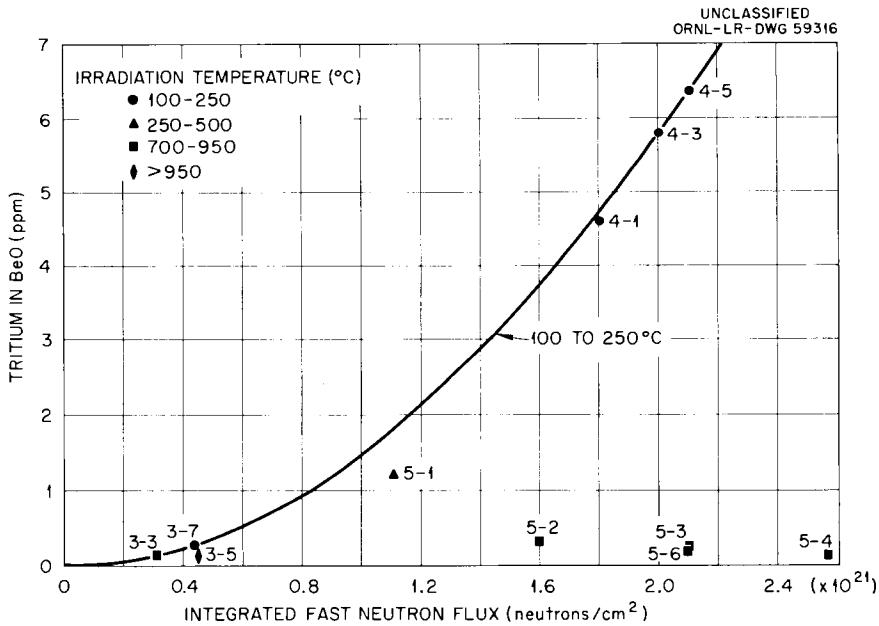

Fig. 30. Tritium Concentration in Irradiated BeO vs Integrated Fast Neutron Flux. (>1 Mev).

Changes in Thermal Conductivity of BeO During Irradiation

Since the thermal conductivity of BeO is known to decrease during irradiation, these experiments were scrutinized routinely for manifestations of this phenomena during the time each assembly was operating in the reactor. A primary purpose of recording the thermal gradient in each capsule by means of the center and sidewall thermocouple pairs was to facilitate observations of the rate and extent of change at the various irradiation temperatures provided in the subject series. Ideally, it should be possible to observe directly any saturation behavior or anneal recovery temperature levels by simple monitoring of the ΔT recordings. Experimentally, however, it proved difficult to provide a complete set of thermocouples that would survive the physical problems associated with the in-pile measurement at elevated temperature under the conditions unique to these particular capsules. As a result, ΔT information for extended operation is limited, since many of the sidewall thermocouples failed after 2000 to 3000 Mwd of operation. The observed ΔT's for two high-temperature capsules which have provided the most consistent information available are shown in Fig. 31.

The radial temperature differences through the BeO specimens increased gradually during the period of irradiation. Final changes of 50 to 100% were observed. These changes were thought not to be caused

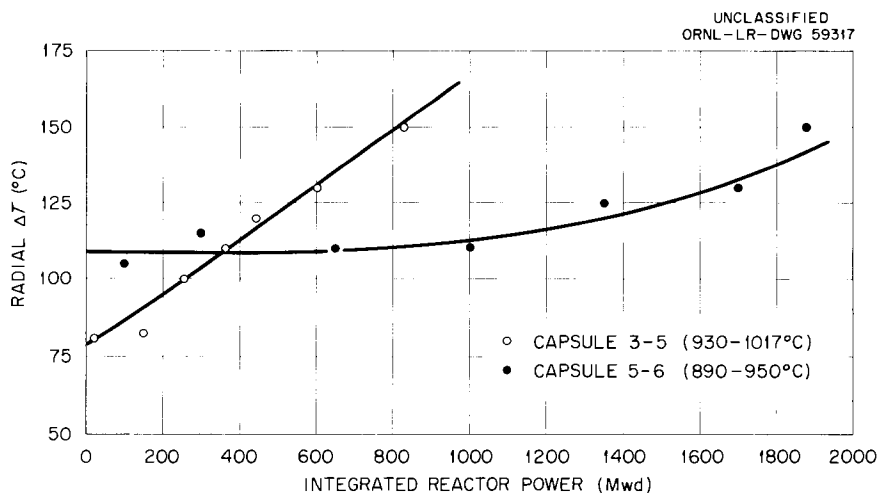

Fig. 31. Radial ΔT in BeO at 175 Mw vs Integrated Reactor Power.

by changes in reactor power distribution, since the ΔT for full reactor power was the same before and after shutdowns for refueling, when the most abrupt changes in power distribution would be expected.

Changes in Crystal Structure of Irradiated BeO

X-ray diffraction studies of irradiated BeO were made by H. L. Yakel of the Metallurgy Division. Debye-Scherrer photographs were taken in an 11.46-cm-diam camera with Cu Kα radiation (λ = 1.5418 A). Exposure time was adjusted to give optimum contrast between reflections and background intensities. A standard comparator was used to measure reflected positions, and the films were also measured with a photometer to give more quantitative line profile data.

The results of measurements on the irradiated samples and on two unirradiated samples are listed in Table 7. Considering the samples irradiated at 120°C as a group, the following observations were made by visual inspection of the patterns. (1) There are weak reflections which are not associated with the zincite lattice. Some of them are the same as those for lead. (2) There is symmetric broadening of all BeO (hk.ℓ) reflections with ℓ = 2n, except for the (hk.0) reflection, which is apparently unaffected. (3) There is an asymmetric broadening of all BeO (hk.ℓ) reflections with ℓ = 2n + 1.

Detailed measurements of the patterns give the following additional information. (1) The average hexagonal a_0 parameter from (hk.0) reflections alone is expanded about 0.1% relative to the a_0 of the unirradiated sample. (2) The average c_0 parameter computed from symmetrically broadened (hk.ℓ) reflections with ℓ = 2n is expanded by about 0.7%. (3) Measurement of the (hk.ℓ) reflections with ℓ = 2n + 1 is virtually impossible due to the asymmetric profile of the lines. (4) The positions of the maxima of the asymmetric (hk.ℓ) reflection with ℓ = 2n + 1 differ slightly from positions calculated from the a_0 and c_0 parameters. The measured differences of these maxima are the Δ values for the 10.1, 10.3, 20.1, 20.3, and 21.1 planes listed in Table 7.

Considering the samples which were irradiated at higher temperatures, the following generalizations may be made. (1) Some expansion of lattice parameters is present for all samples, but, in general, expansion is

Table 7. Lattice Parameters from X-Ray Diffraction Examination of Irradiated BeO

Specimen	a_0	Δa	$\Delta a/a_0$	c_0	Δc	$\Delta c/c_0$	c/a	Δ Values				
								(10.1)Δ	(10.3)Δ	(20.1)Δ	(20.3)Δ	(21.1)Δ
Unirradiated Specimens												
Powdered BeO[a]	2.6980 ± 0.0005 A			4.3780 ± 0.0010 A			1.6227 ± 0.0003					
Control BeO[b]	2.6978 ± 0.0001 A			4.3778 ± 0.0003 A			1.6227 ± 0.0001					
Irradiated Specimens												
3-33	2.6981 ± 0.0003 A	2.6981 − 2.6978 A = 0.0003 A	0.11×10^{-3}	4.385 ± 0.003 A	4.385 − 4.378 A = 0.007 ± 0.003 A	$1.60 \times 10^{-3} \pm 0.69 \times 10^{-3}$	1.625 ± 0.001					
3-51	2.6981 ± 0.0003 A	2.6981 − 2.6978 A = 0.0003 A	0.11×10^{-3}	4.382 ± 0.003 A	4.382 − 4.378 A = 0.004 ± 0.003 A	$0.91 \times 10^{-3} \pm 0.68$	1.624 ± 0.001					
3-73[c]	2.6999 ± 0.0003 A	2.6999 − 2.6978 A = 0.0021 A	0.78×10^{-3}	4.401 ± 0.003 A	4.401 − 4.378 A = 0.023 ± 0.003 A	$5.23 \times 10^{-3} \pm 0.68 \times 10^{-3}$	1.630 ± 0.001					
4-17	2.6991 ± 0.0003 A	2.6991 − 2.6978 A = 0.0013 A	0.48×10^{-3}	4.394 ± 0.003 A	4.394 − 4.378 A = 0.016 A	3.64×10^{-3}	1.628 ± 0.001	0.00394 ± 0.00100	0.01006 ± 0.00200	0.00399 ± 0.00100	0.01081 ± 0.00300	0.00351 ± 0.00100
4-19	2.6997 ± 0.0003 A	2.6997 − 2.6978 A = 0.0019 A	0.70×10^{-3}	4.398 ± 0.005 A	4.398 − 4.378 A = 0.020 A	4.57×10^{-3}	1.629 ± 0.001	0.00380 ± 0.00100	0.01187 ± 0.00300	0.00434 ± 0.00100	0.00895 ± 0.00300	0.00343 ± 0.00100
5-13	2.6983 ± 0.0002 A	2.6983 − 2.6978 A = 0.0005 A	0.19×10^{-3}	4.386 ± 0.003 A	4.386 − 4.378 A = 0.008 A	1.82×10^{-3}	1.625 ± 0.001					
5-22	2.6982 ± 0.0002 A	2.6982 − 2.6978 A = 0.0004 A	0.15×10^{-3}	4.384 ± 0.003 A	4.384 − 4.378 A = 0.006 A	1.37×10^{-3}	1.625 ± 0.001					
5-33	2.6982 ± 0.0002 A	2.6982 − 2.6978 A = 0.0004 A	0.15×10^{-3}	4.384 ± 0.003 A	4.384 − 4.378 A = 0.006 A	1.37×10^{-3}	1.625 ± 0.001					
5-41	2.6982 ± 0.0002 A	2.6982 − 2.6978 A = 0.0004 A	0.15×10^{-3}	4.383 ± 0.002 A	4.383 − 4.378 A = 0.005 A	1.14×10^{-3}	1.624 ± 0.001					
5-63	2.6984 ± 0.0002 A	2.6984 − 2.6978 A = 0.0006 A	0.22×10^{-3}	4.384 ± 0.002 A	4.384 − 4.378 A = 0.006 A	1.37×10^{-3}	1.625 ± 0.001					
5-7b(P)	2.7007 ± 0.0003 A	2.7007 − 2.6978 A = 0.0029 A	1.08×10^{-3}	4.408 ± 0.005 A	4.408 − 4.378 A = 0.030 A	6.85×10^{-3}	1.632 ± 0.001	0.00344 ± 0.00100	0.00945 ± 0.00250	0.00321 ± 0.00100	0.00863 ± 0.00300	0.00333 ± 0.00100

[a]Used for fabrication of specimens.
[b]From fabricated specimens.
[c]$c' = 4.36 \pm 0.01$ A (diffusion reflections).

greatest for samples irradiated at low temperatures and less for samples irradiated at higher temperatures. The $\Delta a/a$ and $\Delta c/c$ values decreased by about 80% for the samples irradiated at the highest temperatures. (2) There is no marked change in the lattice parameters of any of the samples irradiated in the range 450 to 1000°C. (3) Samples irradiated at 735°C and higher do not give diffusion patterns with asymmetric line broadening. In sample 5-13, which was irradiated at 450°C, asymmetric line broadening is barely detectable. (4) Patterns from samples irradiated at 735°C and higher show symmetric line broadening for reflections of the $(hk.\ell)$ plane with $\ell \neq 0$. A slight tendency is noticed for this broadening to become less as irradiation temperatures increase. (5) Sample 3-7 is unique. The characteristic variations of other samples irradiated at 120°C are not found. The pattern shows two distinct sets of $(hk.\ell)$ reflections with $\ell \neq 0$. The more intense of these are not broadened appreciably but correspond to a highly expanded lattice, and the less intense ones are broadened considerably and correspond to a lattice with an expanded a_0 parameter but with a c_0 parameter equal to or less than that of the unirradiated lattice. (6) The pattern from 5-63 contains, in addition to the continuous Debye-Scherrer arcs, discrete single-crystal reflections.

Samples of the irradiated BeO were also studied by x-ray diffraction at Battelle Memorial Institute. The following observations are from a preliminary report. (1) There was an expansion along the hexagonal c axis of 0.2 to 0.6%. (2) Crystal strain was observed from defects which appeared to be concentrated between oxygen layers in the BeO lattice. This produced faulting of the oxide layers, the amount of which increases with the integrated flux and decreases with temperature. (3) At low irradiation temperature there is a decrease in the crystallite size. (4) The layer defects also produce local faulting or blistering, whose concentration is expressed as the possibility (α) per layer in Tables 8 and 9. (5) Sample 5-32 showed the least change, with no indication of strain within the oxide layer. The other low-density samples exhibited either strain within oxide layers or sufficient concentration of defects to cause a decrease in crystal size. (6) The results on the high-density specimens are not conclusive. Only 3-52 and 3-72 exhibited increased x-ray line broadening relative to the unirradiated specimen. The parameters and irradiation conditions are listed in Tables 8 and 9.

Table 8. Structure Changes in Low-Density BeO from Neutron Irradiation

Specimen	Temp (°C)	Exposure (nvt)	Δc/c, Lattice Change (%)	Layer Faulting, α*	Crystallite Size (A)		Intralayer Strain (%)
					L_c	L_a	
		$\times 10^{21}$					
5-32	827	2.1		0.006	760		
5-42	900	2.6	0.13	0.014	270		0.18
5-12	444	1.1	0.18	0.018	210	1400	0.05
5-62AA	950	2.1	0.55	0.019	290		0.20
5-52	944	2.3	0.55	0.018	220	330	
4-12	110	2.0	0.7	0.034	84	360	

*A measure of concentration of layer faulting.

Table 9. Structure Changes in High-Density BeO from Neutron Irradiation

Specimen	Temp (°C)	Exposure (nvt)	Δc/c, Lattice Change (%)	Layer Faulting, α*	Crystallite Size (A)	
					L_c	L_a
		$\times 10^{20}$				
3-52	1025	4.5	0.23	0.008	340	500
3-72	120	4.4	0.46	0.007	560	
3-32	858	3.1	0.23	0.006		
2-12	219	1.1	0.37			
1-12	722	1.4	0.23			

*A measure of concentration of layer faulting.

In addition to the x-ray studies of crystal structure, sample 4-19 was examined by use of the polarized-light microscope and compared with the control sample. Particles in the control sample occur as needle-like crystals approximately 5 μ or less in size. Most of the particles in sample 4-19 are approximately 50 by 10 μ, and there is no evidence

that these particles are constituted of smaller aggregates. The BeO in this sample has a noticeably lower index of refraction than the control. The index of refraction increased upon annealing in the range 700 to 1050°C, as shown in Fig. 32. Certain lines which had been broadened in the x-ray diffraction pattern were restored almost to normal by annealing, as shown in Fig. 33. The information from examination by polarized-light microscopy and annealing studies was supplied by R. E. Thoma.

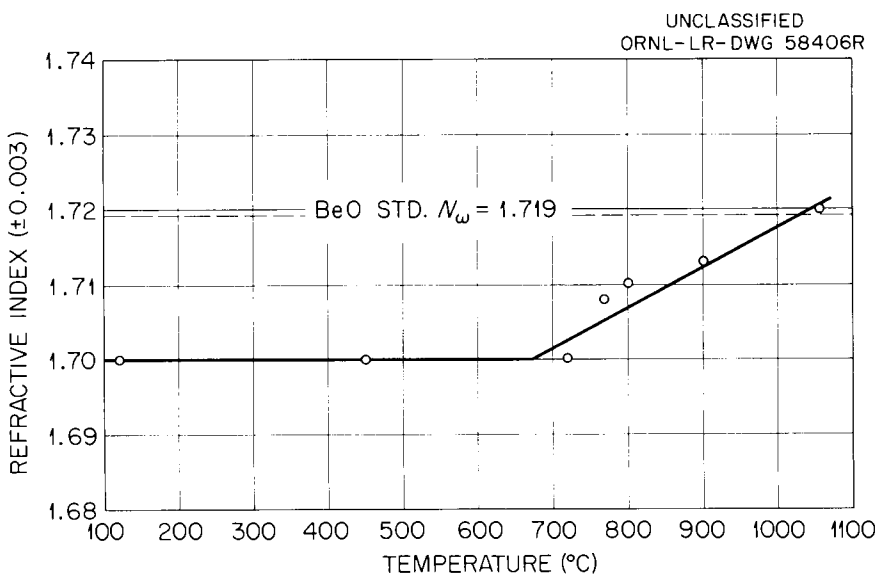

Fig. 32. Refractive Index of Irradiated BeO Samples Series X-41 as a Function of Annealing Temperature.

Electron Microscopy Studies of Irradiated BeO

Specimens of BeO which had been irradiated at both high and low temperatures were examined on the electron microscope at Battelle Memorial Institute. The high-density specimens were examined before and after postirradiation heat treatment at 1025°C. Control specimens of both high- and low-density BeO which had received no irradiation were compared with the irradiated samples.

Specimens were prepared by crushing to present fractured surfaces. Photographs were made from negatively shadowed carbon replicas of the fractured BeO. They were made from thick plastic replicas (10 mils of

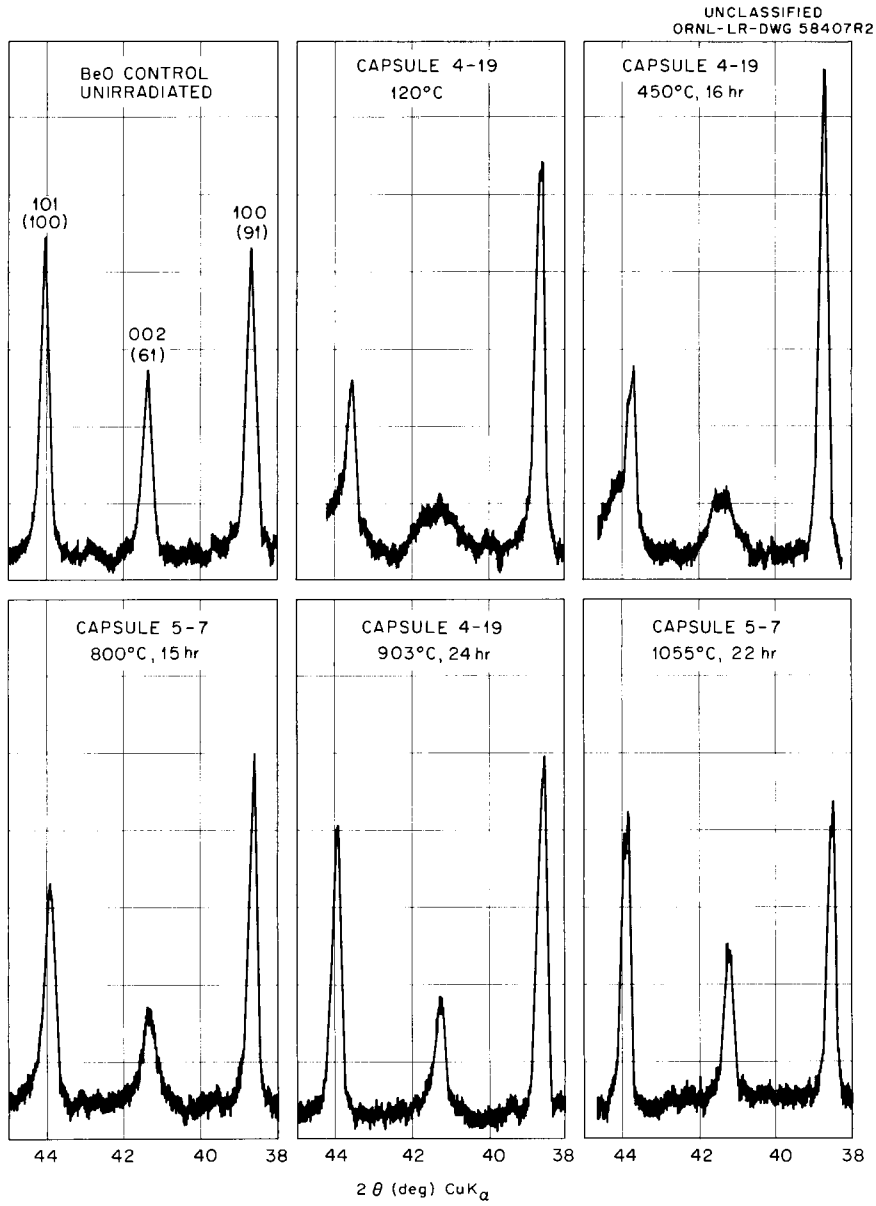

Fig. 33. Diffraction Patterns of Irradiated BeO Samples.

cellulose acetate) by vapor deposition of platinum and carbon followed by the dissolution of the plastic to leave the thin platinum-carbon composite. This technique results in a replica in which the surface relief is opposite that of the specimen; for example, high areas are expressed as depressions.

Electron micrographs were taken at 5000 and 10,000× and subsequently photographically enlarged to 17,500 and 34,000× respectively. Sufficient

detail can be seen and a more representative field shown at the lower magnification; therefore, it was considered preferable to include only one micrograph of each density at 35,000×. Table 10 lists the specimens examined, the irradiation conditions, and the treatment given.

Electron microscopy of the unirradiated control specimens revealed that the high-density BeO is comprised of larger grains and exhibits transgranular fracture rather than intergranular fracture as does the low-density BeO. The characteristic striations of transgranular fracture are shown in Fig. 34. The smooth faceted surfaces in Fig. 35 are typical of intergranular fracture. The unirradiated material contained voids which are generally characteristic of sintered BeO. They are shown in Fig. 34 in the lower left and upper right corners. The surfaces in these voids have developed the growth steps during sintering which are often seen on free surfaces of many metals and ceramics. The voids are displayed as raised portions but are actually depressions.

Observations of fractured surfaces of irradiated BeO indicate that irradiation has produced voids presumably filled with helium and that

Table 10. Specimens and Treatment Before Electron Micrographs Were Made

Sample Designation	Estimated Density, Per Cent of Theoretical	Irradiation Temperature (°C)	Postirradiation Heat Treatment	Integrated Exposure (nvt)
3 control	93		None	
3-1 control	93		24 hr at 1025°C	
3-52	93	1025	None	4.5×10^{20}
3-52	93	1025	24 hr at 1025°C	4.5×10^{20}
3-72	93	120	None	4.4×10^{20}
3-72	93	120	24 hr at 1025°C	4.4×10^{20}
5 control	86		None	
5-52	86	944	None	2.3×10^{21}

Fig. 34. Unirradiated Control (High-Density) Specimen, Experiment 3. Note the striations indicating transgranular fracture. Two very large voids are also shown with the structure typical of a free surface. 17,500X. Reduced 18%.

Fig. 35. Unirradiated Control (Low-Density) Specimen, Experiment 5. The smooth surfaces indicate intergranular fracture. Dark shadowlike areas indicate thin flaps in the replica which penetrated cracks in the surface of the specimen. 17,500X. Reduced 17%.

upon heat treatment, these voids coalesce to form blisters. Higher temperatures create larger blisters. These findings agree with studies made by Frisbie, Bisson, and Caillat.[17] An important difference between these two studies is that the present one found the high-density BeO fracture to be transgranular before irradiation, after irradiation, and after postirradiation heat treatment and that the low-density BeO fracture was intergranular before as well as after irradiation. The French study stated that there was a predominance of intergranular fracture after irradiation, as opposed to a transgranular fracture before irradiation.

There are voids in the BeO of both densities, irradiated at high temperature, which were not present in the unirradiated material. The voids are larger in the low-density material and are present only in certain facets of the grains exposed by the intergranular fracture. Figure 36 shows these voids, present on only certain faces of the grain, and Fig. 37 is a more detailed view. An interesting conclusion suggested by this phenomenon is that helium diffuses more readily in certain crystallographic directions. In the high-density material, irradiated at high temperature, both large and small bubbles are found but are, in general, smaller than those in the low-density material. An interesting fact is that these bubbles are sometimes found in parallel alignment, as shown in Fig. 38. This also suggests a crystallographic relationship to direction of helium diffusion. Heat-treating this sample for 24 hr at 1025°C caused the number of voids to decrease and the size to increase. This is shown in Fig. 39.

No voids were found before heat treatment in the high-density specimen irradiated at low temperature (Fig. 40). However, there were a few voids after heating for 24 hr at 1025°C (Fig. 41). This may be attributed to agglomeration of helium. The high-density control specimen which received a 24-hr heat treatment at 1025°C was unchanged (Fig. 42).

---

[17]H. Frisbie, A. Bisson, and R. Caillat, J. Nuclear Materials 1, 106–8 (1959).

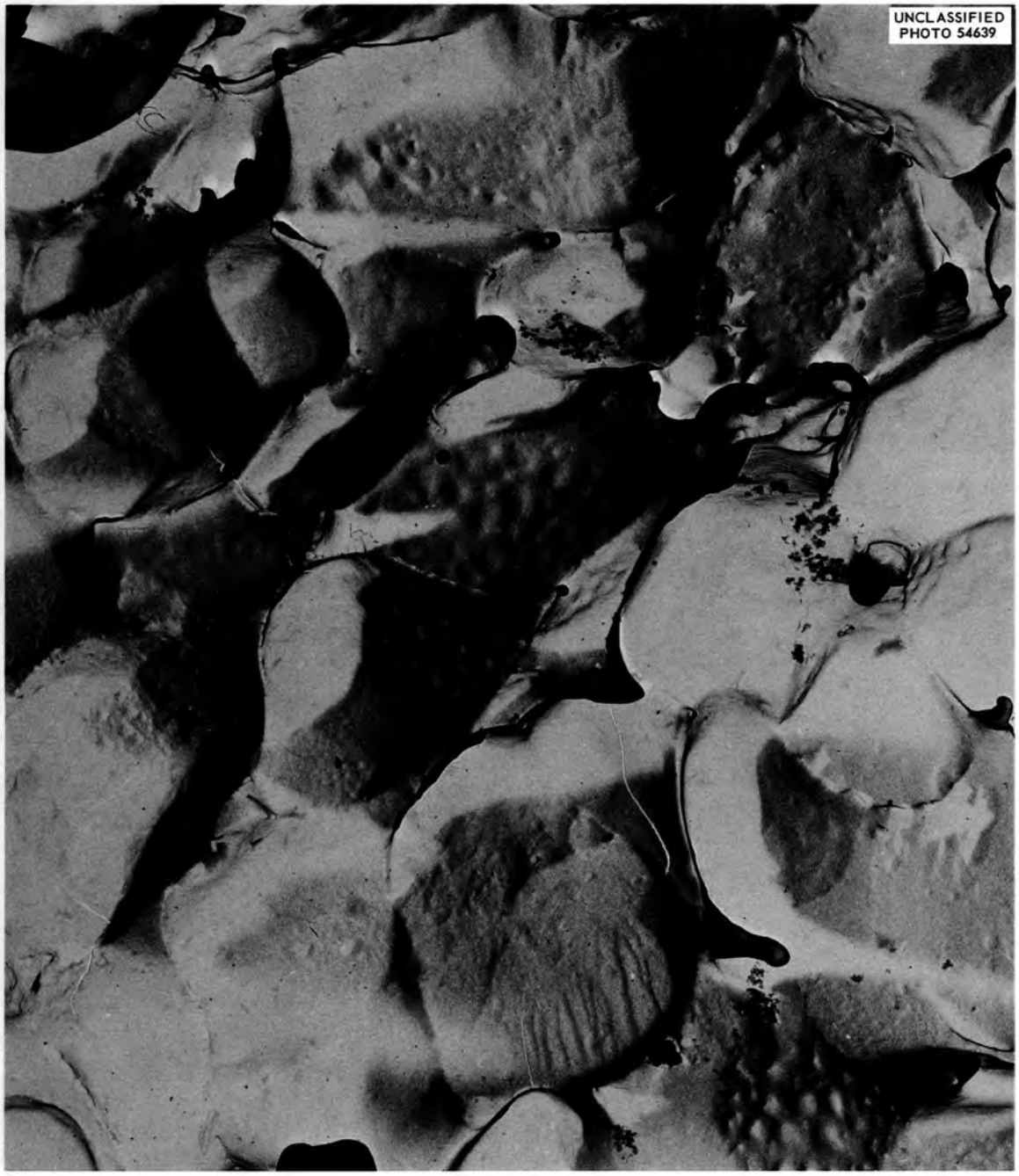

Fig. 36. Irradiated (2.3×10^{21} nvt, fast, 944°C) Specimen 5-52 (Low Density). Note the appearance of voids indicated by the small raised areas in the replicas. Note that the voids appear only on certain facets of the grains exposed by intergranular fracture. 17,500X. Reduced 17%.

Fig. 37. Irradiated Specimen 5-52 (Low Density). A more detailed view of the void locations is shown. 35,000X. Reduced 20%.

Fig. 38. Irradiated (4.5×10^{20} nvt, fast, 1025°C) Specimen 3-52 (High Density). Voids were much smaller than in the low-density material. Note that voids appear in parallel alignment in some areas. Transgranular fracture. 35,000X. Reduced 18%.

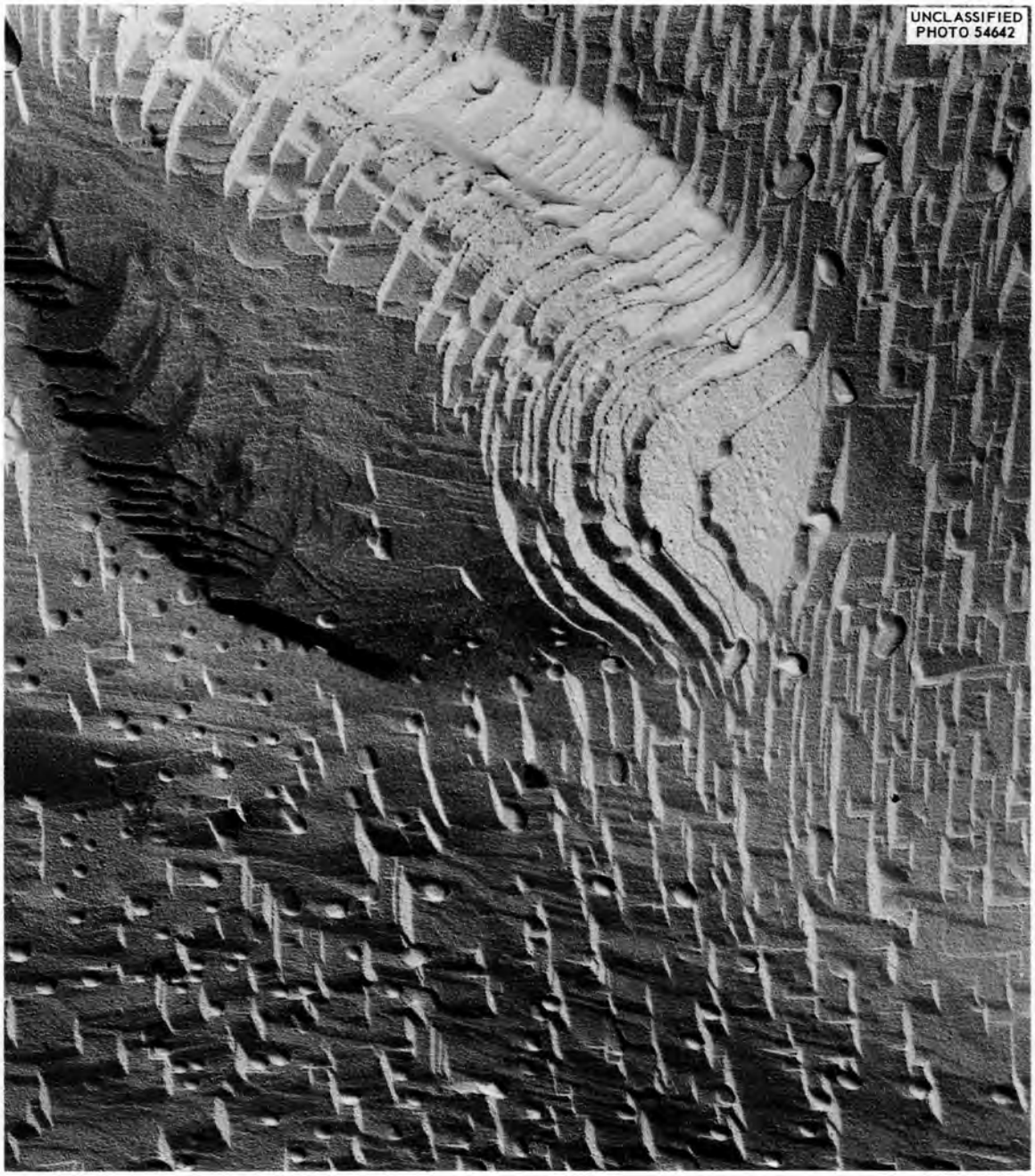

Fig. 39. Irradiated Specimen 3-52 (High Density) After Heat Treatment at 1025°C for 24 hr. Note that small voids disappeared and large voids are now evident. Transgranular fracture still evident. 17,500X. Reduced 18%.

Fig. 40. Irradiated (4.4×10^{20} nvt, 120°C) Specimen 3-72 (High Density). Transgranular fracture. Note that void structure is not visible as in the case of the high-density irradiated at 1025°C. 17,500X. Reduced 20%.

Fig. 41. Irradiated Specimen 3-72 (High Density) After Heat Treatment at 1025°C for 24 hr. The development of some porosity is evident. Transgranular fracture. 17,500X. Reduced 18%.

Fig. 42. Unirradiated Control Specimen, Experiment 3 (High Density) After Heat Treatment at 1025°C for 24 hr. Transgranular fracture. Resembles original appearance. Compare with Fig. 34. 17,500X. Reduced 17%.

Metallographic Examination of Irradiated BeO

Metallographic examination of most of the BeO specimens was performed in an effort to observe irradiation damage in terms of grain growth, porosity changes, void development, and any other detail in microstructure which might become evident. Specimen mounts of the end faces of each recovered pellet were prepared and examined in the polished and etched condition with a light microscope at magnifications up to 800×. The BeO specimens were, in general, difficult to polish, especially to get a uniform condition across the entire face of a single sample. The edges were frequently poorly prepared, with extreme pullout present. The problem occurred in both irradiated and control specimens.

Various quantities of voids were observed in the prepared surfaces of the hot-pressed material in experiments 1–3. A considerable quantity of voids could be seen just below the surface by careful focusing. By use of this technique it was possible to differentiate to a considerable extent between pullout, which occurred at the surface as a result of metallographic preparation, and the voids, which were characteristic of the material. Void spaces were generally spherical in shape in the center of the BeO grains and irregularly shaped along grain boundaries and at grain boundary intersections. It seems evident after comparison with control material that there is no readily measurable difference in the quantity or size of void structure between the irradiated and control BeO and that the observed incidence of this type of detail must be attributed solely to the fabrication techniques. This is supported to a certain extent by the much smaller grain-size structure and absence of porosity noted in the isostatically pressed and sintered material of experiments 4, 5, and 6.

Cursory examination of structures shown in the photomicrographs suggests that there is grain growth evident at both high and low temperatures in the material irradiated at the intermediate and higher neutron dosages. The observed growth may not be firmly defined, since it is random in nature and could possibly vary to as great an extent within a single specimen as from one sample to another. The interpretation is further obscured by the fact that comparisons here can be made only to a limited number of representative control samples instead of to the

same samples observed before irradiation. An estimate of apparent average grain diameter was made by using a random line intersection technique, and the values determined in this manner are listed for comparative purposes in Table 11.

Table 11. Comparison of Grain Sizes Observed in BeO

Specimen	Average Grain Diameter at 100× (in.)
Hot-Pressed	
1-1	0.14
2-1	0.05
2-3	0.10
3-1	0.09
3-3	0.10
3-5	0.10
3-7	0.11
Control	0.04
Isostatically Pressed	
4-19	0.02
Control	0.01

Metallographic pullout experienced during polishing of the specimens served as an effective qualitative indication of intergranular fracture. Severest pullout occurred in specimens receiving the highest neutron dose but irradiated at similar temperatures. A somewhat lesser degree of pullout was experienced in the specimens irradiated at high temperature than in those irradiated at low temperatures for similar neutron dosages. This observation may be evidence as to the results of annealing effects which could relieve radiation-induced stresses.

Several observations of a more random nature were noted. The presence of a white foreign material was detected on capsules 3-51 and 3-52 on two surfaces which were in direct contact with each other during

irradiation at a high temperature. The presence of the material is unexplained but is not believed to be the result of metallographic preparation procedures. No evidence could be found for new crystalline phases within the irradiated BeO specimens. The isostatically pressed and sintered BeO material contains random large grains included in the general small grain size. This condition persists for both the irradiated and control material. This same type of material when irradiated to high neutron dosage becomes too soft to polish metallographically. It accordingly becomes impractical to prepare large surfaces, and the observations on this material are limited to small pieces. Although excessive pullout is sustained, a large enough number of grains become polished to permit an estimate of typical grain diameter.

Figures 43–57 show the grain structure. An example of material from each capsule is presented, along with a representative control preparation for each of the two types of BeO studied.

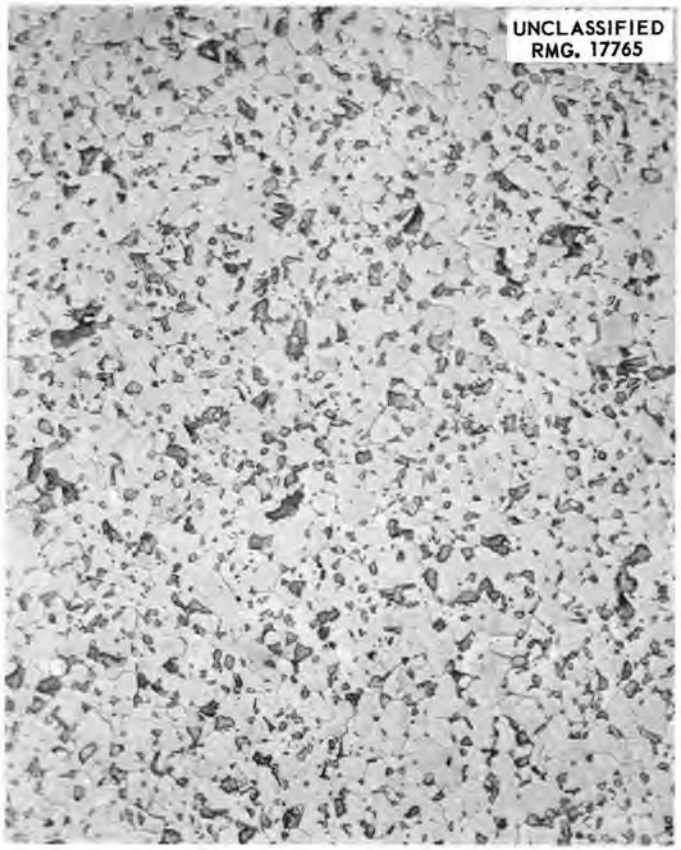

Fig. 43. Beryllium Oxide Control Specimen (Hot-Pressed), Typical Structure. 250X.

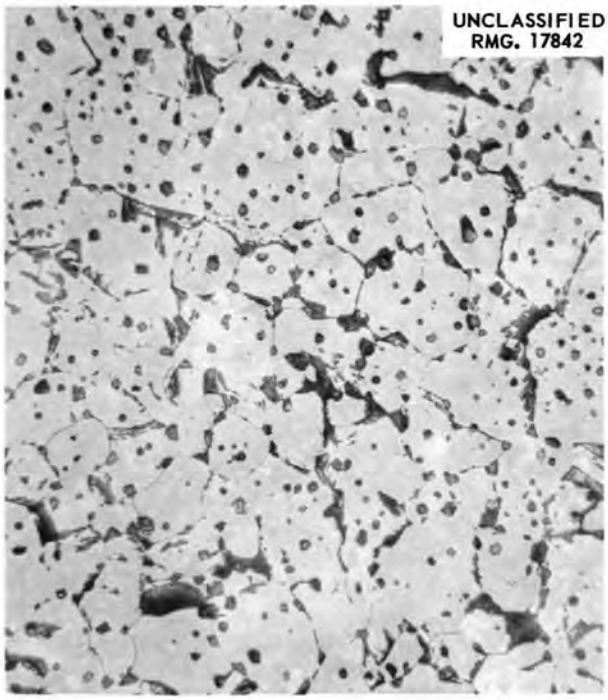

Fig. 44. Specimen 1-1, Etched, Typical Structure. 250X.

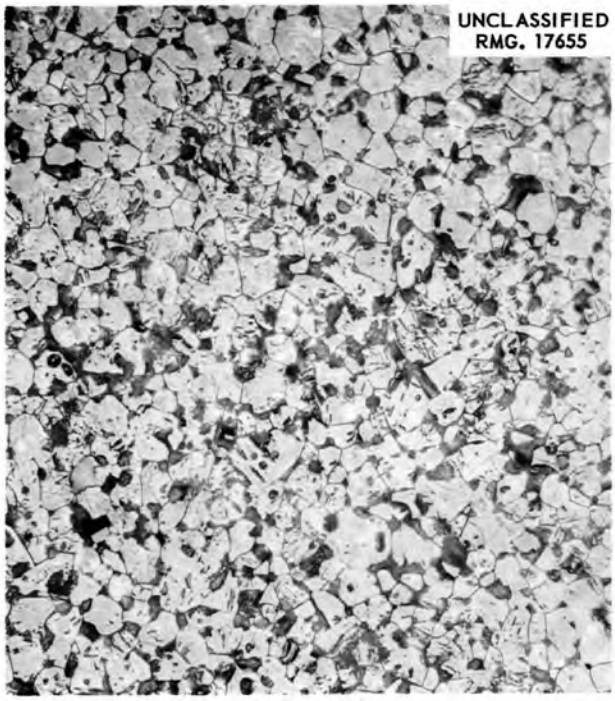

Fig. 45. Specimen 2-1, Etched, Typical Structure. 250X.

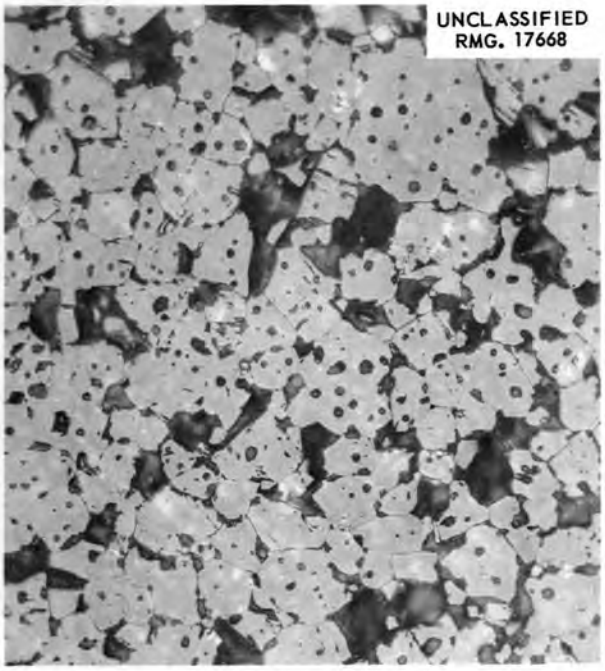

Fig. 46. Specimen 2-3, Etched, Typical Structure. 250X.

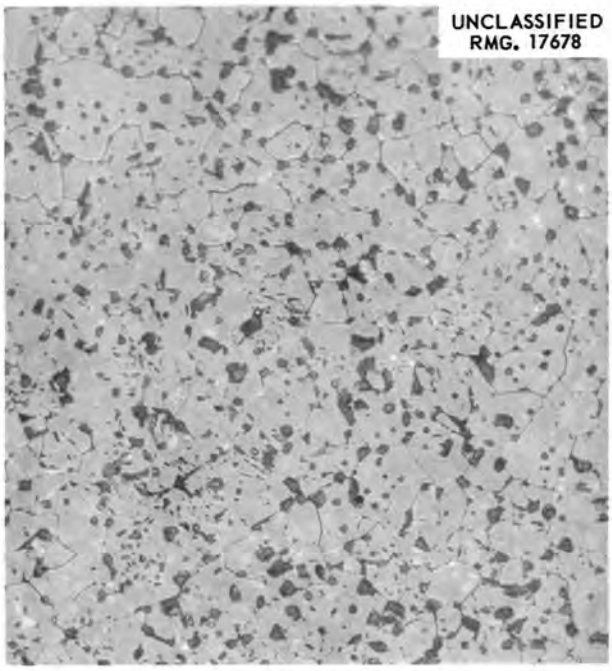

Fig. 47. Specimen 3-1, Etched, Typical Structure. 250X.

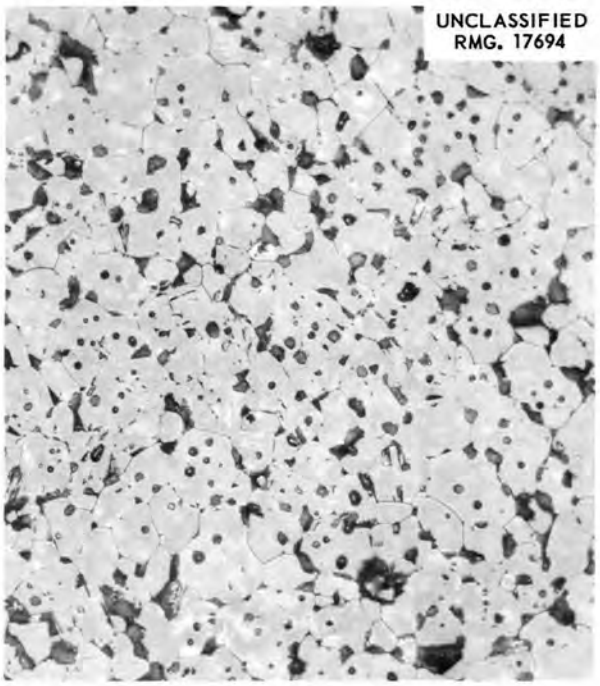

Fig. 48. Specimen 3-3, Etched, Typical Structure. 250X.

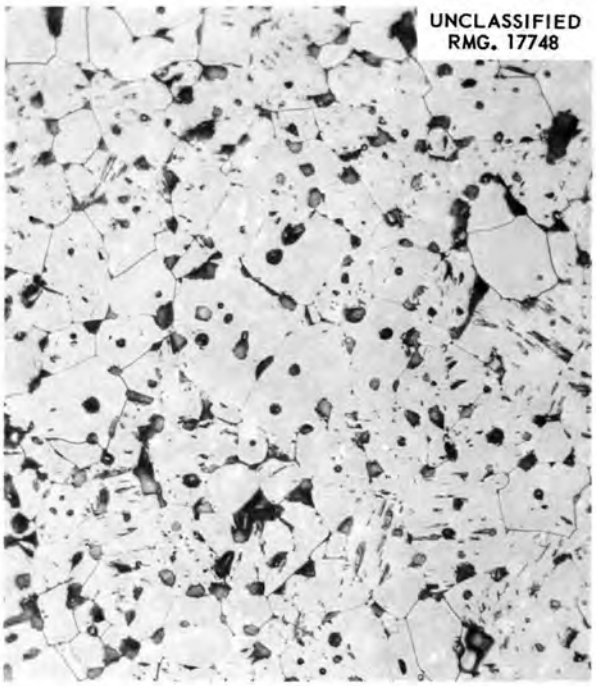

Fig. 49. Specimen 3-5, Etched, Typical Structure. 250X.

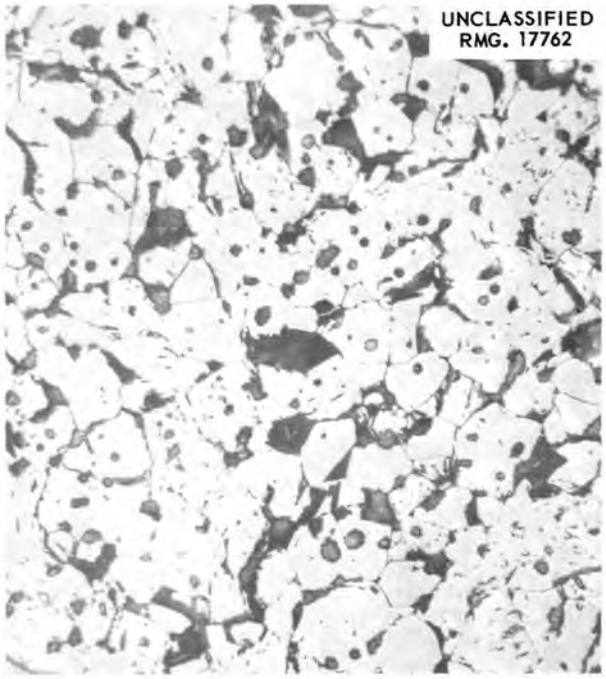

Fig. 50. Specimen 3-7, Etched, Typical Structure. 250X.

UNCLASSIFIED
RMG. 18481

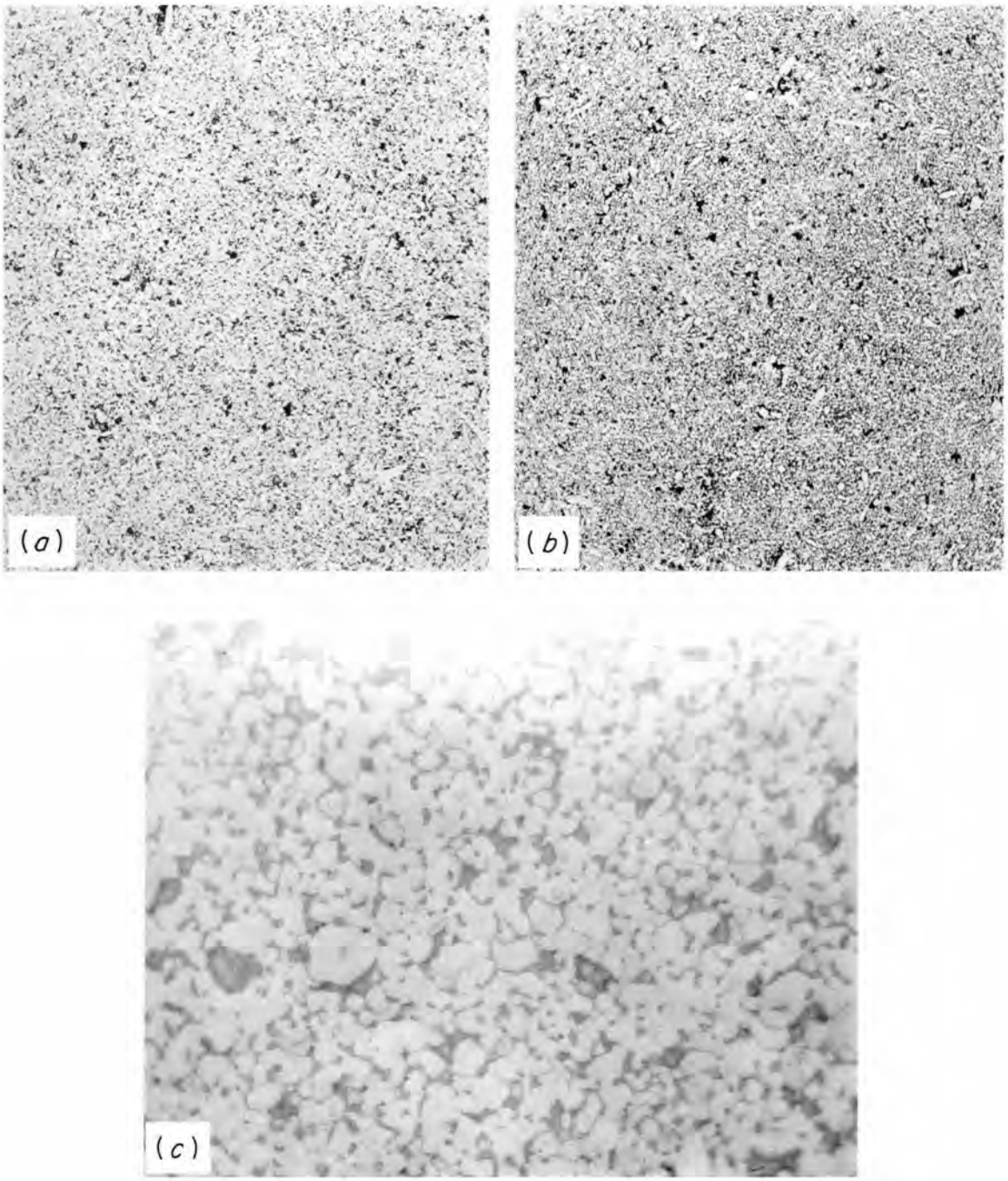

Fig. 51. Microstructure of Unirradiated Control Specimen Experiment 5. Final polish on lintless cloth, Linde-A abrasive, 1700 rpm. Etchant: boiling 25% $NH_4F \cdot HF$ in water. Note general small grain size with scattered large grains and porosity. (a) As polished. 100X. (b) Etched. 100X. (c) Etched. 750X.

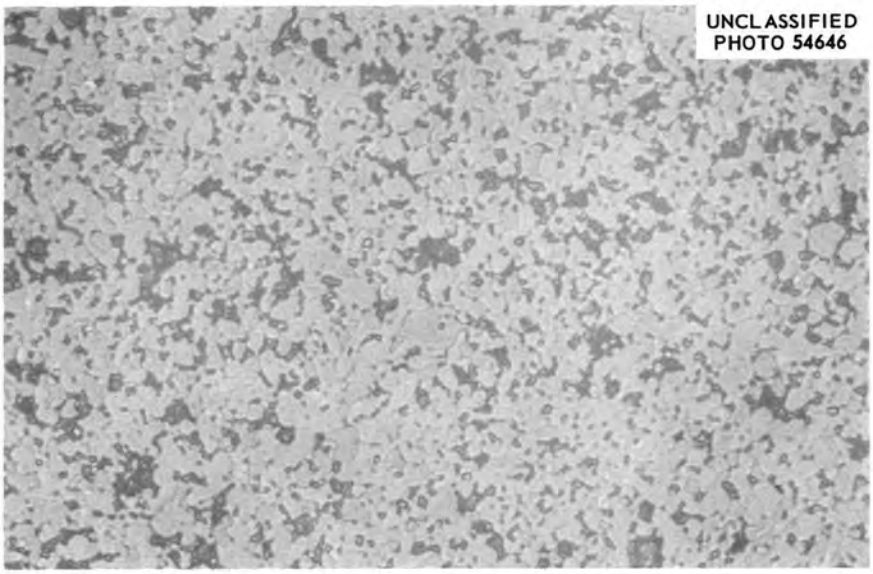

Fig. 52. Irradiated Specimen 5-12; Etched. 750X.

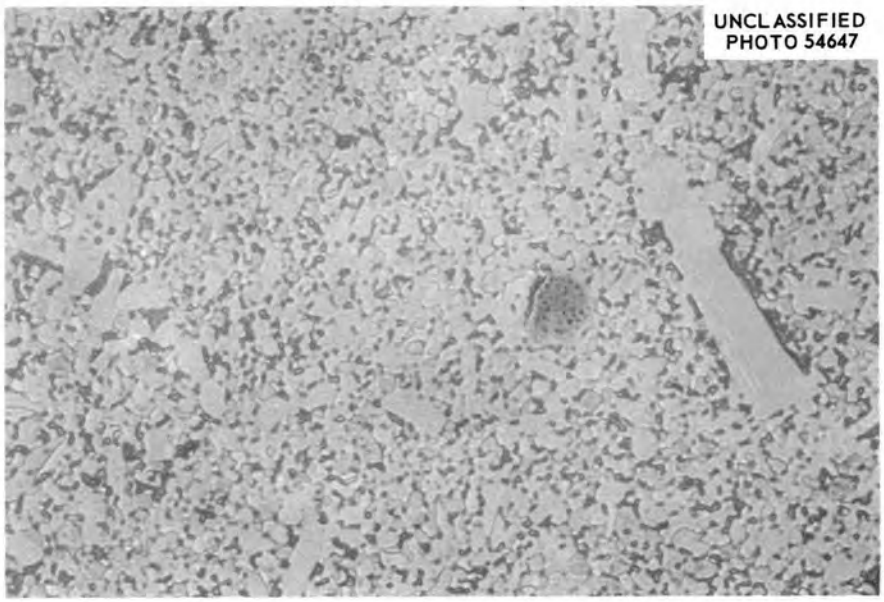

Fig. 53. Irradiated Specimen 5-22; Etched. 750X.

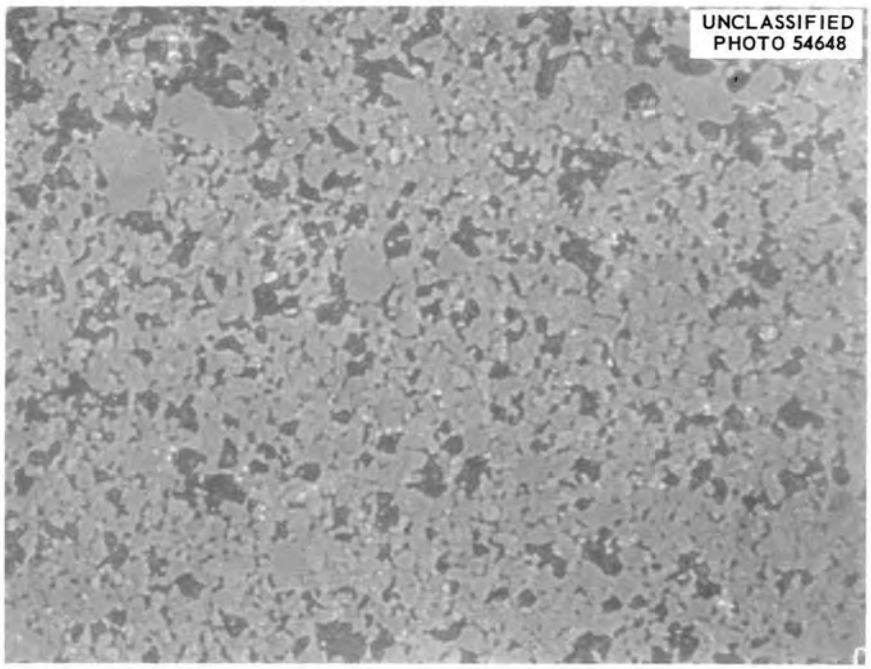

Fig. 54. Irradiated Specimen 5-32. The etching process tended to remove grains from the surface. As polished. 750X.

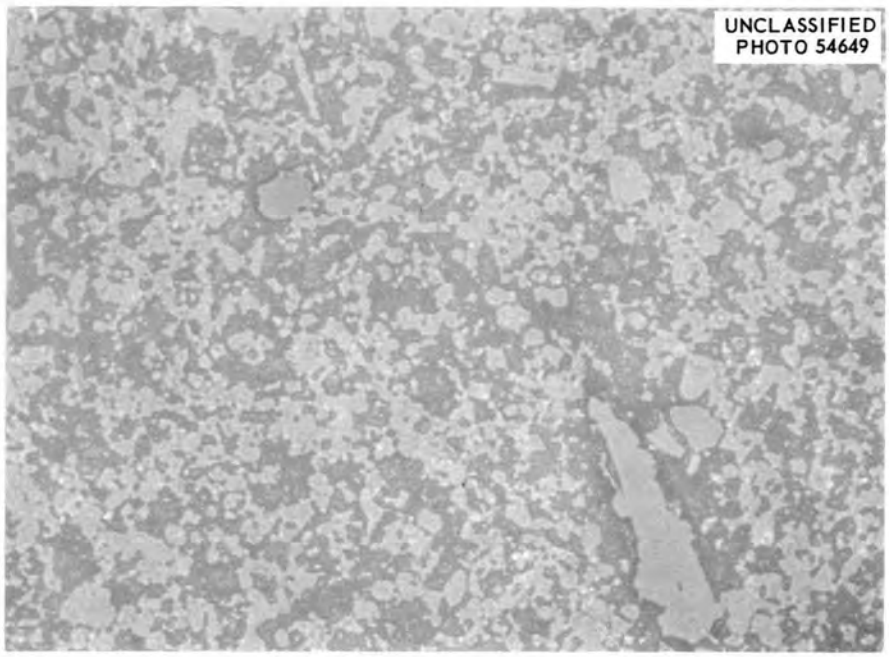

Fig. 55. Irradiated Specimen 5-42. The etching process tended to remove grains from the surface. As polished. 750X.

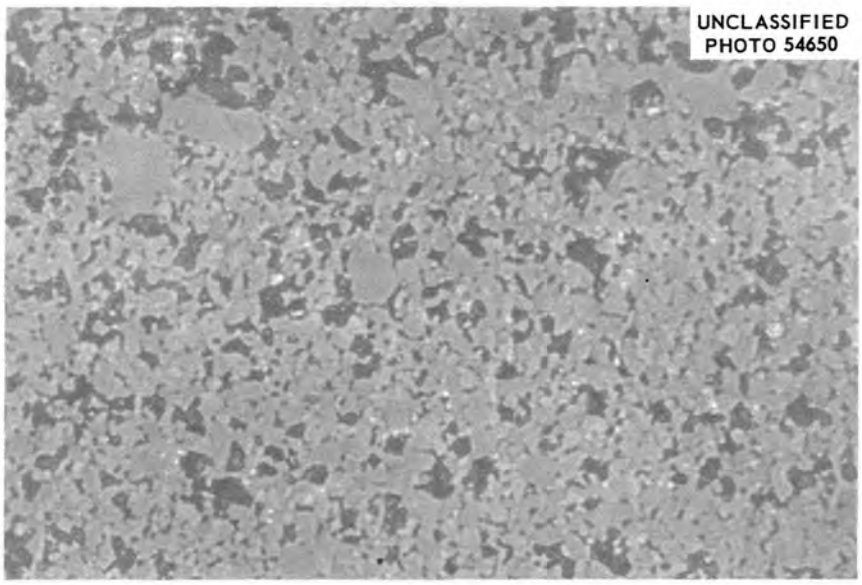

Fig. 56. Irradiated Specimen 5-52. Very difficult to observe any structure as polished or etched. Etched. 750X.

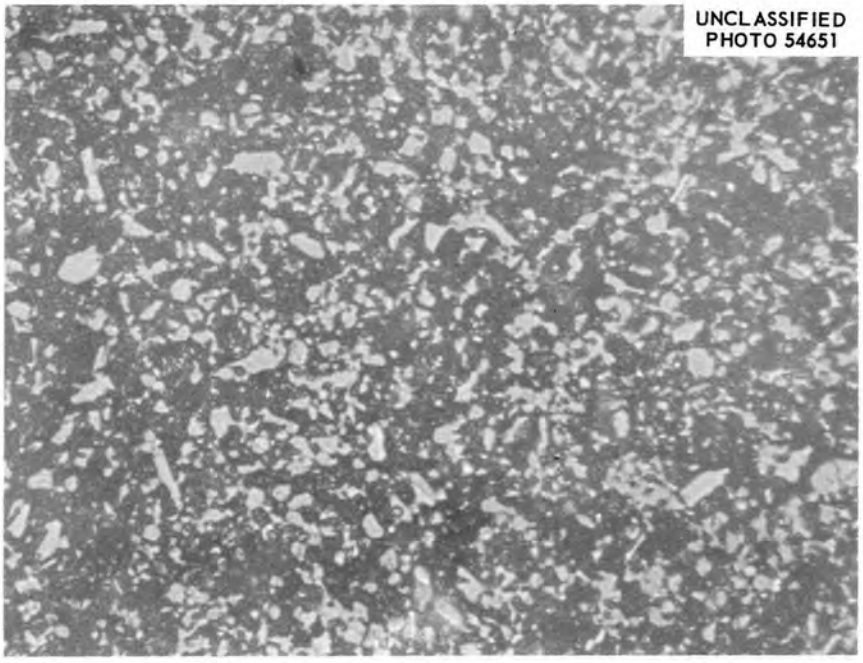

Fig. 57. Irradiated Specimen 5-62. Very difficult to observe any structure as polished or etched. Etched. 750X.

DISCUSSION OF RESULTS

In considering the behavior of BeO in a nuclear reactor, it is desirable to keep in mind the changes which are theoretically possible when a material of this type is exposed to nuclear radiations. The interaction of nuclear radiation with matter can be divided into three types for the purposes of this discussion:

1. Interaction with electrons. These interactions produce ionization and excitation of the atoms in the material.
2. Momentum-transfer collisions. For example, Rutherford-type collisions between nuclei and fast neutrons; these interactions result in thermal excitation of the atoms in the material and, in some cases, translation of the atoms from their normal lattice positions. Such atomic displacements are produced primarily by fast neutrons rather than by gamma radiation. The kinetic energy transmitted to an atom by a gamma ray is generally not sufficient to exceed the binding energy of the atom in the solid.
3. Nuclear reactions. These reactions in some cases produce transmutations in the atoms which are struck, resulting in a change in their chemical form. Of particular interest is the production of helium and tritium by fast neutrons in (n,2n) and (n,α) reactions.

These three kinds of primary interactions of nuclear radiation with matter result in (1) generation of heat within the material, with the attendant thermal gradient and thermal stresses; (2) chemical decomposition of compounds; (3) atomic displacements, with the production of lattice defects such as interstitial atoms and vacancies in the structure of the material; and (4) the generation of the gases helium and tritium in the material.

Effects of Thermal Stress

Internal heat generation in a material produces a thermal gradient which results in differential thermal expansion between different parts of the material. In the case of a nonductile material such as BeO, this differential thermal expansion produces relatively high thermal stresses which under certain circumstances can exceed the strength of the material and result in fracture. If the material is maintained at a very high temperature, stress relaxation can occur, preventing damage to material. Failure by thermal stress alone would be expected to occur when the material is first exposed to radiation. If the thermal conductivity of

the material decreases when it is exposed to radiation, the thermal gradient resulting from a given heat generation will increase and the thermal stress will increase with continued exposure. If the strength of the material decreases when it is exposed to radiation, the damage produced by a given amount of thermal stress will increase with continued exposure. It is clear that failure due to thermal stress alone will manifest itself at the beginning of the irradiation period, whereas failure which appears after continued irradiation is associated with a gradual change in physical properties.

A cursory examination of the information on fracturing of BeO specimens in Fig. 8 indicates that damage to the material is associated with high integrated radiation dose and apparently does not occur at the time the sample is first exposed to radiation. The increase in diameter of the capsule cladding described is apparently associated with the dimension change in the BeO and with the cracking of the BeO specimens. In an effort to identify the cause of these changes, it is of interest to examine the changes in diameter as a function of integrated neutron flux and temperature. Figures 58 and 59 show these relationships. It can be seen that the dimension change increases with radiation exposure at all temperatures but is more pronounced at temperatures less than 400°C. For any given integrated dose the change in diameter decreases as temperature increases. Apparently, whatever is producing the increase in capsule dimensions occurs not abruptly at the beginning of the irradiation period, but gradually over the entire period of irradiation and is reduced in its effectiveness at temperatures greater than 400°C.

Further evidence as to the time at which changes occur in the material is contained in Fig. 31, which shows the observed radial ΔT for some of the specimens during irradiation. If failure of the specimens were produced by thermal stress alone, and if the change in ΔT were produced by fracturing of the BeO, all of the change in ΔT would have occurred at the beginning of the irradiation period. However, the change in ΔT was greater toward the end of the irradiation period, indicating that the effect is associated not with the initial thermal stress but with some factor associated with integrated radiation dose. The hypothesis that the change in ΔT is the result of fracturing is not tenable

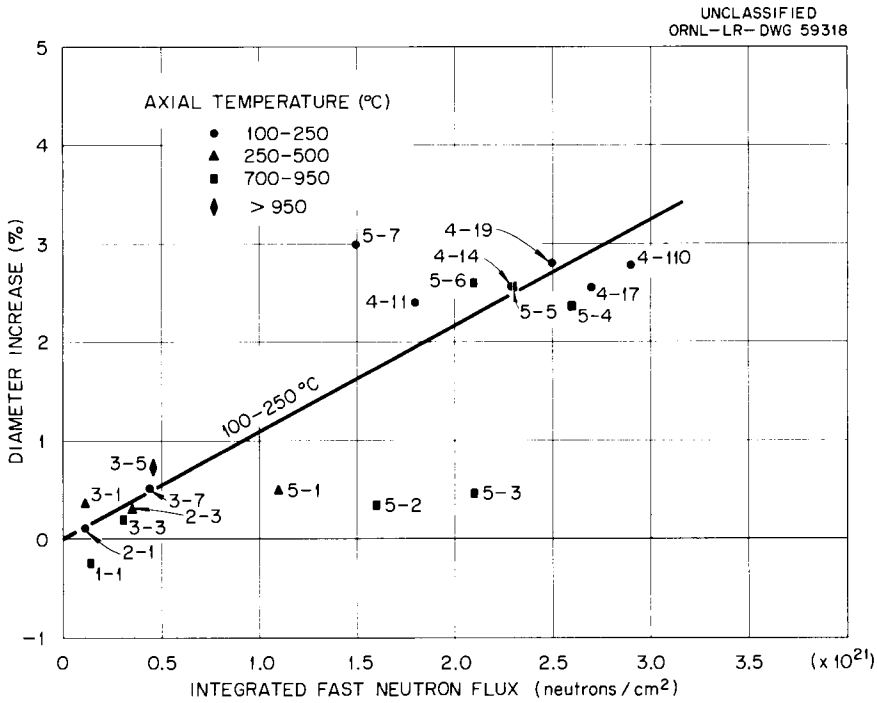

Fig. 58. Increase in Clad Diameter vs Integrated Fast Neutron Flux.

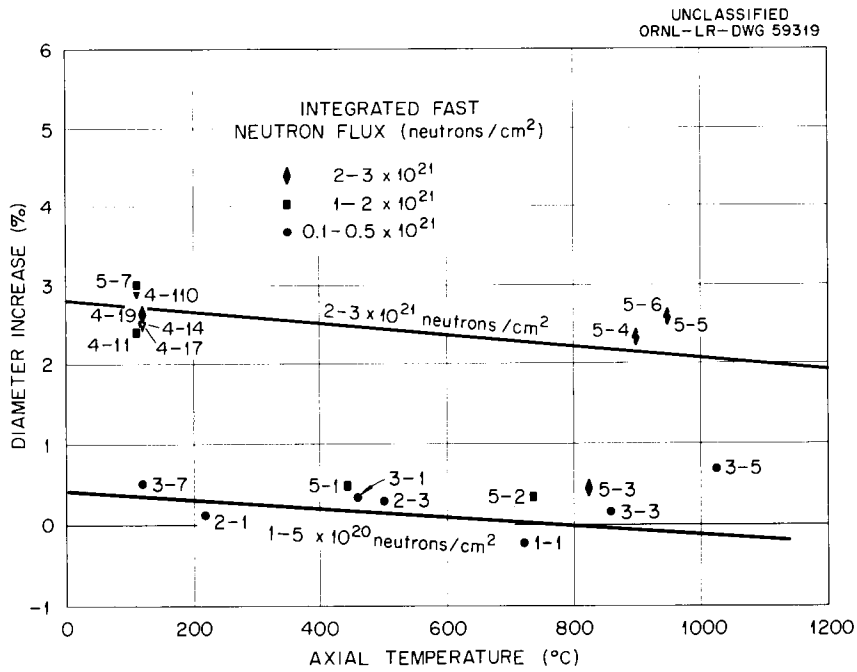

Fig. 59. Increase in Clad Diameter vs Temperature.

for these two specimens, since more change occurred in capsule 3-5 than in 5-6, and capsule 3-5 exhibited only initial fractures, while capsule 5-6 fractured extensively (Fig. 31).

In a cylindrical specimen the maximum tensile stress resulting from internal heat generation is proportional to the internal heat generation times the square of the diameter if all other factors are considered constant. Figure 60 is a plot of the observed changes in capsule diameter vs the function nvD^2. In this figure the fast flux, nv, is taken as a crude measure of the relative gamma-heating intensity in the material. The effect of temperature must be considered in interpreting this data. If the change in capsule diameter is produced by failure of the BeO under thermal stress, with no contribution by other factors, then the change in diameter should increase monotonically with the quantity nvD^2. The random variation of the change in gross capsule dimensions with the relative thermal stress in the specimen at each temperature indicates that failure by thermal stress alone is not a sufficient explanation. The fact that more change in capsule dimensions occurs at lower temperatures cannot be explained by the variation of thermal conductivity with temperature. The thermal conductivity of BeO is higher at low temperatures (Fig. 2), and

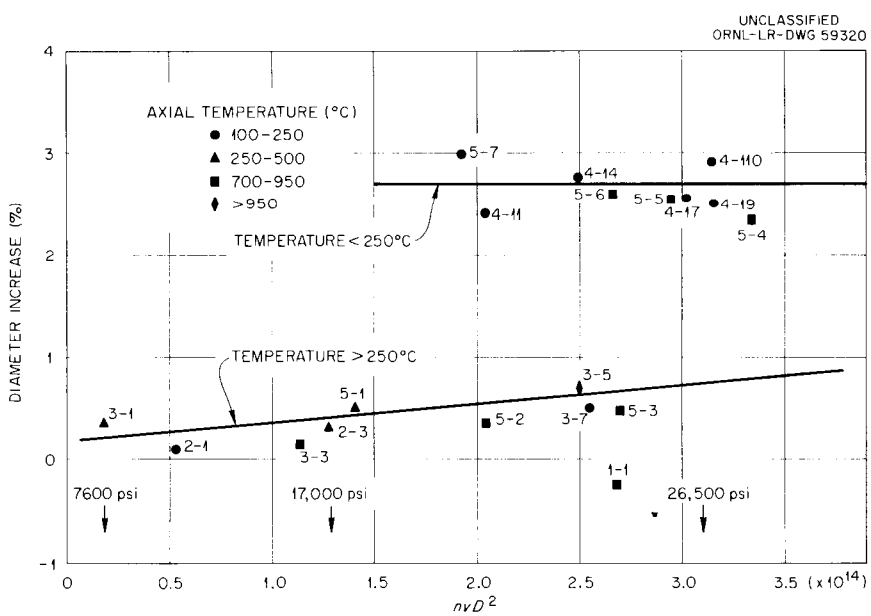

Fig. 60. Increase in Clad Diameter vs Thermal Stress Function.

would result in reduced thermal stresses. However, it does not rule out the possibility that changes in physical properties such as thermal conductivity or strength of the material could produce a condition where the specimen fails under thermal stress over long periods of irradiation.

Chemical Decomposition of Compounds

Chemical decomposition of BeO could result in the appearance of neutral beryllium atoms or oxygen atoms. These could appear as defects in the BeO lattice or could aggregate and appear as metallic beryllium in a separate phase or as oxygen gas. Such chemical changes are not considered probable in an ionic crystal such as BeO because of the stability of the ionized form of the atoms within the crystal. No new phases were observed during metallographic examinations. No x-ray diffraction lines corresponding to metallic beryllium could be found. Small amounts of oxygen were observed in the gases released from the samples. The range of amounts of oxygen is equivalent to decomposition of 7 to 50 ppm of the BeO. On the basis of this evidence, it must be concluded that chemical decomposition of the BeO did not play an important role in the effects of radiation.

Effects of Atomic Displacements

Momentum transfer interactions between radiation and atoms sometimes result in the displacement of atoms from their normal positions in the solid lattice. Such an event produces an atomic vacancy and an interstitial atom where the struck atom comes to rest. The beryllium atom receives a greater amount of energy than oxygen in a neutron collision because of its lower mass, and for a given amount of energy a greater fraction of atoms will be displaced with beryllium than with oxygen because the beryllium ion has only 1/5 the radius of the oxygen ion in the BeO lattice and is therefore more mobile in the lattice. In fact, the doubly charged beryllium ion is smaller than the neutral helium atom, since it has an electronic structure like that of neutral helium, but the increased positive charge on the nucleus results in smaller orbital radii. Consequently, it is to be expected that a greater amount of beryllium atom displacements than oxygen atom displacements will occur.

When a beryllium atom is displaced in the BeO lattice, it results in a positively charged interstital beryllium ion and a negatively charged vacancy at the site normally occupied by the beryllium ion. When an oxygen atom is displaced it results in a negatively charged oxygen ion interstitial and a positively charged vacancy at the site normally occupied by an oxygen ion. These vacancies and interstitials pair off to preserve electrical neutrality in an ionic lattice, forming Frenkel defects where a vacancy and interstitial of the same type of atom are paired, Schottky defects where oppositely charged interstitials pair, and various other combinations. The higher the temperature, the greater the mobility of these defects. They diffuse in the material, even at room temperature, and can form aggregates or can mutually annihilate each other or disappear at grain boundaries. The abundance of lattice defects would be expected to increase with continued exposure to radiation until a saturation condition is reached where the rate of disappearance of defects equals the rate of production of new defects. The initial rate of change of concentration of defects would be proportional to the intensity of radiation. The time to saturation would depend upon the intensity of the radiation and upon factors such as temperature which affect the rate of disappearance of defects. The concentration of defects at saturation would also depend upon the intensity of radiation and upon the factors affecting disappearance of defects and aggregates. Defects and their aggregates in a solid material are essentially alterations in the structure of the material and can manifest themselves in changes in such physical properties as thermal conductivity, density, refractive index, elastic modulus, strength of the material, and chemical reactivity as seen in metallographic etching. These changes in structure of the material result in distortions of the adjacent structure and produce lattice strain which can be detected by line broadening in x-ray diffraction patterns. The aggregation of defects at sites within the grains or the alignment of point defects at preferrred sites can also be detected by x-ray diffraction measurements. The diffusion of defects to grain boundaries in sufficient quantities could result in displacement of grain boundaries. It is conceivable that defects, upon annihilation, could produce crystal forms different from that of the

original material. If such a form were stable, new crystalline forms would be detected by x-ray diffraction measurements, or if they are sufficiently abundant they would be detected by metallographic examination. Any of these changes in structure could produce distortions which would cause fracture of the material for extreme exposure unless thermal healing occurs.

The x-ray diffraction measurements reported contain ample evidence that lattice defects are produced. The c parameter of the BeO lattice was the most consistently changed quantity obtained by x-ray diffraction measurements. Figures 61 and 62 show relative changes in this parameter as a function of integrated neutron flux and temperature. Data from the French work are also shown for comparison.[18] There is very good agreement between the French data and the data obtained in this study. In

[18]M. Salesse and R. Caillat of French Commission Energie Atomique, personal communication (1961).

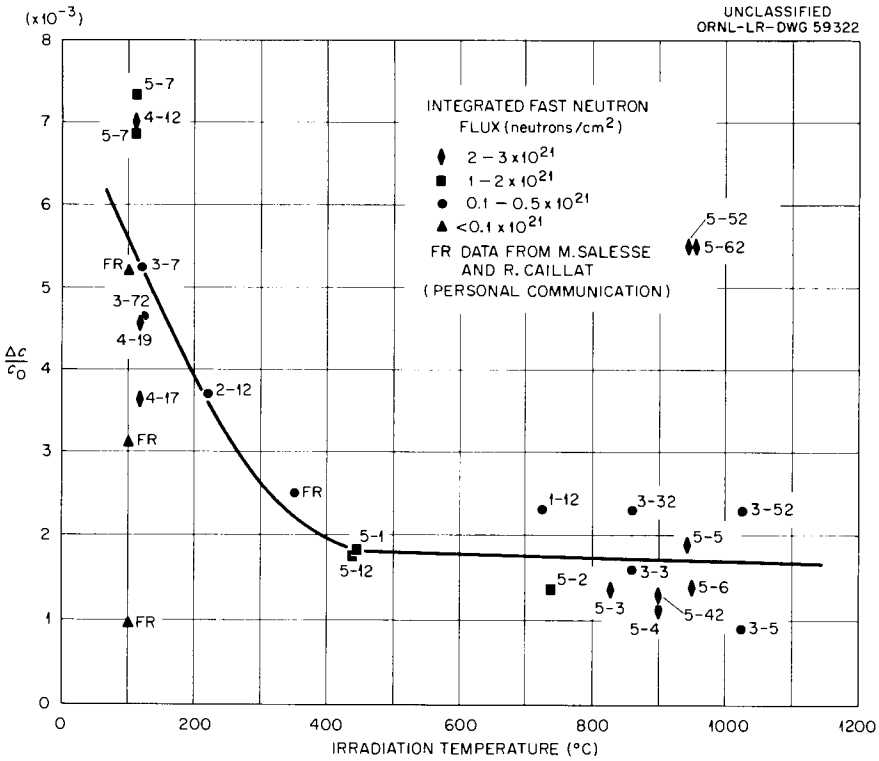

Fig. 61. Changes in c Parameter in X-Ray Diffraction Pattern of Irradiated BeO vs Irradiation Temperature.

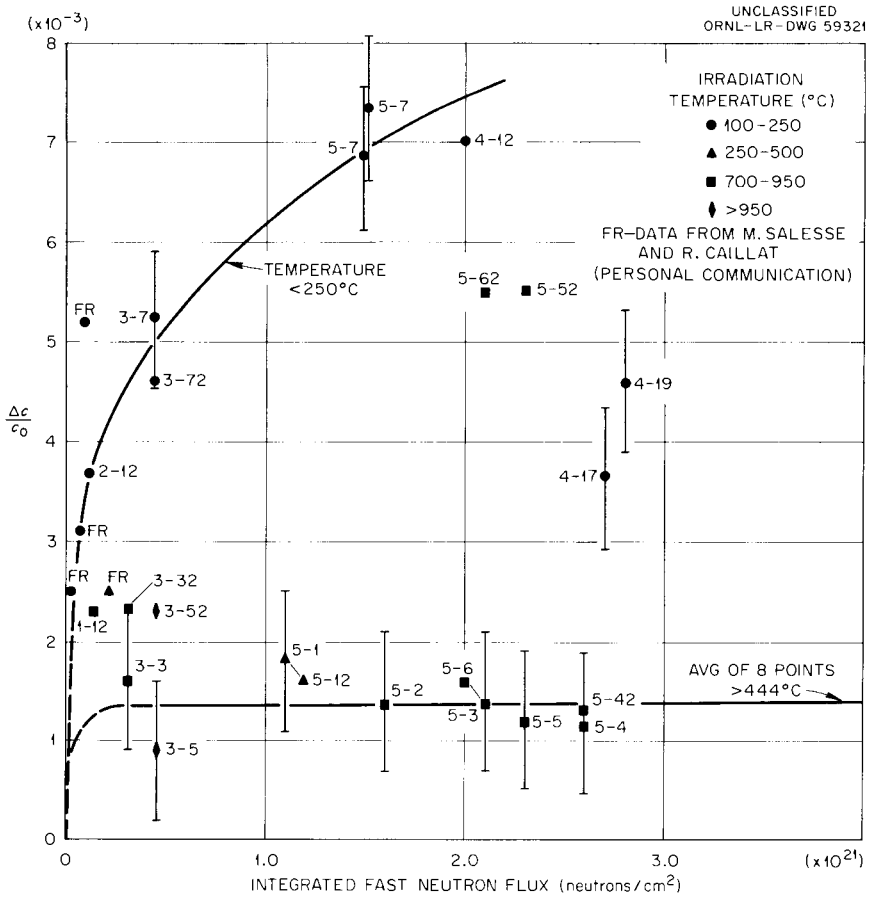

Fig. 62. Change in c Parameter in X-Ray Diffraction Pattern of Irradiated BeO vs Integrated Exposure.

Fig. 61 it can be seen that large changes in the c parameter are observed only in those specimens irradiated at 110 to 220°C. Specimens irradiated over the range 444 to 1025°C exhibited a fractional change of only 1.5×10^{-3} in the c parameter. Figure 62 shows that at temperatures greater than 250°C the change in the c lattice parameter reaches saturation by an integrated dose of 3×10^{20} neutrons/cm^2 and has no further significant change up to 2.6×10^{21} neutrons/cm^2. At a temperature of 110 to 120°C, however, fractional changes in the c parameter as large as 7.3×10^{-3} occur as exposure is continued, but there is a tendency for the effect to level off. Apparently, the lattice defects and their ultimate products are eliminated by a thermally activated process which is dominant at temperatures greater than 440°C and which has some effect even in the range 110 to 220°C.

The presence of lattice defects and their products could produce the observed changes in physical properties such as thermal conductivity, linear dimension, refractive index, and strength of material, as indicated by the pullout of grains during metallographic examination, and in chemical reactivity, as indicated by a need for changing etching procedures. A change in mechanical strength could result in cracking of the material during thermal cycling, and this in turn could gradually produce an apparent change in thermal conductivity as indicated by ΔT in the specimen during irradiation.

Among the products of lattice vacancies and interstitials are changes produced by their appearance at grain boundaries. Apparently, processes of this kind take place in these specimens at temperatures as low as 110°C, as evidenced by the tendency for the low-temperature curve in Fig. 62 to saturate. Presumably, interstitial atoms upon arriving at the grain boundary take a lattice position at the crystal face, resulting in an extension of the grain, and vacancies result in a retreating of the crystal face. Possibly, faces having certain orientations are preferred by one or the other of these processes, and, if so, for very large radiation doses significant changes in grain size or shape could occur. It hardly seems possible that changes in grain size of the magnitude described could occur in this way, however.

There was no metallographic or electron microscopic evidence for the formation of new crystalline forms of BeO such as could result from the rearrangement of beryllium and oxygen atoms as vacancies and interstitials rearranged themselves.

Most of the effects observed could be explained by the production of interstitial ions and vacancies in the lattice and their products.

Effects of Gas Generation

Nuclear reactions can produce elements which were not present in the original material. Reactions which produce gas are of special interest because of their effect on the material. In the case of BeO, there are two nuclear reactions which have sufficient yield to be important. Both of these are produced by fast neutrons in the range of energies which appear in nuclear reactors.

1. The (n,2n) reaction:

$Be^9 + n \rightarrow Be^8 + 2n$ (threshold energy, 2.7 Mev) (ref 19),
$Be^8 \rightarrow 2He^4$.

The cross section for the primary reaction has been variously reported to be 100 to 600 mb.[19] The second step occurs with a half-life of less than 10^{-14} sec.

2. The (n,α) reaction:

$Be^9 + n \rightarrow He^6 + He^4$ (threshold energy, 0.71 Mev) (ref 19),
$He^6 \rightarrow Li^6$,
$Li^6 + n(th) \rightarrow He^4 + H^3$.

The cross section reported for the primary reaction is in the range 1.9 to 50 mb.[19] The second step occurs with a half-life of 0.82 sec, and the cross section of Li^6 for thermal neutrons is 945 barns. The tritium decays to He^3 with a half-life of 12.6 years. Helium and tritium have been observed in irradiated beryllium metal[20-22] and in BeO.[23,24]

The data plotted in Fig. 29 indicate that internally generated helium is retained by the BeO even at high temperatures up to fast-neutron doses of 1.6×10^{21} neutrons/cm^2. The scatter among the points above this dose is probably caused by the release of helium by fracture of the BeO. The fact that the plot is linear rather than varying as the square of neutron dose indicates that the (n,2n) reaction contributes predominantly and the (n,α) reaction only negligibly to the production of helium.

---

[19] J. E. Evans, Reaction Products in High nvt Irradiated Beryllium, IDO-16364 (September 1956).

[20] C. E. Ells, The Swelling of Beryllium from Neutron-Induced Gases, CrMet-809 (1958).

[21] C. E. Ells, The Effect of Temperature During Irradiation on the Behavior of Helium in Beryllium, CrMet-864.

[22] R. S. Barnes and G. W. Greenwood, "Effects of Gases Produced in Reactor Materials by Irradiation," A/Conf.15/P/29 (1958).

[23] R. C. McGill and J. A. G. Smith, The Thermal Conductivity of Irradiated and Unirradiated BeO, AERE-R-3019 (1959).

[24] H. Frisbie, A. Bisson, and R. Caillat, J. Nuclear Materials 1, 106–8 (1959).

This is to be expected from the cross-section values for the two reactions. The slope of the line in Fig. 29 indicates a helium yield of 205 std μl of helium per g of BeO per 10^{21} neutrons/cm^2. This compares favorably with the range of values of 250 to 269 μl per g of BeO per 10^{21} neutrons/cm^2 which would be expected, based on data reported by Rich and Walters[25] for metallic beryllium. Similar data reported by Ells[20] are equivalent to a higher value of 460 μl per g of BeO per 10^{21} neutrons/cm^2.

The data plotted in Fig. 30 indicate that internally generated tritium is largely retained by the BeO at 120°C but is lost to an increasing degree at higher temperature. The fact that the tritium content varies as the square of the neutron dose agrees with theoretical expectation, since two neutrons are required to produce tritium. Strictly speaking, the yield of tritium is approximately proportional to the product of the integrated fast flux and the integrated thermal flux, since a two-step reaction is involved, the rate of the first step being proportional to fast flux and of the second to thermal flux. Within the ETR facility used in this work the fast flux is approximately proportional to thermal flux. By use of the analytical data and of the curved line in Fig. 30 as an indication of the amount of tritium generated, it is possible to calculate the fraction of the tritium which escaped from the BeO during irradiation. Booth[26] has developed an expression for diffusion of gaseous fission products from a spherical region during continuous generation of the gas.

The differential equation for diffusion with continuous generation is

$$\frac{\partial C}{\partial t} = D\left(\frac{\partial^2 C}{\partial r^2} + \frac{2}{r}\frac{\partial C}{\partial r} \right) + B \ , \qquad (1)$$

where C is the concentration of tritium, at radius r at time t, D is the diffusion coefficient, and B is the tritium production rate. Application

---

[25] J. B. Rich and G. P. Walters, The Mechanical Properties of Beryllium Irradiated at Various Temperatures, AERE-R-3684 (1961).

[26] A. H. Booth, A Method of Calculating Fission Gas Diffusion from UO_2 Fuel and Its Application to the X-2-f Loop Test, CRDC-721 (September 1957).

of this equation imposes the simplifying approximation that the tritium concentration increased linearly to its final value for each specimen. The solution to Eq. (1) is used to obtain the amount of tritium passing through the surface up to time t. This is divided by the total amount generated to give the fraction of tritium released,

$$f = 1 - \frac{6a^2}{90Dt} + \frac{6a^2}{\pi^4 Dt} \sum_{n=1}^{\infty} \frac{1}{n^4} \exp(-n^2\pi^2 Dt/a^2) \ , \qquad (2)$$

where a is the radius of the equivalent sphere in which diffusion is occurring. The observed fraction of tritium released for each data point in Fig. 30 may be substituted into Eq. (2) and solved graphically to obtain Dt/a^2. Dividing by t, the duration of irradiation yields D/a^2. The results of these calculations are plotted in Fig. 63. From the slope of the line the effective activation energy for diffusion is 10.8 kcal/mole. The diffusion rate, D/a^2, at 950°C is 2.5×10^{-7} sec^{-1}. For comparison, the activation energy of hydrogen in another ionic lattice, SiO_2, is 9.3 to 12 kcal/mole.[27] The data are not sufficient to indicate whether more than a single mode of diffusion is at work.

The effect of generated gas depends upon the amount of gas retained and the strength properties of the material. The amount of gas retained depends upon the rate of production and the rate of escape of gas and the duration of the experiment. At temperatures low enough that gas cannot diffuse out of the grains in which it is born, or into voids, the concentration would accumulate with continued exposure to radiation until the equilibrium pressure of the gas at a potential fracture surface exceeds the strength of the material. When this happens the material would fracture at intervals small enough that gas could escape from the remaining fragments by diffusion as fast as it is formed. At higher temperatures the same general behavior would occur except for the effects of changes in diffusion rate, solid solubility of gas, and strength of the material. The increased diffusion rate would increase the size of regions which could survive intact, although reduction of strength of the material would lessen this effect somewhat.

---

[27] R. M. Barrer, J. Chem. Soc. 1934, 378.

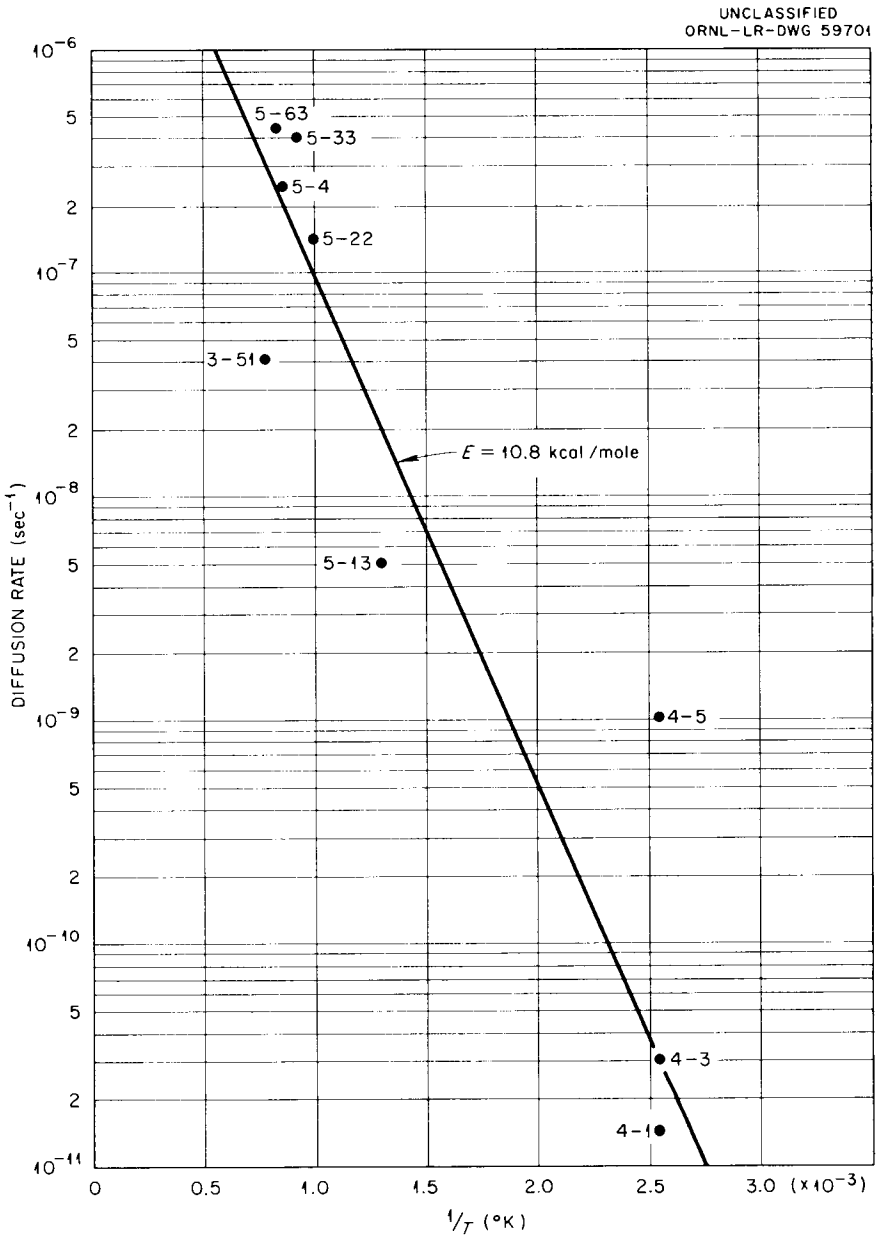

Fig. 63. Diffusion Rate for Tritium in BeO.

This model for explaining damage to BeO fits the observations which are represented in Figs. 8, 58, and 59. At low temperature, BeO fractures at a lower radiation dose than at high temperature; and for high radiation dose and low temperatures the material is degraded to a fine powder. This can be explained by the hypothesis that at low temperature, helium is able to diffuse from only small particles of BeO as fast as it is formed. At

high temperatures the escape of helium by diffusion to void spaces is fast enough for BeO to survive.

This model can be used to explain many of the observed changes in irradiated BeO. The changes in physical dimensions are the result of deformation of the BeO by helium either as interstitial atoms or in submicroscopic voids. The fact that the helium is retained in the BeO even during deformation indicates that it is traveling to voids rather than out of the specimen. Probably the helium first diffuses to submicroscopic voids of the kind pictured in Figs. 37 and 38. These voids were not detected by metallographic examination because they are too small to be seen (0.1 to 0.3 μ). As deformation of the BeO becomes extensive the submicroscopic voids enlarge and finally make connection with voids of the kind shown in Fig. 34, which existed in the BeO before irradiation. The calculated pressure of the maximum amount of helium in the pores of the corresponding form of BeO (low density) is 180 psi at room temperature, or 840 psi at 1000°C. These pressures are well below the strength of BeO, so the propagation of cracks would be expected to halt as soon as this occurs.

The changes in thermal conductivity described can be explained by the voids or by the introduction of helium into the lattice as interstitials. The effects on the crystal lattice of BeO can be explained by the loss of beryllium atoms and the appearance of helium and tritium atoms in the lattice. These changes would, in fact, produce lattice defects of the kind observed by x-ray diffraction measurement. Stresses produced by gas pressure in the submicroscopic voids would produce the lattice strain which appeared as line broadening.

Most of the observed changes in BeO during irradiation can be explained as effects of gas generation.

CONCLUSIONS

Behavior of BeO Under Irradiation

Beryllium oxide bodies when exposed to nuclear radiation inside a nuclear reactor will fracture or degrade to a fine powder under some conditions. The conditions favoring this damage are high integrated fast neutron flux (>1 Mev) and low temperature. The effect is large at a dose

of 2×10^{21} fast neutrons/cm^2 at 100°C and appears to be reduced substantially at temperatures of 400 to 1000°C. These changes are accompanied by changes in dimension, thermal conductivity, crystal structure, and strength of intergranular bonds. The changes in crystal structure at 400 to 1000°C reach a saturation value at less than 3×10^{20} neutrons/cm^2, and no further change occurs up to 2.6×10^{21} neutrons/cm^2.

The cause of the changes appears to be either atomic displacements or gas generation or a combination of both. It is not possible to distinguish between these two causes by the data in this report. The damage to BeO is not caused by thermal stresses alone, since the changes occur gradually over the period of irradiation. There was no detectable chemical decomposition of BeO.

It is not possible to determine whether high-density BeO resists radiation damage better than low-density BeO, since the two kinds of specimens were subjected to different ranges of radiation dose.

Helium produced by fast-neutron reactions is retained by BeO at all irradiation temperatures from 100 to 1000°C, and tritium is retained at 100°C but is released at temperatures of 400 to 1000°C. New voids 0.1 to 0.3 μ in diameter appear in the irradiated BeO both within grains and at grain boundaries.

Additional irradiation experiments with various kinds of BeO are needed to determine whether the behavior of the low-density BeO used in these tests is representative. A program of development should be conducted in which fabrication parameters are made a part of the statistical design of the experiment. Such a program should determine the stability of BeO fabricated in various ways when exposed to various combinations of irradiation conditions. Factors which should be explored are grain size of BeO powder from which bodies are made, sintering temperature, intensity of fast-neutron and gamma radiation, specimen diameter, irradiation temperature, and duration of exposure. By varying these factors in a statistical design, it will be possible to resolve many of the questions involved in the use of BeO in nuclear reactors.

Implications for Reactor Design

The results of this series of experiments indicate that great caution must be exercised in designing BeO moderators for nuclear reactors. Under some conditions physical deterioration occurs to such a degree as to render the material unsuitable for use. For greatest life the moderator should be kept above 400°C, and probably 800 to 1000°C is more desirable.

The fact that at least one specimen remained intact after an exposure of 1.6×10^{21} fast neutrons/cm^2 at 737°C implies that conditions exist under which BeO can be used. The optimum conditions for long moderator life must be found before BeO-moderated reactors can be designed with confidence.

ACKNOWLEDGMENTS

The authors wish to acknowledge the contributions of R. Hamner and T. N. McVay of the Ceramics Laboratory, H. L. Yakel, R. M. Steele, and B. S. Borie of the X-Ray Laboratory, and E. Long of the Metallography Laboratory (all of the Metallurgy Division); A. Meyers of the Analytical Chemistry Division, for gas analysis; and R. E. Thoma of the Reactor Chemistry Division.

J. E. Gates, C. Melton, and A. E. Austin of Battelle Memorial Institute rendered invaluable support in the hot-cell work and in x-ray diffraction, metallography, and electron microscopy. Fred McMillan, R. Nertney, Howard Watanabe, R. B. Van Sice, and J. L. Walker of Phillips Petroleum Company at the ETR site in Idaho supervised in-pile operation. G. W. Keilholtz, W. R. Grimes, and G. M. Watson gave valuable support and encouragement.

ORNL-3164
UC-40 — Radiation Effects on Materials
TID-4500 (17th ed.)

INTERNAL DISTRIBUTION

1. Biology Library
2-3. Central Research Library
4. Reactor Division Library
5. ORNL — Y-12 Technical Library Document Reference Section
6-40. Laboratory Records Department
41. Laboratory Records, ORNL R.C.
42. C. J. Barton
43. D. S. Billington
44. F. F. Blankenship
45. A. L. Boch
46. E. G. Bohlmann
47. G. E. Boyd
48. R. B. Briggs
49-63. W. E. Browning, Jr.
64. R. H. Chapman
65. W. E. Clark
66. J. H. Coobs
67. F. L. Culler
68. A. P. Fraas
69. J. H. Frye, Jr.
70. R. J. Gray
71. W. R. Grimes
72. R. L. Hamner
73. W. O. Harms
74. T. Hikido
75. R. G. Jordan (Y-12)
76-81. G. W. Keilholtz
82. M. T. Kelley
83. A. Larson
84. C. E. Larson
85. J. A. Lane
86-97. J. E. Lee, Jr.
98. G. H. Llewellyn
99. R. A. Lorenz
100-119. W. D. Manly
120. H. G. MacPherson
121. R. E. MacPherson
122. H. F. McDuffie
123. D. L. McDonald
124. A. S. Meyer
125. A. J. Miller
126. C. E. Miller, Jr.
127. R. E. Moore
128. J. P. Murray (K-25)
129. M. W. Rosenthal
130. G. Samuels
131. J. H. Shaffer
132-141. R. P. Shields
142. C. H. Secoy
143. M. J. Skinner
144. C. D. Susano
145. J. A. Swartout
146. D. B. Trauger
147. E. H. Taylor
148-187. G. M. Watson
188. J. C. White
189. A. M. Weinberg
190. M. C. Wittels
191. H. L. Yakel
192. A. F. Zulliger
193. F. Daniels (consultant)
194. F. T. Gucker (consultant)
195. F. T. Miles (consultant)

EXTERNAL DISTRIBUTION

196. Division of Research and Development, AEC, ORO
197-795. Given distribution as shown in TID-4500 (17th ed.) under Radiation Effects on Materials category (75 copies — OTS)